Fall 2013

A structural analysis of the El Kasr structure in the western desert of Egypt

Trevor Charles Ellis

A STRUCTURAL ANALYSIS OF THE EL KASR STRUCTURE IN THE WESTERN DESERT OF EGYPT

by

TREVOR CHARLES ELLIS

A THESIS

Presented to the Faculty of the Graduate School of the

MISSOURI UNIVERSITY OF SCIENCE AND TECHNOLOGY

In Partial Fulfillment of the Requirements for the Degree

MASTER OF SCIENCE IN GEOLOGY AND GEOPHYSICS

2013

Approved by

John P Hogan, Advisor
Fransisca Oboh-Ikuenobe
Andreas Eckert

ABSTRACT

The El Kasr structure was studied in order to investigate the origins and evolution of the enigmatic Desert Eyes structures of the Western Desert due to its accessibility and uniqueness among the structures. The El Kasr structure, an elongate structural basin with low limb dips, is unique among the "Desert Eyes" structures in that it: 1) occurs in isolation in otherwise horizontal sedimentary rock, 2) the long dimension of the basin is oriented NNW, 3) it is closely spatially associated with the less common NNW fault zones, and 4) is composite in nature. The structure was investigated using remote sensing and field mapping techniques. The structure is defined by basins of prominent carbonates and associated siliclastics. Both basins defining the structure have broad interlimb angles. The structure is truncated along the southwest by a prominent normal fault zone. Evidence for an eastern fault system includes truncation of layers of Dakhla Formation that strike at a high angle to the structure and terminate along possible drag folds and layers of Dakhla Formation that are locally steeply dipping, offset by numerous small faults, and rotated from the strike of the basin. The El Kasr structure occurs in the hanging wall(s) between two fault systems, which appear to merge south of the structure, as an elongated basin sub-parallel to the trace of these faults. Balanced cross-sections of the structure suggest that the El Kasr structure formed within a transtensional zone between overlapping left-lateral strike-slip zones. The sedimentary cover within this zone deformed by drape folding along the margins of the transtensional zone as well as plastic deformation over a graben that developed in the Precambrian basement. The investigation of the El Kasr structure suggests that other Desert Eye structures may have formed through interactions between fault segments and deformation related to rheology.

ACKNOWLEDGMENTS

I would like to extend my sincerest gratitude to Dr. John Hogan for his exceptional guidance and assistance throughout my academic career. To my committee, Drs. Oboh-Ikuenobe and Eckert for their time and talents. To the Department of Geological Sciences and Engineering for the tremendous opportunities and exceptional instruction as well as the peerless camaraderie that makes it special. To the National Science Foundation through the Office of International Science and Engineering, grant number 1030230, entitled Desert Eyes: Origin and Evolution of enigmatic domes and basins in the stable platform of Egypt. To Dr. Barbara Tewksbury for her pioneering work on the Desert Eye structures as well as her tremendous assistance with literature and imagery. To the other members of the Desert Eyes team, including but not limited to, Dr. Kelly Liku, Dr. Charlotte Mehrtens, Dr. Simon Kattenhorn, Dr. Elhamy Tarabees, Cory Reed, Brock Alldredge, Susan William, Steven Gohlke, Claire Sayler, Tucker Keren, Peter Laciano, and Eric Doubet, To the graduate students of the department that continuously offer guidance and support. To Tom Jerris for his assistance with figures. To all the special friends I’ve made along the way. Finally, I would like to thank my wife as well as the rest of my family for their patience and support throughout my studies.

TABLE OF CONTENTS

LIST OF ILLUSTRATIONS

LIST OF TABLES

1. INTRODUCTION

Understanding the relationship between folding and faulting is a fundamental question to structural geology. This relationship may be manifested in a variety of forms and mechanisms related to the tectonic setting (Suppe, 1983; Sharp et al., 2000) and the mechanical strength properties of the material (Erickson, 1995). Folds have been well documented in compressional environments and their mechanisms and geometries well constrained by field investigations (Rich, 1934; Bucher et al., 2003; Robert-Charrue and Burkhard, 2008;) as well as various modeling experiments (Storti et al., 1997).

Recently, many field investigations have focused on the development and classification of folds associated with normal faults found in extensional settings (Khalil and McClay, 2001; Janecke et al., 1998). These folds have been shown to display a wide variety of mechanisms and characteristics related to fault-plane geometry, fault segment length, and along-strike variations in displacement (Schlishe, 1995).

A variety of folds have been documented along strike-slip zones as well, such as en echelon folds with complex geometries (Sylvester, 1988) and Accordion-style folding (Sylvester and Smith 1976). These folds associated with strike-slip faulting have been investigated as potential hydrocarbon reservoirs (Harding, 1974; Dibblee, 1977).

Spectacular folds associated with faults occur within both the Stable and Unstable Shelf regions of the Western Desert of Egypt (Issawi, 1968) and are clearly visible in remote sensing imagery (Thurmond et al., 2004; Tewksbury et al., 2009). First mentioned by Issawi (1968) the presence of the largest of these folds was noted throughout the southern portions of the Western Desert but the origins of these structures remained a mystery. Tewksbury et al. (2009) investigated these structures using remote sensing methods as well as field work, cataloguing 479 individual structures and coining the term "Desert Eyes" for these folds. They demonstrated that these structures are both structural basins and structural domes that deform the sedimentary cover. Many of the "Desert Eyes" define linear arrays along east-west trends with a close spatial association to or located along and cross-cut by visible east-west fault traces (Figure 1.1). However, other well developed Desert Eyes without a close spatial association to a clear surface trace of a fault are visible as well (Figure 1.2). Tewksbury et al. (2009) speculate that these structures may be related to the propagation of faults in the subsurface, but note that other factors such as shale mobilization and rock rheology may play a significant role in their formation.

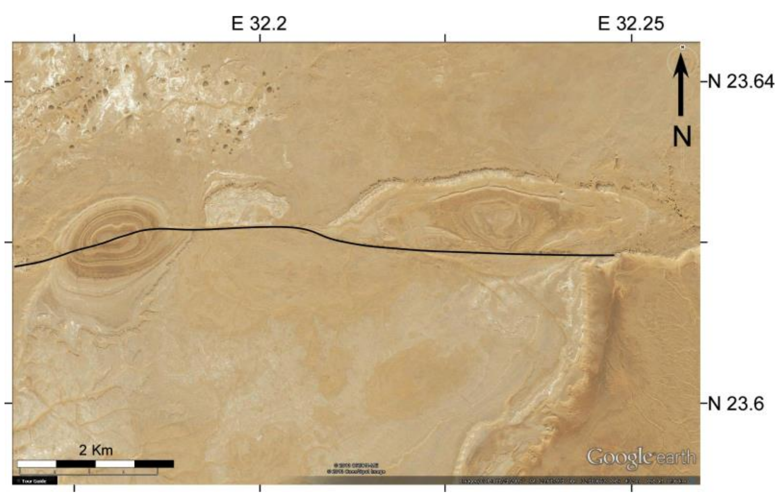

Figure 1.1 "Desert Eye" **s**tructures associated with the visible trace of a fault. The Seiyal cuts a structural dome on the left and a structural basin on the right.

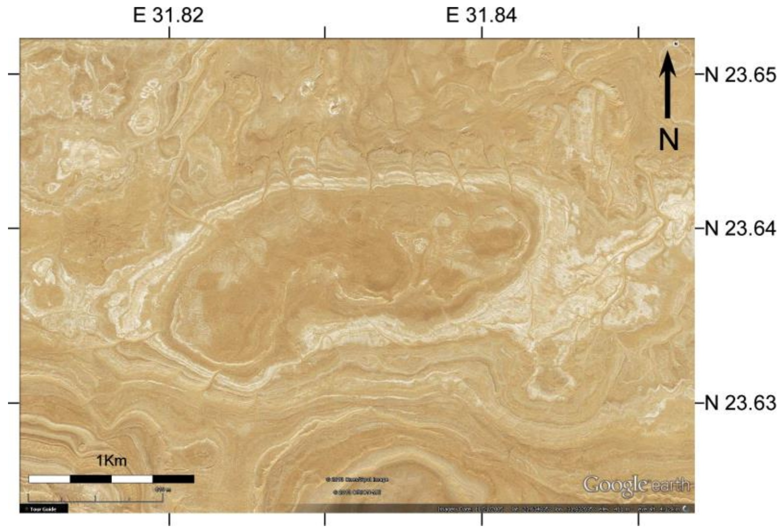

Figure 1.2 “Desert Eye” structure not associated with a visible fault trace.

The Desert Eyes structures crop out throughout the Shelf regions of Egypt: however, the character of these structures changes dramatically from north to south. In the north the Desert Eyes are defined by pseudo-circular structures of very low relief within Kohman chalk and are more closely associated with the development of a polygonal fault network (Tewksbury et al., 2009). Tewksbury et al. (2009) suggest that the structures to the north represent onshore analogues of structures previously reported from the North Sea. The structures to the south are remarkably different in character and expression. Currently little research has been done on these structures, further complicated by the lack of any known analogs corresponding to structures of this scale and spatial distribution.

The El Kasr structure, the subject of this paper, belongs to the group of Desert Eyes located in the Stable Shelf near the Arabian-Nubian Massif southwest of Aswan. The Desert Eyes structures in this region are both structural domes and basins that display a wide variety of geometries as well as various degrees of asymmetry and elongation. They also commonly exhibit a close spatial association with faults, faults that have demonstrable multiple and variable displacement histories, but examples of Desert Eye structures isolated from any visible trace of a fault also occur (Tewksbury et al., 2009).

The close spatial relationship observed between many of the Desert Eyes southwest of Aswan, including the El Kasr structure, and the regional fault systems suggest a genetic relationship. Woodward-Clyde (1985) and Thurmond et al., (2004) both noted the presence of these structures and speculated that the folds are related to local transpression produced by strike-slip motion along these faults. Tewksbury et al. (2009) noted that displacement of Desert Eye structures necessitates a component of dip-slip motion in their past, even though modern focal mechanisms indicate strike-slip as demonstrated by Mohamed et al. (2001). Dip-slip motion along these faults could allow for the formation of both longitudinal and transverse folds related to extension (Schlishe, 1995).

This study investigates the El Kasr structure in an effort to constrain the potential relationship between episodes of faulting in this region and the folding responsible for the formation of this Desert Eye. Like many of the Desert Eyes, the El Kasr is a structural basin closely associated with and partially truncated by faults. The El Kasr structure differs from other Desert Eyes in that it occurs in relative isolation, is associated with the less common N-S trending faults, and is larger, ~5 Km in length, than many of the Desert Eyes in this region. The El Kasr is easily identifiable in remote sensing data and readily accessible in the field, allowing for detailed field mapping and study. The structure is similarly visible in ASTER data and is clearly visible in images processed using

Optimum Index Factor, Principal Components Analysis, and Band Math techniques. The combination of field and remote sensing investigation, stereographic analysis, and construction of balanced cross-sections suggests that the formation of the El Kasr structure has formed in association with normal faults that have developed in a local area of extension related to overlapping left-lateral strike-slip faults, resulting in transtension.

2. REGIONAL GEOLOGIC SETTING

Egypt and northeast Africa may be subdivided into three major geologic provinces: 1) the Unstable Shelf, 2) the Stable Shelf, and 3) the Arabian-Nubian Massif (Henson, 1951; Guiraud and Bosworth, 1999; Guiraud et al., 2001; Youssef 2003; Figure 2.1). These divisions take into account both the tectonic history and the stratigraphy of northeast Africa (Youssef 2003). The Shelf regions have seen repeated transgressions and regressions, resulting in a broad carbonate and mixed facies deposition in the north and clastics in the south of Cretaceous to Eocene age (Guiraud et al., 2001). Youssef (2003) states that the Shelf regions are portions of a trough the follow the edges of the Nubian-Arabian Massif, which is visible to the south.

Guiraud et al., (2001) described the Unstable Shelf in the north as extending from Cyrenaica in the west to the Palmyrides in the east. The Unstable Shelf represents the area in which the Cretaceous to Eocene sedimentary cover has undergone severe tectonic deformation. This deformation was manifested in rifting through the Permian and Triassic, resulting in the separation of discrete blocks from the north coast of Africa, intense compression during the Santonian, resulting in basin inversion and folding, and finally a return to extension punctuated by brief extensional periods (Bosworth et al., 2008). Similarly the Stable Shelf represents the Cretaceous to Eocene sedimentary cover that has undergone relatively little deformation, although Precambrian structural trends have been repeatedly reactivated and propagate up through the cover rocks in this region (Said and El Kelany, 1990).

The El Kasr structure (Figure 2.1) is located approximately 45 km southwest of Aswan in the Stable Shelf region of Egypt near the Arabian-Nubian Massif and deforms

Cretaceous to Eocene sediments. In Google Earth imagery the El Kasr structure appears as a bold white and blue elongate basin, bound to the west and south by tan ridges (Figure 2.2).

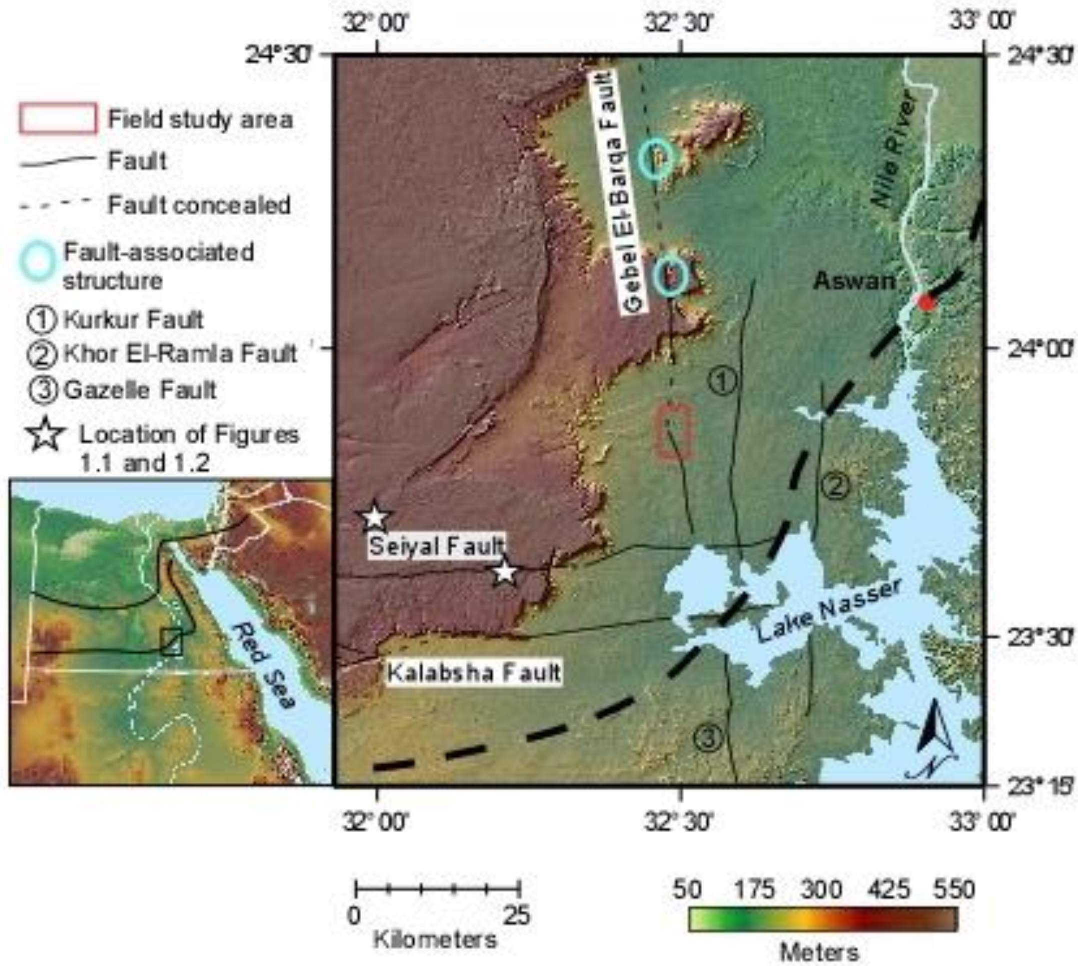

Figure 2.1. Southeastern portion of the Western Desert. Prominent faults are clearly visible and the location of observed structural domes and basins has been identified. The general boundary between the Stable Shelf and Nubian-Arabian Massif regions are indicated by the heavy dashed line, with the Stable Shelf to the north and the massif to the south.

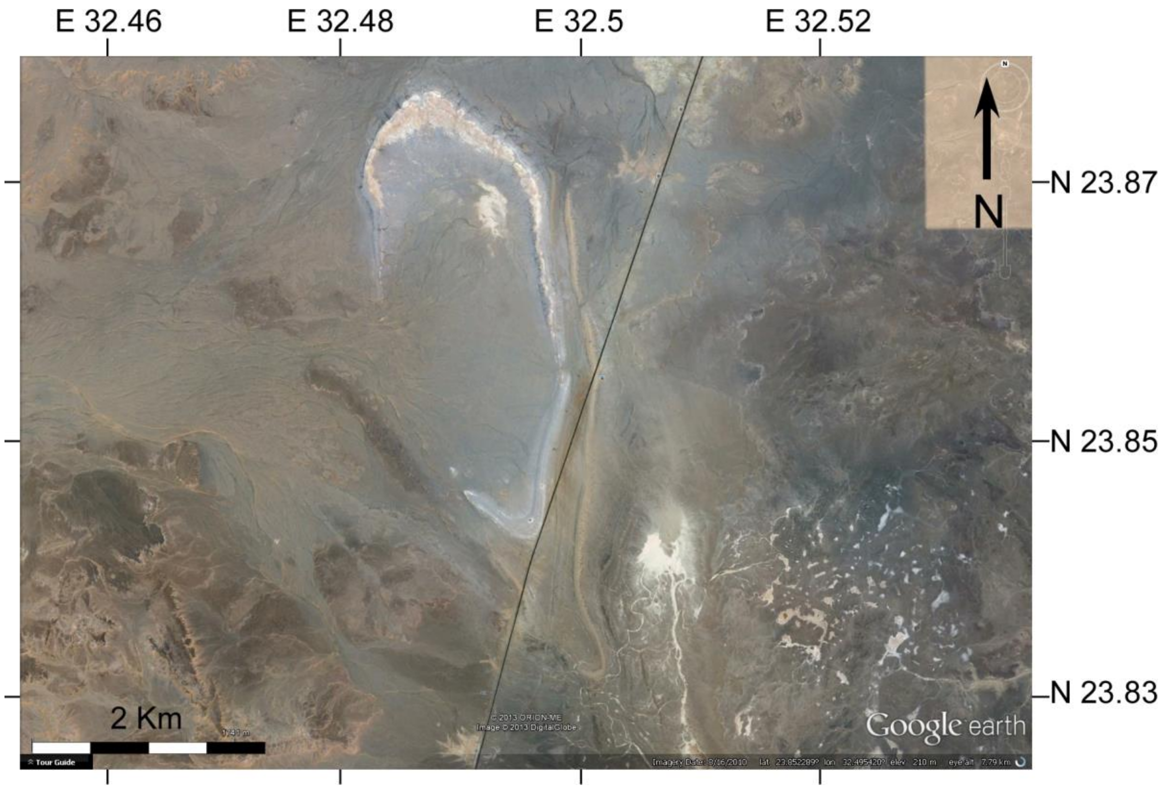

Figure 2.2 Google Earth image of the El Kasr structure. The Garra Formation crops out as a bold blue/white and the Kurkur as a dull tan. The Dahkla and alluvium may be seen in the adjacent plain in shades of brown.

The Precambrian basement exposed in the Nubian-Arabian Massif and the Red Sea hills of the Eastern Desert are composed of metamorphosed shelf sediments, gneisses, undifferentiated granites and weakly tectonized calc-alkaline granites (Conoco, 1981). These rocks are primarily exposed in southern Egypt and Northern Sudan as well as the Eastern Desert but are generally poorly exposed throughout the Western Desert.

Major Precambrian fault trends exist in the region and have been studied extensively relating to the geologic history of the region as well as the potential for seismicity related to the Aswan High Dam and Lake Nasser (Issawi, 1968, Woodward-Clyde Consultants, 1985, Mohamed et al., 2001,). These trends have been reported in studies done by Thurmond et al., (2004), Guiraud et al., (2005) and Roden et al. (2011) though their origin and history have not been investigated thoroughly. The most prominent of these trends are the Guinean-Nubian Lineaments, a series of transcontinental faults that trend approximately E-W. These features have repeatedly been reactivated as both strike-slip, dextral along E-W faults and sinistral along N-S faults, (Woodward-Clyde Consultants, 1985; Abdeen et al., 2000) and dip-slip (Issawi, 1978) and propagated up through the sedimentary cover. Similar, though more localized, north-south faults exist near Aswan. Issawi (1968) described these north-south faults as trending approximately due north with variations up to 10° to either east or west. These faults have also been reactivated as both strike-slip (Youssef, 2003) and dip-slip (Issawi, 1978).

The tectonic history of North Africa and Arabia is defined by a series of compressional and extensional episodes that were manifested in deformation within the Unstable Shelf and reactivation and propagation of preexisting faults in the Stable Shelf (Guiraud and Bosworth 1999; Guiraud et al., 2001). Prior to the Santonian the sinistral motion of Eurasia relative to Africa induced a transtensional to extensional stress fields across North Africa, leading to rifting in the Sirte, Abu Gharadiq, and Shushan-Matruh Basins during this time (Guiraud and Bosworth, 1999; Guiraud et al., 2001; Bosworth et al., 2008).

During the Santonian, the motion between Africa and Eurasia was rearranged, resulting in the brief but severe Santonian Compressional Event (Bosworth et al., 2008). This compressional event resulted in basin inversion as well as localized folding and faulting within the Unstable Shelf (Bosworth et al., 2008). This change in stress fields reactivated pre-existing basement faults (Bosworth et al., 1999) and the Guinean-Nubian Lineaments within the Stable Shelf registered dextral motion during this event (Guiraud et al., 2001). Youssef (2003) attributes much of the present day geomorphology of the region to the Santonian compressional event.

There is some evidence to suggest that these events induced local folding within the northern portions of what has traditionally been referred to as the Stable Shelf (Bosworth et al., 1999). These findings serve to demonstrate that the so-called Stable Shelf of Egypt may have undergone more severe deformation than previous studies suggest.

Rifting continued once again in the Late Cretaceous and into the Paleocene and Eocene, interrupted briefly by compression within the Unstable Shelf (Guiraud and Bosworth 1999). Compression occurred again in the late Eocene reactivating the east-west trending faults near Aswan (Guiraud and Bosworth 1999).

2.1 REGIONAL GEOLOGY OF THE SOUTHERN WESTERN DESERT

2.1.1 Geomorphology and Structures. The region around Aswan is dominated by a few broad geomorphologic features; the Sinn El-Kaddab Plateau, the Nubian Plain, the Red Sea Hills, and the Nubian Swell. The Sinn El-Kaddab Plateau is on the order of 100 Km wide in an east-west direction and stretches for about 300 Km from north to south with relief on the order of 200 m. The plateau is capped by the Eocene Dungul Formation while Garra, Kurkur, and Dahkla formations are exposed along the scarp (Conoco, 1981). The Sinn El-Kaddab Plateau is cross-cut by faults belonging to both the N-S and E-W trending fault trends. Woodward-Clyde Consultants (1985) suggest that the erosion of the scarp of the plateau may be structurally controlled by the many faults in the region. The Nubian Plain lies adjacent to the plateau and is approximately 30 to 50 Km wide with little to no relief. The plain slopes gently to the east, exposing roughly parallel bands of Dahkla and Nubian formations, reflecting their sub-horizontal nature. The Red Sea Hills to the east of the Nile are underlain by the Precambrian Basement which is composed of metamorphosed sediments, calc-alkaline granites, amphibolites, and gneisses, and are cross-cut by multiple faults, joints, and dikes (Issawi 1968; Woodward-Clyde Consultants, 1985; Conoco, 1981). To the south the Nubian Swell dominates southern Egypt and Northern Sudan. The Nubian Swell is defined a “complex, east-west trending structural high in southern Egypt and northern Sudan” and is composed of Neoproterozoic crystalline basement and Paleozoic sediments (Thurmond et al., 2004).

2.1.2 Stratigraphy As seen in Figure 2.3, the sedimentary cover of southern Egypt is approximately 1 km thick with large variation in the thickness of the individual units (Issawi 1978; Woodward-Clyde Consultants, 1985;).The Cretaceous Nubian Formation is the most extensive of these units and uncomformably overlies the Precambrian Basement, varying in thickness on the order of 400-600 m, reaching a maximum measured thickness of 592 m in the Kurkur oasis (Issawi, 1968; Woodward-Clyde Consultants ,1985). The varying thickness of the Nubian along with low dip angles suggests that the Precambrian Basement has an irregular surface (Issawi 1968). The Nubian is comprised of well sorted, poorly cemented 2 mm quartz sandstone with tabular cross-bedding and asymmetric ripple marks (Issawi, 1968; Woodward-Clyde Consultants ,1985).

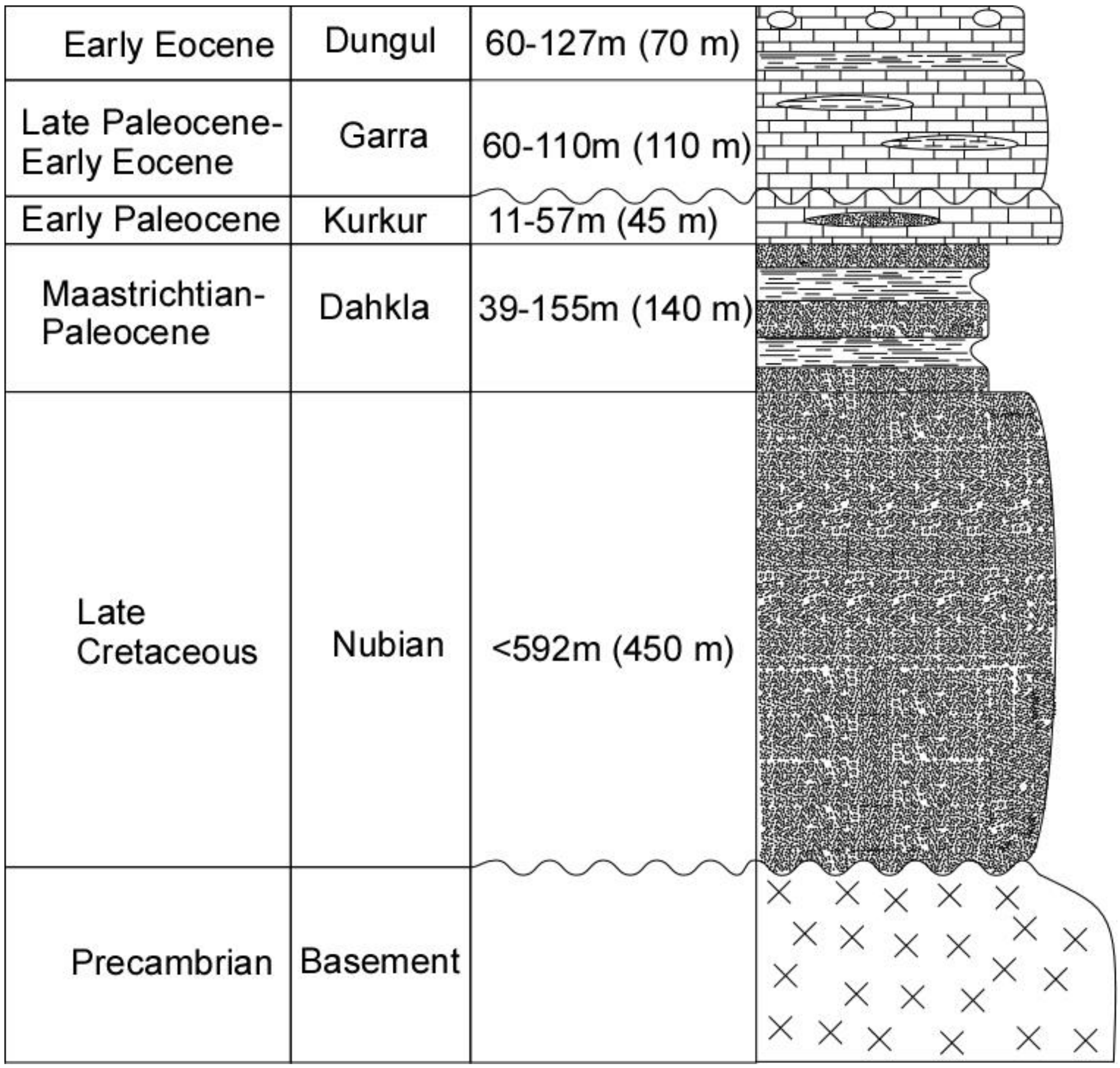

Figure 2.3 Stratigraphic Column of the study area. Thickness ranges are given as well as the unit thicknesses used in the cross-sections given in parentheses (Issawi, 1968; Woodward-Clyde Consultants, 1985).

The marine Maastrichtian Dakhla Formation conformably overlies the Nubian and is composed of interbedded shales, sandstones, and conglomerates near the base with carbonate beds near the top. The Dakhla ranges in thickness between 39 m and 155 m, thinning to the west (Woodward-Clyde 1985). In the field the Dakhla was observed as a brown medium grained sandstone with a calcite cement. Oyster beds and rip up clasts within the Dakhla were observed during this study.

The Paleocene Kurkur Formation is a thin fossil rich limestone, ranging between 11 m and 57 m, that conformably overlies the Dakhla. In the field the Kurkur Formation cropped out as resistant ridges of a buff, dull gray massive limestone with severe spheroidal weathering. The late Paleocene to early Eocene Garra Limestone uncomfortably overlies the Kurkur and ranges from 60 m to 110 m. The Garra is composed of thick limestone beds with chalk and shale intercalations (Woodward-Clyde Consultants, 1985). In the field area the Garra crops out as alternating massive and thinly bedded limestone with some stromatolites. The Early to Middle Eocene Dungul Formation caps the Sinn El-Kaddab Plateau but was not observed cropping out near the El Kasr. The Dungul is reported to consist of alternating shale and limestone beds and range from 60 m to 127 m (Issawi, 1968; Woodward-Clyde Consultants, 1985).

2.2 MAJOR STRUCTURAL TRENDS

Figure 2.1 displays the location of major structural trends in the Aswan area. The Guinean-Nubian Lineaments are the dominant features in the region and manifest as an east-west transcontinental trend as the Seiyal and Kalabsha faults. Issawi (1978) described these faults as “the most important…fault system in south west Egypt.” El Etr et al. (1982) indicates that these faults have undergone dextral motion and suggest that the east-west fault segments that comprise the Guinean-Nubian Lineaments are the modern manifestations of the basement faults that have not yet coalesced into continuous features.

Major N-S trending Precambrian faults that have been reactivated with dip-slip (Issawi, 1978) as well as sinistral strike slip motion (Abdeen et al., 2000) are also found in the region. These north-south trending faults are much more localized than the Guinean-Nubian Lineaments but have also been repeatedly reactivated with varying motions (Issawi, 1978). According to Woodward-Clyde Consultants (1985) some of these faults may be on the order of ~100 km in length, and Issawi (1978) indicated that none are found west of Darb El Arbain, approximately 32° W. According to Issawi (1968) these north-south faults have steep dips and indicate normal motion on the order of 20 m. A consistent but subdued down to the east escarpment may be observed along the length of these faults. Woodward-Clyde Consultants (1985) note numerous slip-indicators indicate that sinistral motion has occurred along these faults

The two orthogonal fault zones (N-S and E-W) located in the Aswan area have been repeatedly reactivated by far field stresses to accommodate the compression or extension of northeast Africa (Guiraud and Bosworth 1999; Guiraud et al., 2001). These events include long periods of extension punctuated by brief periods of compression (Guiraud and Bosworth 1999; Guiraud et al., 2001; Youssef 2003). The E-W trending Guinean-Nubian Lineaments as well as the N-S trending faults have been shown to have been reactivated during at least two compressional events, specifically the Santonian compressional event, and a late Eocene event (Guiraud and Bosworth 1999; Guiraud et al., 2001).

The "Desert Eye" structures of the region are a collection of 479 spectacularly exposed bedrock structures visible across both the stable and unstable shelf regions of the Western Desert (Tewksbury et al., 2009). The Eyes exposed to the south across the stable shelf represent both structural domes and basins on the order of kilometers in scale. These structures tend to display linear trends that may or may not be associated with the visible trace of a fault.

2.3 STATE OF STRESS

2.3.1 Modern State of Stress. Reflecting the tectonic divisions of Egypt, similar divisions may be drawn concerning the modern state of stress in the region. Two distinct stress provinces are present in the country, divided along 27°N. This division closely corresponds to the division between the Stable and Unstable shelf regions as defined by Youseff (2003). The north is predominantly transtensional in which the stress field is defined by an even mixture of NW-SE and E-W S_{Hmax} alignments, while the south is mainly strike-slip and defined by a uniform E-W S_{Hmax} alignment (Badawy, 2001). The intra-plate stress patterns are attributed to plate boundary forces (Zoback, 1992). This modern E-W alignment of S_{Hmax} as presented by Badawy (2001) is in good agreement with the evidence presented by Bosworth and Strecker (1997) including bore-hole breakouts.

The state of stress in North Africa is locally complicated by the interactions between the Sinai micro plate and the Levant Transform fault. Overprinted structures attributed to both the Dead Sea stress field and the Syrian Arc stress field suggests that both stress fields are present in the region. The Dead Sea stress field is dominated by left-lateral motion along the Levant Transform associated with opening of the Red Sea whereas the Syrian Arc stress field is defined ENE-WSW compression. The dominance of one stress field over the other may be controlled by large earthquakes along the Levant

Transform. The Dead Sea stress field has been found to dominate in pre-seismic periods with the Syrian Arc stress field dominating in interseismic periods.

2.3.2 Paleo State of Stress. Bosworth and Strecker (1997) present findings that indicate that the modern stress field throughout eastern Africa, particularly the Afro-Arabian rift system, has resulted from counterclockwise rotation since the Late Pleistocene but before 125,000 years ago. This rotation resulted in S_{Hmin} oriented approximately N-S. Prior to this rotation, S_{Hmin} was oriented NE-SW. This state of stress may have been favorable for reactivation of the N-S trending faults in the region (Figure 2.4). Bosworth and Strecker (1997) speculate that this change in orientation of S_{Hmin} may be due to either rift related processes or reflect far field stresses affecting the entire continent, citing similar events throughout eastern Africa.

The paleo state of stress in north east Africa as presented by Bosworth and Strecker (1997) may have been favorably oriented to reactivate preexisting faults in the region, particularly the N-S trending faults. This motion would have induced left-lateral motion along the N-S trending faults and right-lateral motion along E-W trending faults (Figure 2.4).

2.3.3 Seismicity. Investigations into seismicity as well as active and potentially active faults in Egypt and the surrounding regions became a priority following the construction of the Aswan High Dam and subsequent formation of Lake Nassar.

This need to understand the hazards associated with local and regional faults has been punctuated by a series of earthquakes in the region including a 5.6M event in 1981 associated with the Kalabsha Fault (Kebeasy et al., 1986; Mohamed et al., 2001; Abdelsalam et al., 2005; Abdel-Monem et al., 2012; Hosny et al., 2013;). Focal mechanisms indicate that the majority of these events are characterized by strike-slip motion or normal motion, with little reverse (Badawy, 2001, Figure 2.5).

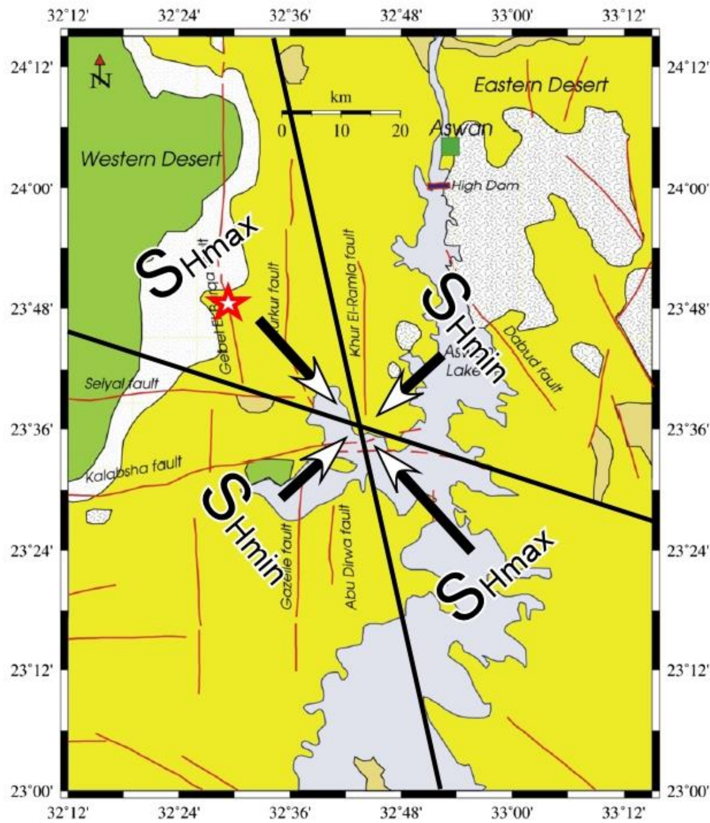

Figure 2.4 Schematic of Early Pleistocene stress-field (Bosworth and Strecker, 1997). The stress-field (solid black) is overlain over the major faults of the region. This stress-field would have been favorable to reactivation of faults oriented parallel to the solid black lines. The red star represents the location of the El Kasr structure. Modified from Deif et al., 2011.

Simpson et al. (1988) defined the seismicity in the Aswan region as being reservoir induced. Unsurprisingly, detailed studies of seismicity in the region have reported that approximately 95 percent of the seismicity in the Aswan region is located within a rectangle (Figure 2.6 and Figure 2.7) bounded by 23.4 N, 23.8 N, 32.4 N, 33.0 N

(Abdel-Monem et al., 2012). This zone includes the much of the northern portion of the lake as well as the intersection of the N-S and E-W trends (Figure 2.6).

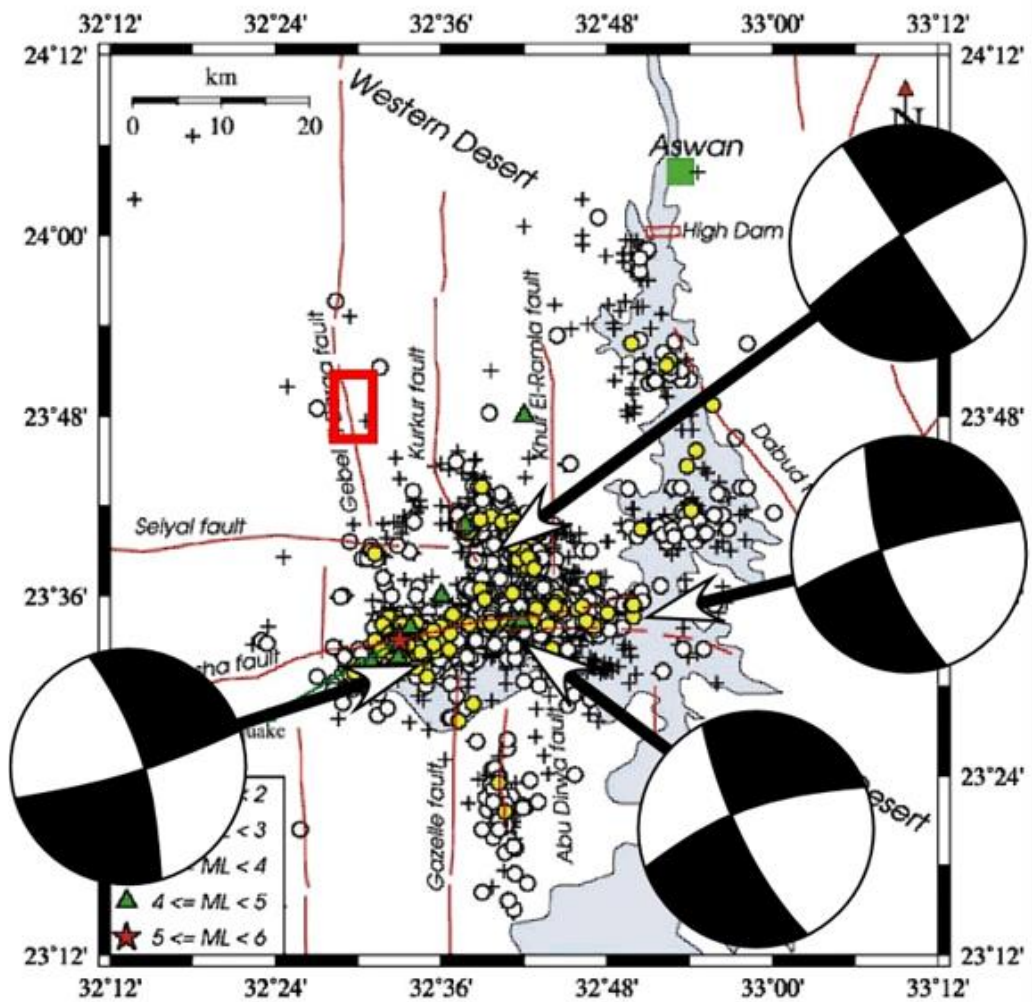

Figure 2.5 Map of the Aswan area with major faults and earthquake epicenters from 1981-2010. The location of the El Kasr marked by the red box. Modified from Deif et al., 2011. Focal mechanisms from El-Khashab et al., 1991 and Hosny et al., 2013.

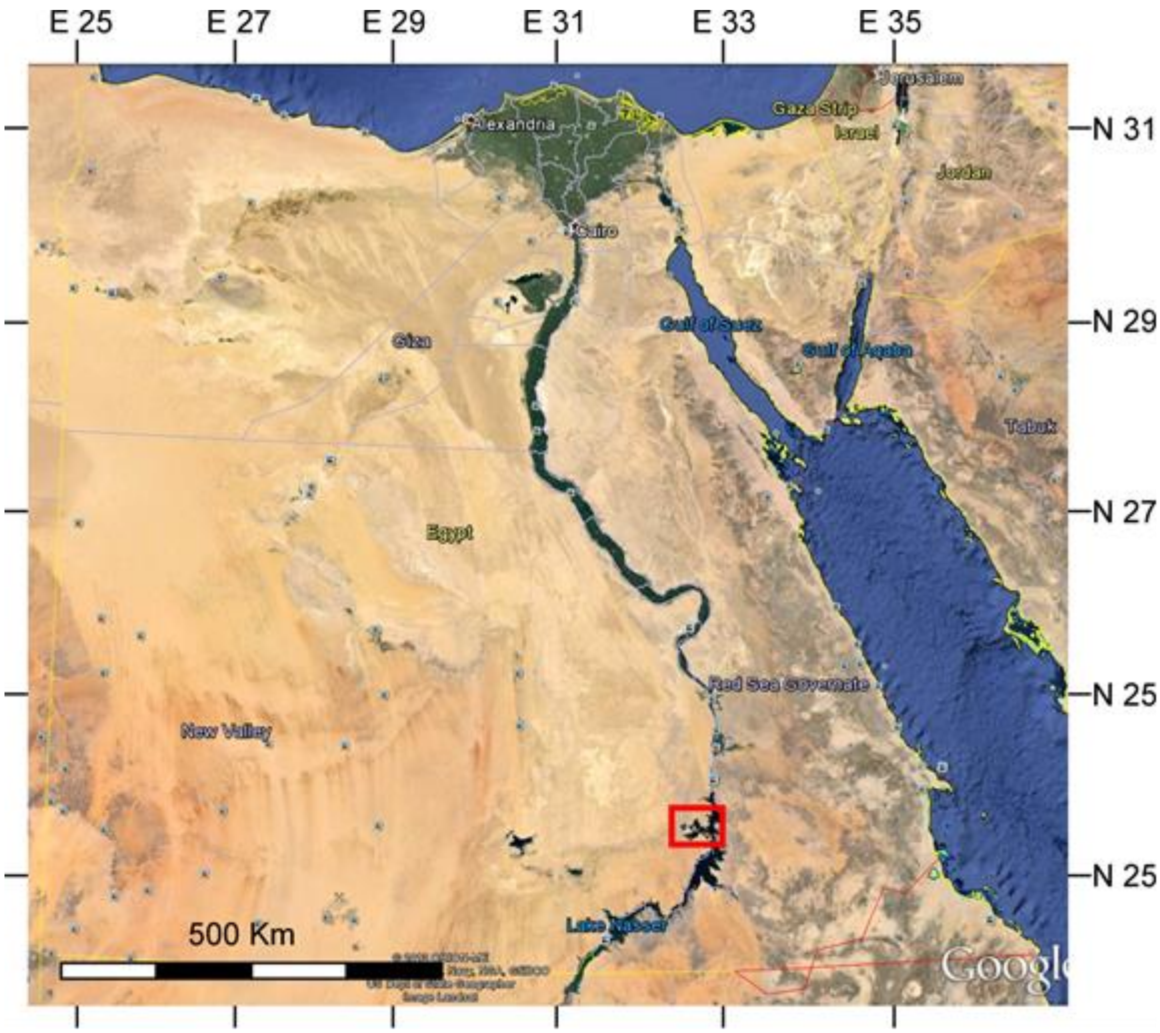

Figure 2.6 Location of 95% of Aswan seismicity. 95% of the seismicity in the Aswan region is within the red box.

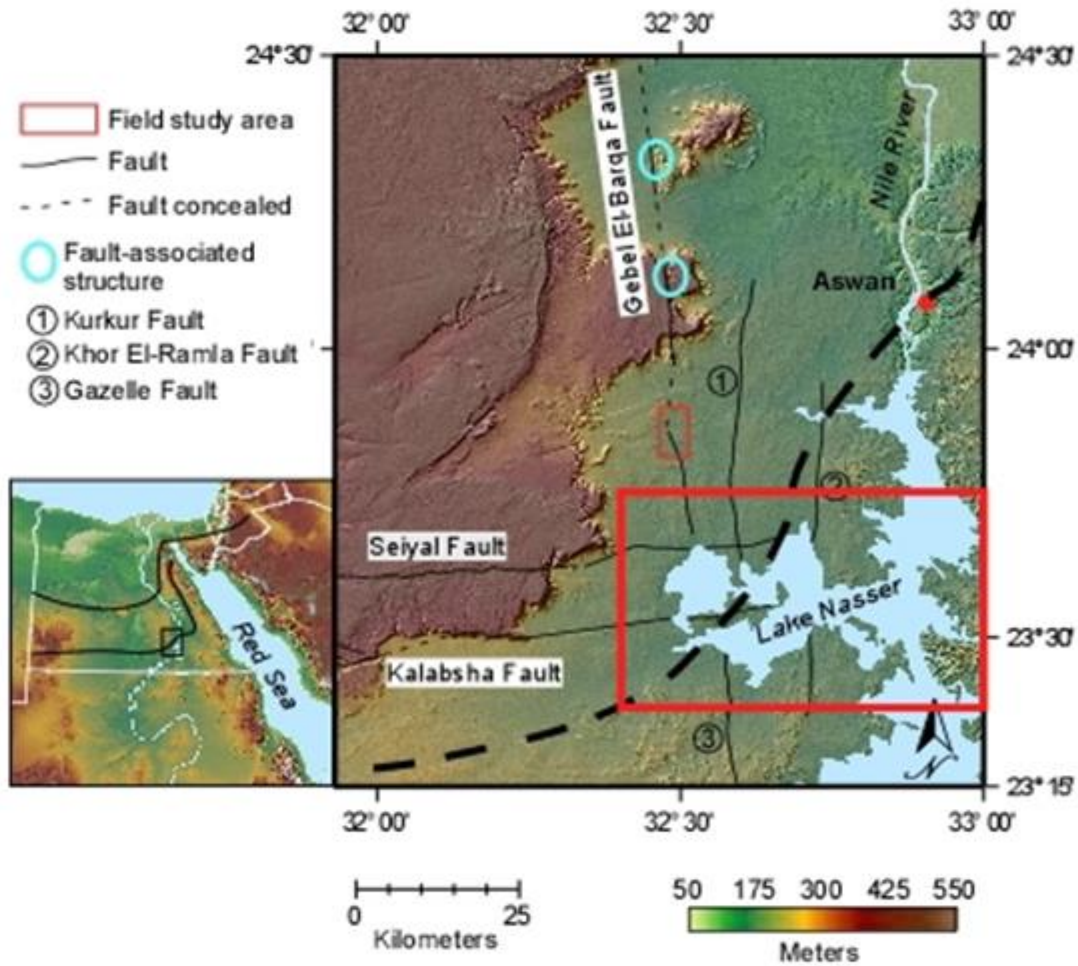

Figure 2.7 Intersection of N-S and E-W fault trends in the Aswan area. The large red box indicates the location of approximately 95% of the seismicity in the Aswan region (Abdel-Monem et al., 2012).

Woodward-Clyde Consultants (1985) and Simpson et al. (1986) found the Kalabsha, Seiyal, Abu-Dirwa, Gazal, Kurkur, and Gebel El-Barqa faults to be “potential seismic sources” and “significant to the High Dam”. Among these faults, the Kalabsha fault is deemed the most seismically active in the region (Mekkawi et al., 2005;Adbel-Monem et al., 2012) The intersection of the N-S and E-W trending faults is characterized by seismicity along the Kalabsha (Mekkawi et al., 2005; Abdel-Monem et al., 2012). It is important to note that the trace of the Kalabsha fault is present along the bottom of lake Nasser (Mekkawi et al., 2005) and shallow seismic events have been shown to be induced by water levels within the lake (Abdel-Monem et al., 2012).

Locally Aswan is considered seismically active with the activity related to local (Lake Nasser), regional (Red Sea rifting), and global (African-Eurasian collision) stresses. Though the Gebel El-Barqa fault is considered active (Woodward-Clyde Consultants, 1985; Simpson et al., 1906) the activity along the fault has been M1-M3 and occurred south of 24.00° N. These observations along with the unfavorable state of stress for reactivation of the Gebel El-Barqa suggest that most of the activity along the fault is reservoir induced (Figure 2.8)

Seismicity in Egypt is not limited to the Aswan area. The Aswan region actually ranks quite low in integrated seismic risk map of Egypt (El-Araby and Sultan, 2000). Greater seismic risks are found in the northeastern portion of the country near Cairo and the Gulf of Suez. The seismicity in this region is attributed to the rifting within the Red Sea as well as sinistral motion along the Levant-Aqaba trend.

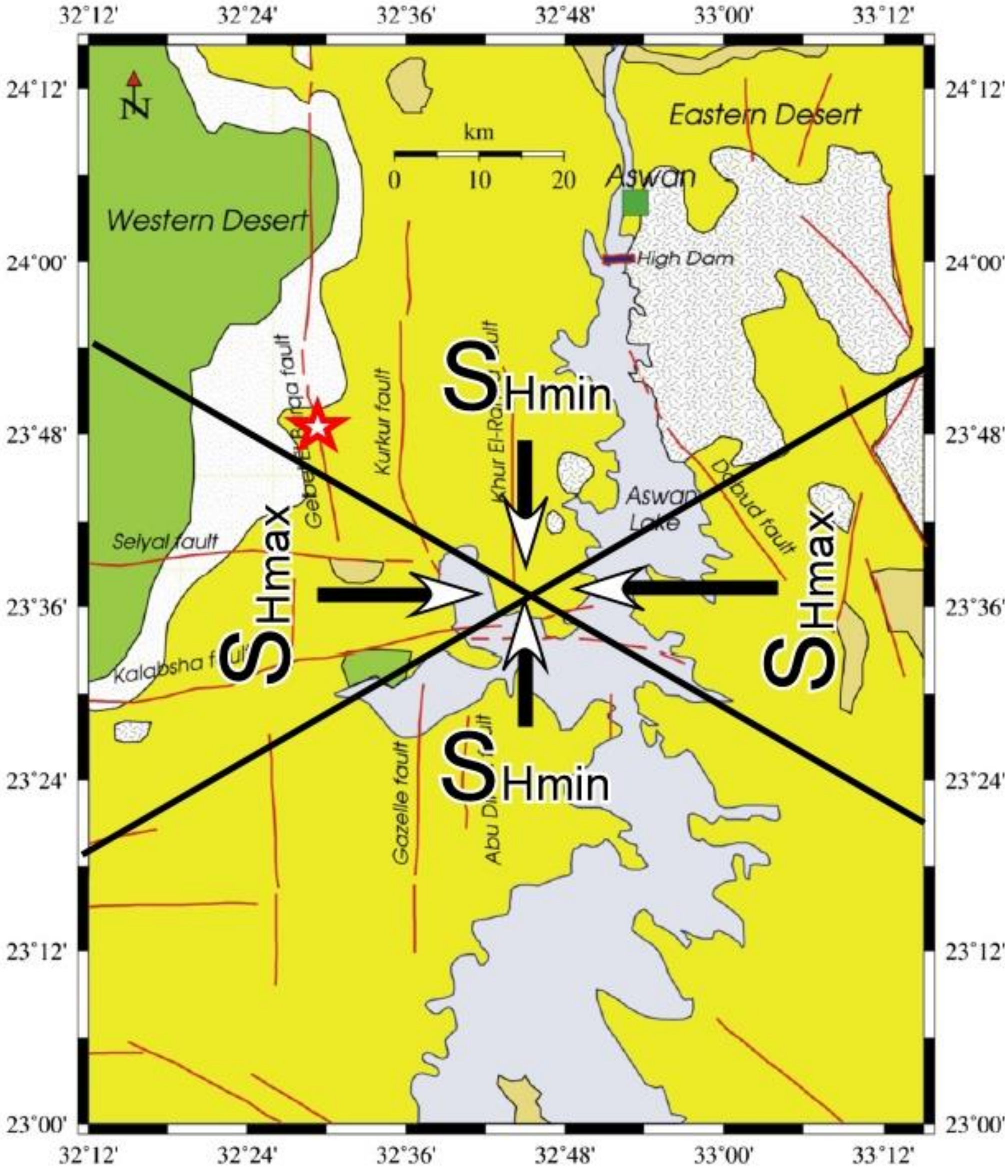

Figure 2.8 Schematic of modern stress-field (Bosworth and Strecker, 1997). This stress-field would be favorable to reactivation of faults oriented parallel to the solid black lines. The red star represents the location of the El Kasr structure. Modified from Deif et al., 2011.

3. METHODS

Analyses of remote sensing images and geologic field investigations has allowed for a three dimensional investigation of the El Kasr structure. Geologic maps were created using imagery from Google Earth, field work, and the results of previous mapping in this area (Issawi, 1968; Conoco, 1981; pers. comm., Tewksbury and Hogan 2012). The field mapping investigation, conducted by the author over three days, targeted high priority areas based upon the Google Earth imagery analysis for collection of structural data and conformation of lithological and structural contacts in the field. Analysis of ASTER (Advanced Spaceborne Thermal Emission and Reflection Radiometer) data was then integrated into completion of the geologic and structural maps for the El Kasr structure.

3.1 GOOGLE EARTH

Google Earth's highest resolution of 1m/pixel allowed for detailed mapping of the study area following the procedures discussed in Tewksbury et al. (2012). Lithological differences were inferred from differences in color and texture. Dip direction of units was determined using rule of v's and sun-shadow relationships (Appendix A). This data revealed that the El Kasr is a composite structural basin deforming multiple stratigraphic units. Faults were mapped by identifying offsets and truncations of stratigraphic units and their contacts. The most striking truncation visible in Google Earth imagery is that of the Garra Formation along the western edge of the structure (see Figure 2.2 where the Garra Formation. is distinctly blue-white in Google Earth imagery). Upon completion of "Remote Mapping" of the structure, several distinct units were identified including:

Quaternary Alluvium, Garra Formation, Kurkur Formation, and the Dakhla Formation. Interbedded members were visible within many of these units. Multiple faults were identified as well, including a bounding fault to the west, and multiple offsets to the southeast. These results were compared with previous geologic studies in the region.

Using dip data and contacts mapped in the field, as well as in remote sensing data, the thickness of units was calculated using simple trigonometric relationships (Davis et al., 2012). These thicknesses were compared to previously recorded thicknesses including drill cores and measured sections. Figure 2.3 shows the stratigraphic column of the study area. Previously recorded thickness ranges are included as well as the thickness of each unit as used in the construction of the various cross-sections.

3.2 FIELD INVESTIGATION

A brief but intense three day field investigation of the structure and immediate surroundings was conducted in the winter of 2011-2012. Based upon previous studies of the structure by other authors and members of this team, Drs. Hogan and Tewksbury (Issaiw, 1968; Woodward-Clyde Consultants, 1985; pers. comm., Tewksbury and Hogan 2012) and analysis of Google Earth imagery, work initially focused on constraining the relationship of the flat-lying units to the east of the structure and the nature of the subtle ridges along the eastern side of the structure. While in the field other features were identified and studied including drag folds, and a ridge of the Dahkla Formation. in the northeast that was discordant to the main trend of the structure.

3.3 ASTER

Advanced Spaceborne Thermal Emission and Reflection Radiometer (ASTER) data of the study area were obtained from the USGS database. ASTER data is 15 m resolution in the VNIR bands and 3 0m resolution in the SWIR bands. Each tile downloaded from USGS is 60 km x 60 km, and was cropped to isolate the structure. Each tile was layer stacked and in order to avoid redundancies in the data the Optimum Index Factor (OIF) was determined. The OIF is a statistical value for an image that is calculated using the standard deviation and variance of each band in order to determine the band combination that reduces redundancies in the image. The optimum band combination was found to be 4-2-1, resulting in the image seen in Figure 3.1.

Outcrop scale study of the structure was performed using both Principal Components Analysis (PCA) on the ASTER data (Figure 3.2) and OIF images. Various band math techniques were attempted in mapping the units as well. Figure 3.3 was created using band math equations sensitive to limestone, dolomite, and ferric iron. In Figure 3.3 (band 7 + band 9) / band 8 corresponds to limestone which appears as red. In the same figure (band 6 + band8) / band7 corresponds to dolomite which appears as blue, while band2 / band1 corresponds to units rich in ferric iron which appears as green (Rowan and Mars, 2003).

Additional remote sensing analysis focused on the Gebel El-Barqa fault trace. Various structures found along the trace of the Gebel El-Barqa fault can be seen in the ASTER image in Figure 3.4. These structures have not been studied in depth but appear to be smaller than the El Kasr and have different characteristics.

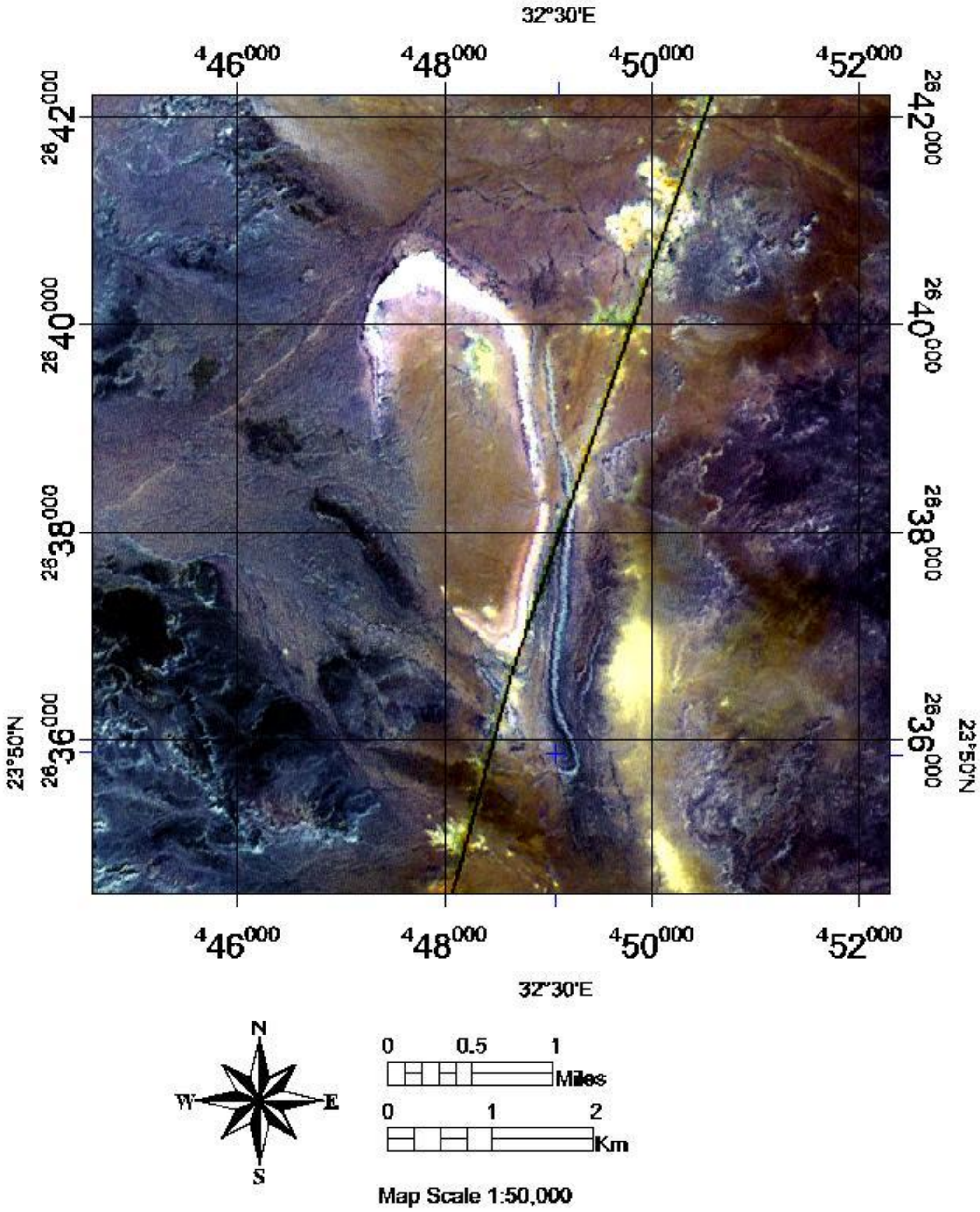

Figure 3.1 ASTER OIF image of the El Kasr structure. The resistant Garra is easily identified by the bold white color. Kurkur is visible as light blue resistant ridges to the east and south.

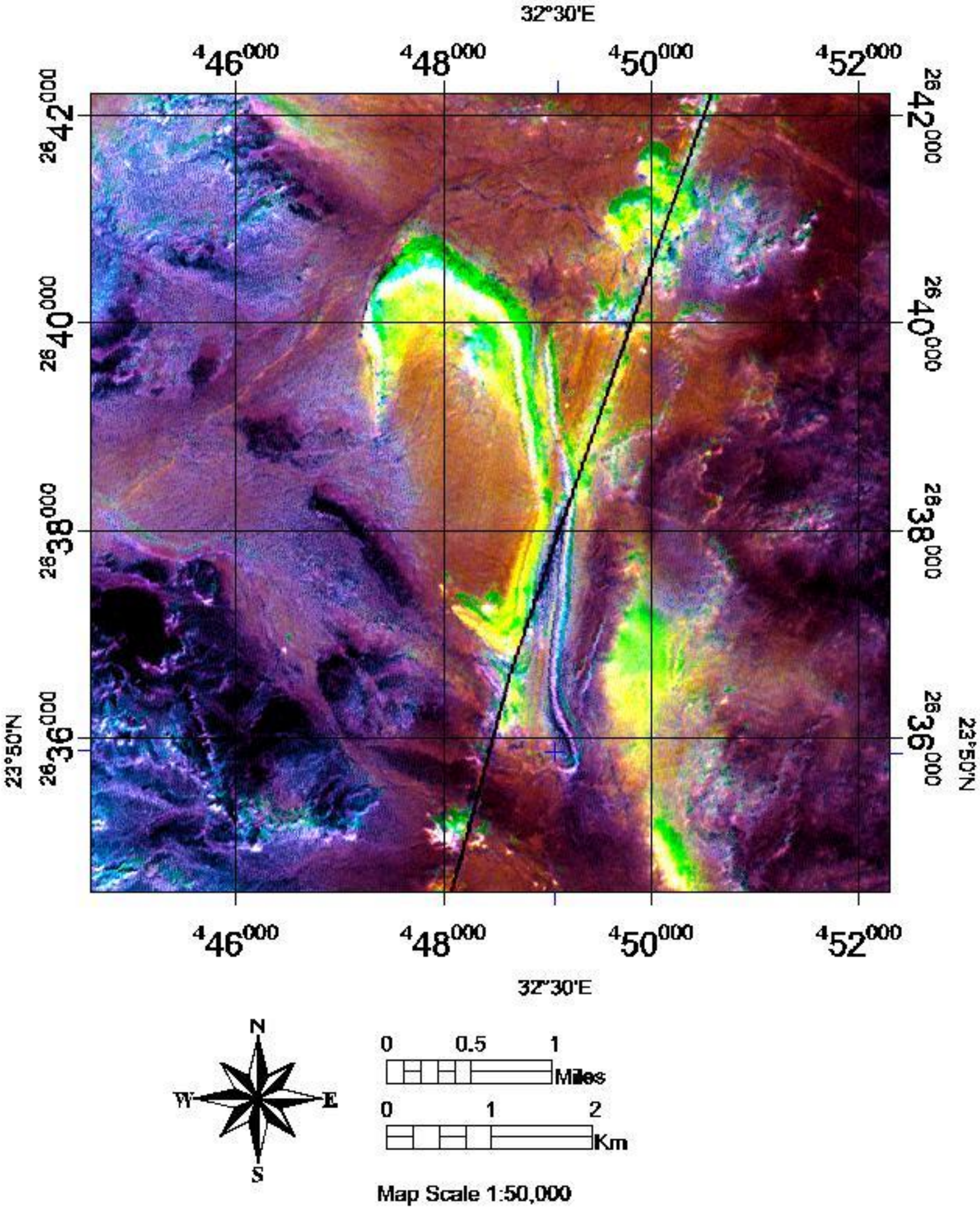

Figure 3.2 Principal Components Analysis image of the El Kasr. The structure is easily identified by the bold green and yellow Garra Formation.

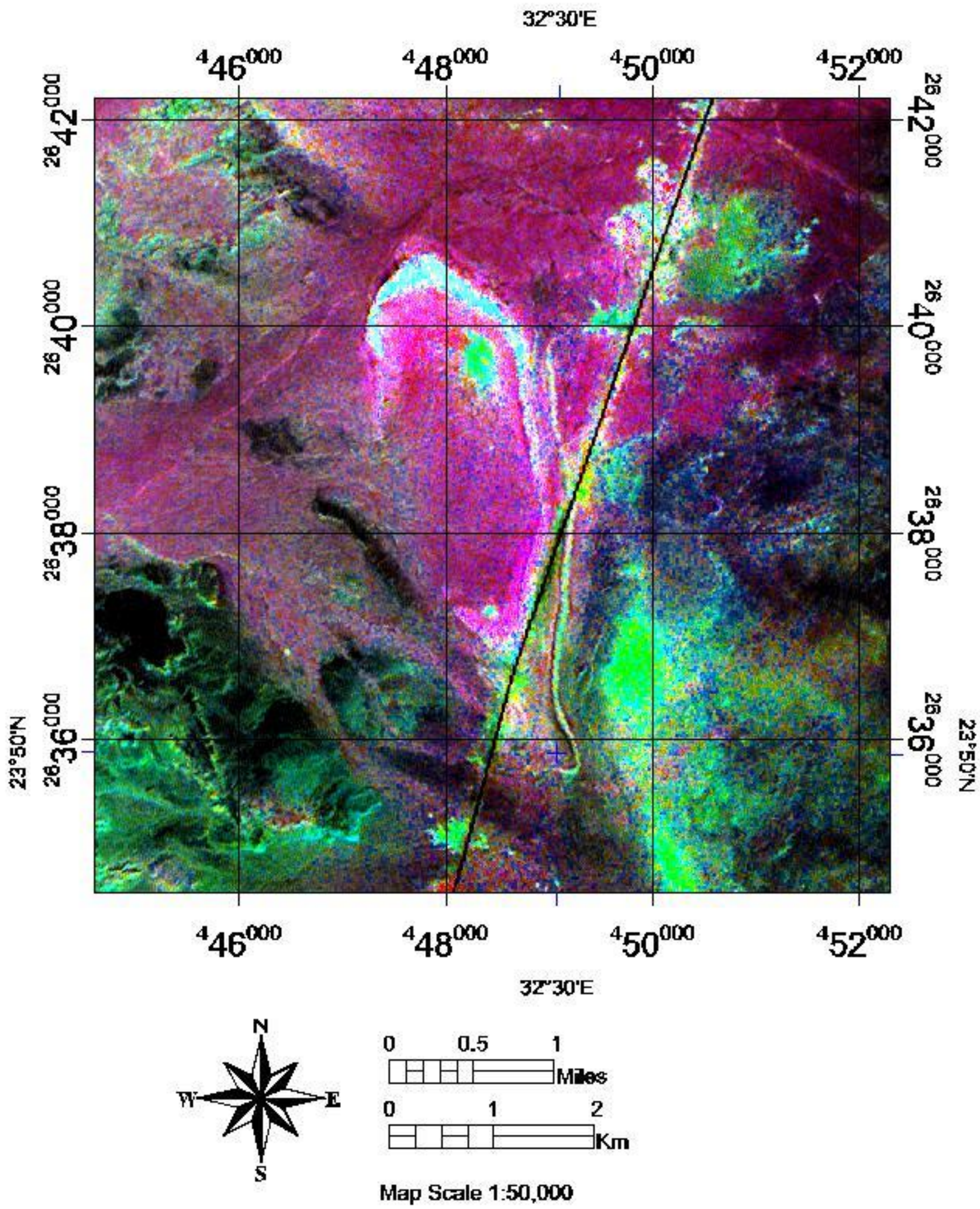

Figure 3.3 Band math image of the El Kasr. Red corresponds to limestone, green to ferric iron, and blue to dolomite. The alluvium appears as a diffuse red and purple reflecting the carbonate nature of the plateau.

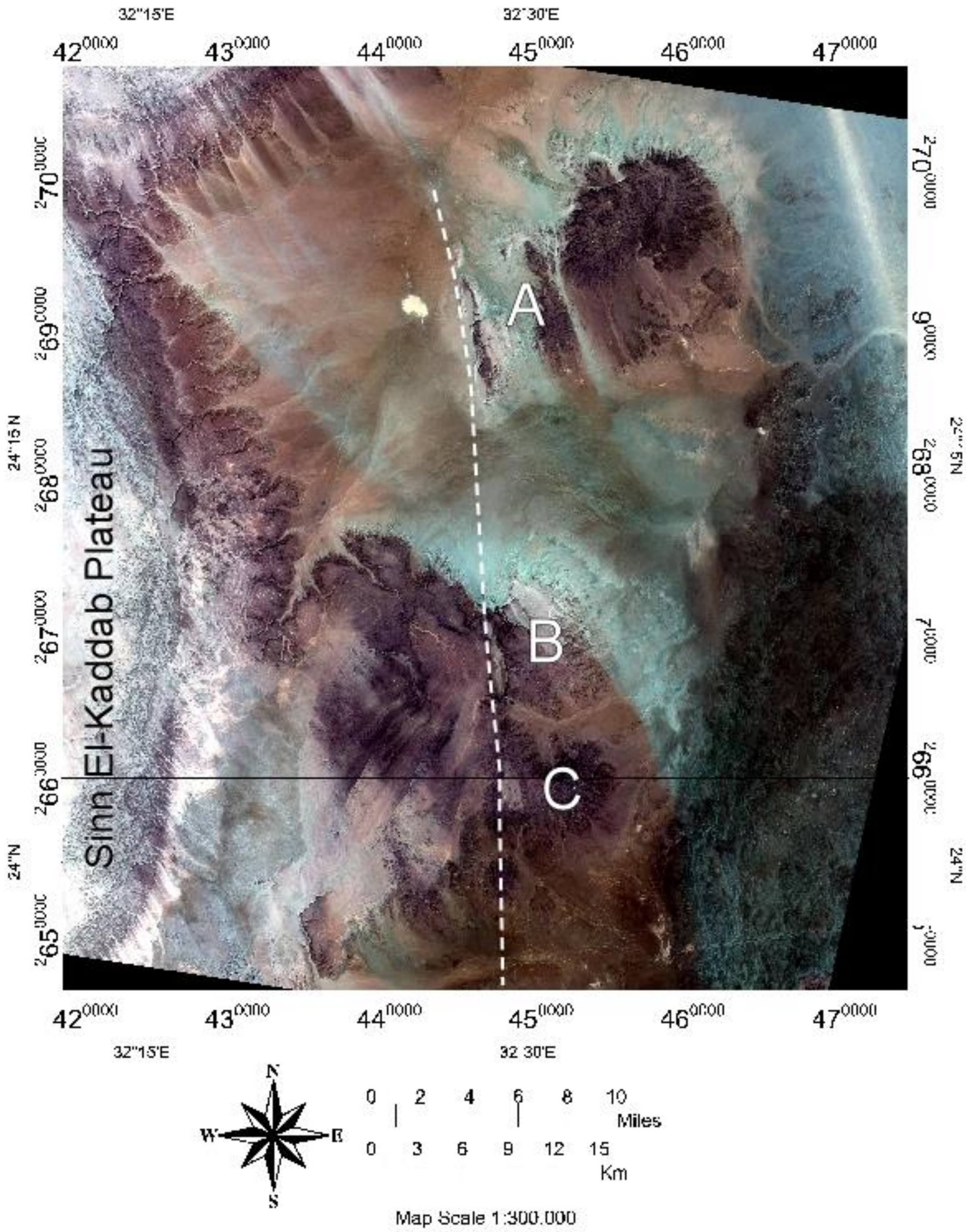

Figure 3.4 ASTER tile north of the El Kasr. The trace of the fault is marked by the occurrence of a number of structures along its length. Details concerning these structures are found in Appendix D.

4. RESULTS

4.1 REMOTE SENSING

The El Kasr structure was investigated with ASTER data (processed using Optimum Index Factor, Principal Component Analysis, and Band Math), Google Earth imagery, and supplemented by previous studies (Issawi 1968; Woodward-Clyde Consultants, 1985; pers. comm., Tewksbury and Hogan 2012) and maps (Conoco, 1981) of the region. Color differences observed in these images are a good indication of differences in lithology (Rowan and Mars, 2002; Gomez et al., 2004) as there is little to no vegetation present. Remote sensing characteristics of the geologic formations as well as field observations are presented in Table 4.1.

Using these characteristics geologic interpretations were constructed for each remote sensing image (Figures 4.1, 4.2, 4.3, and 4.4). Conformable stratigraphic contacts between formations were identified by subtle to abrupt changes in color and/or texture between semi-parallel bands of color evident within the ASTER and Google Earth images (Figures 4.1 and 2.2). Subtle to gradual color changes along an irregular to diffuse boundary and/or pinching out of stratigraphic units are interpreted as unconformable stratigraphic contacts, for example between different ages of alluvium (e.g., the alluvium in the northeast of the ASTER image in Figure 4.1).

Table 4.1 Remote Sensing and field characteristics of lithologic units

Unit	Age	Google Earth Characteristics	ASTER 4-2-1 Characteristics	Characteristics in the Field	Thickness Range	Calculated Thickness*
Alluvium	Recent	Smooth to braided appearance. Diffuse. Variable color	Smooth to braided appearance. Diffuse, variable color	Unconsolidated, poorly sorted	N/A	N/A
Dungul	Early to Middle Eocene	Smooth, medium to light tan	Not seen in study	N/A	60-127m	N/A
Garra	Late Paleocene to Early Eocene	Speckled white to light blue with interbedded darker blue bands	Bright white, some darker interbedded members	Massive tan limestone	60-110m	96 m
Kurkur	Paleocene	Buff uniform tan along prominent ridges, darker brown near nose	Light blue	Massive gray limestone, severe spheroidal weathering, "spackled" appearance	11-57.2m	67m
Dakhla	Late Cretaceous	Dark brown to light gray brown. Lighter patches possibly exposed calcareous members	Blue to purple	Calcareous sandstone, poorly sorted, oyster fragments, rip-up clasts, buff tan weathered surface, rusty orange fresh surface	39-155m	Minimum Thickness 221 m
Nubian	Early Cretaceous	Mottled light tan	Not seen in study	N/A	0-592m	N/A
Basement	Pre-Cambrian	Dark gray to brown. Dull. Cross-cut by drainage that appears to sxploit faults/joints	Not seen in study	N/A		N/A

*Calculated thicknesses determined through mapped contacts and trigonometric relationships (Davis, et al., 2012; Issawi, 1968; Woodward-Clyde Consultants, 1985).

The attitude of the bedding locally can be interpreted using the rule of v's. The attitude of the formations associated with the El Kasr structure indicates this is a structural basin. The color changes in the region surrounding the El Kasr structure follow closely the irregular topographic steps consistent with these formations being nearly horizontal. This change in orientation is evident in the Google Earth imagery (see Figure 4.4) where the Dakhla Formation. east of the structure is near horizontal and the Garra and Kurkur formations can be seen dipping toward the structure. Structural fault contacts are inferred for abrupt truncation of stratigraphic contacts and juxtaposition of linear resistant bedrock ridges with distinctly different strike lines. These were later confirmed by field studies. The western flank of the structure is clearly truncated in the ASTER and Google Earth images (see Figures 4.1-4.4). Juxtaposed and truncated ridges are evident in these images (particularly to the east and northeast of the structure) and shown as faults in the corresponding geologic interpretations.

4.2 STRATIGRAPHY

The oldest and most pervasive unit studied in the field was the Dakhla formation. This formation displayed a variety of characteristics consistent with those reported by Issawi (1968) and Woodward-Clyde Consultants (1985). The flat-lying Dakhla to the east consisted of fine grained laminated sandstone containing some pebbles and shell fragments. Also observed were massive well sorted, well cemented sandstone members containing rip-up clasts above, giving way to a shalely member below (Figure 4.5 Location UTM 36Q 449605.9 m E 2638374.12 m N).

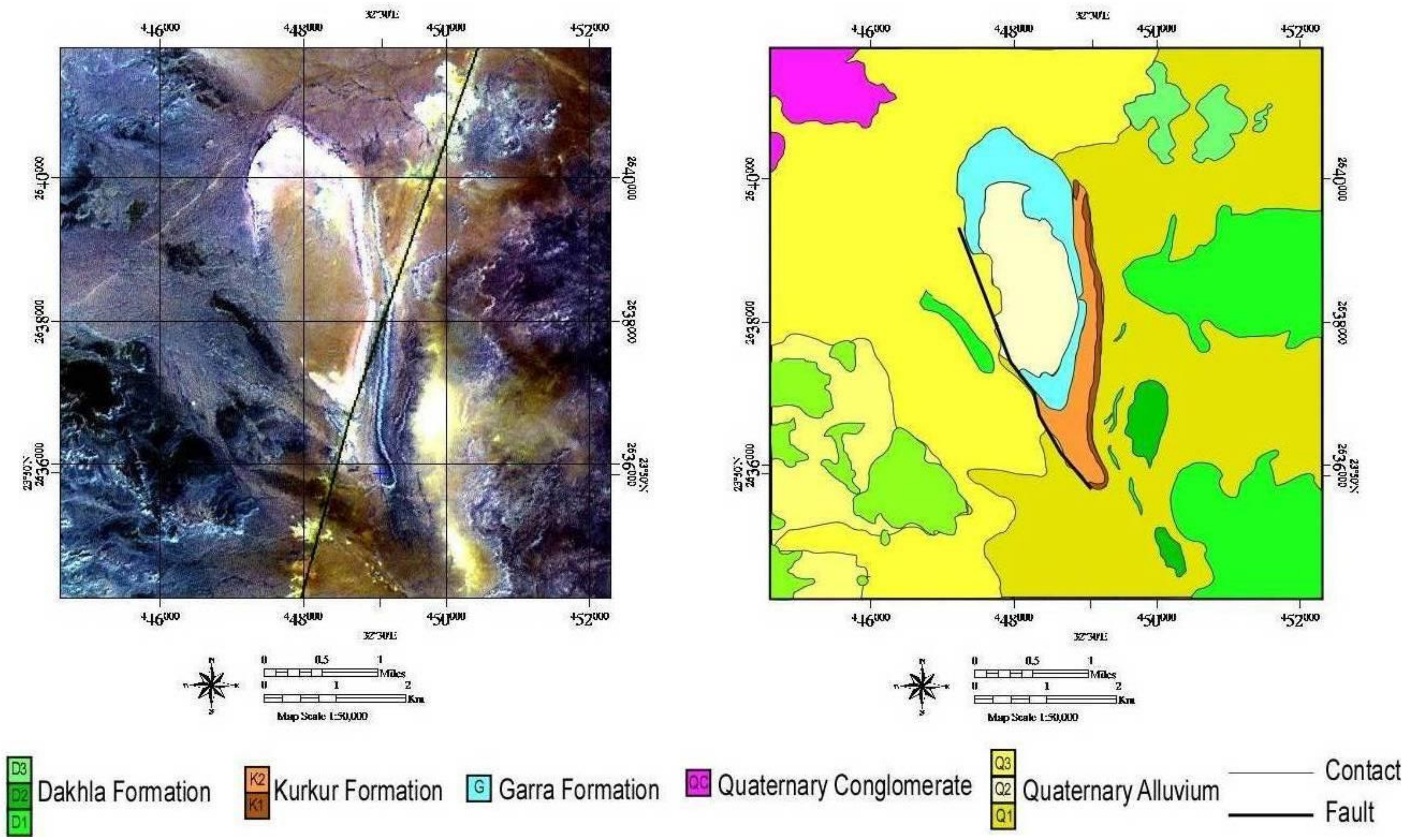

Figure 4.1 4-2-1 image of the El Kasr with geologic interpretation.

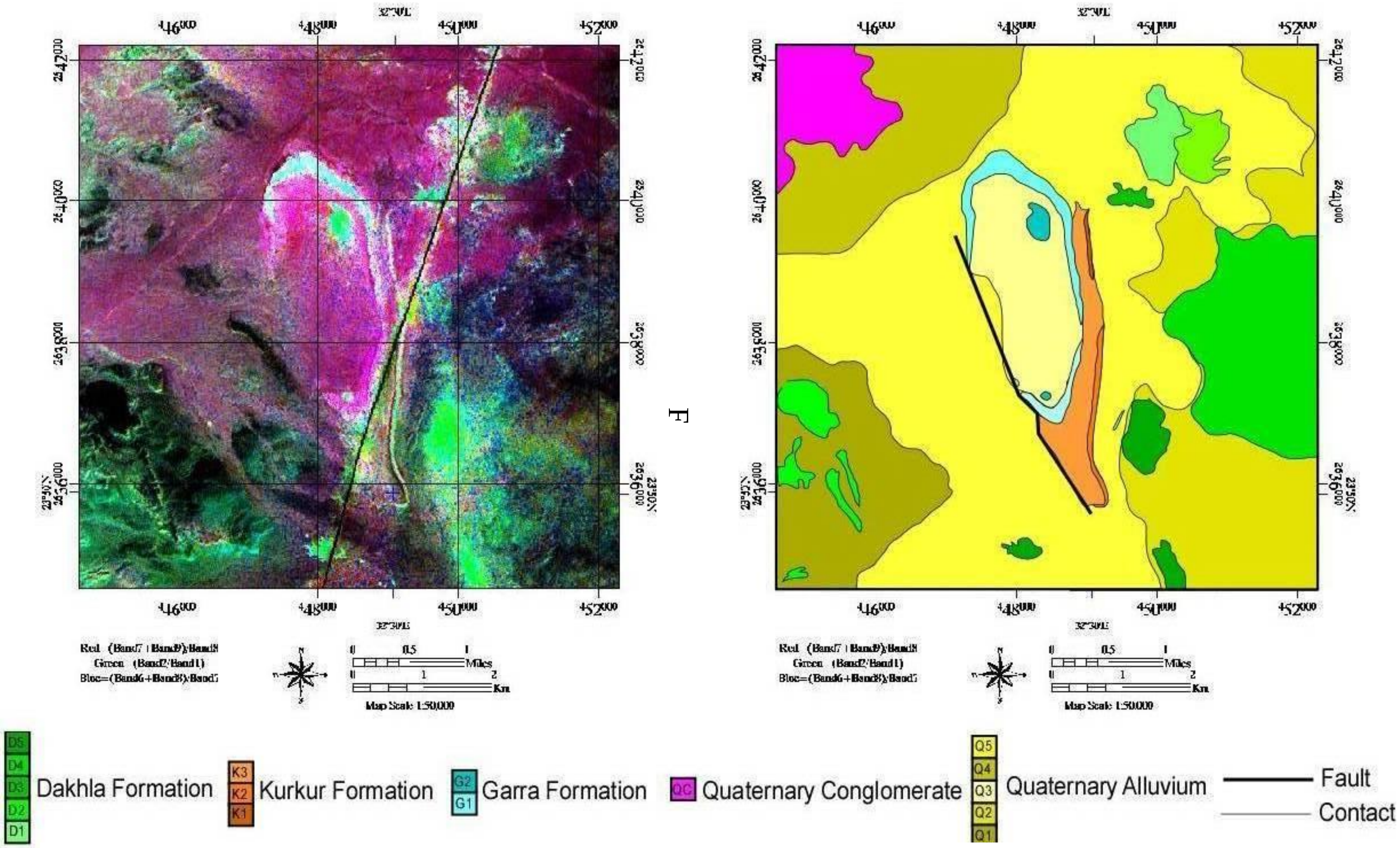

Figure 4.2 Band math image with geological interpretation.

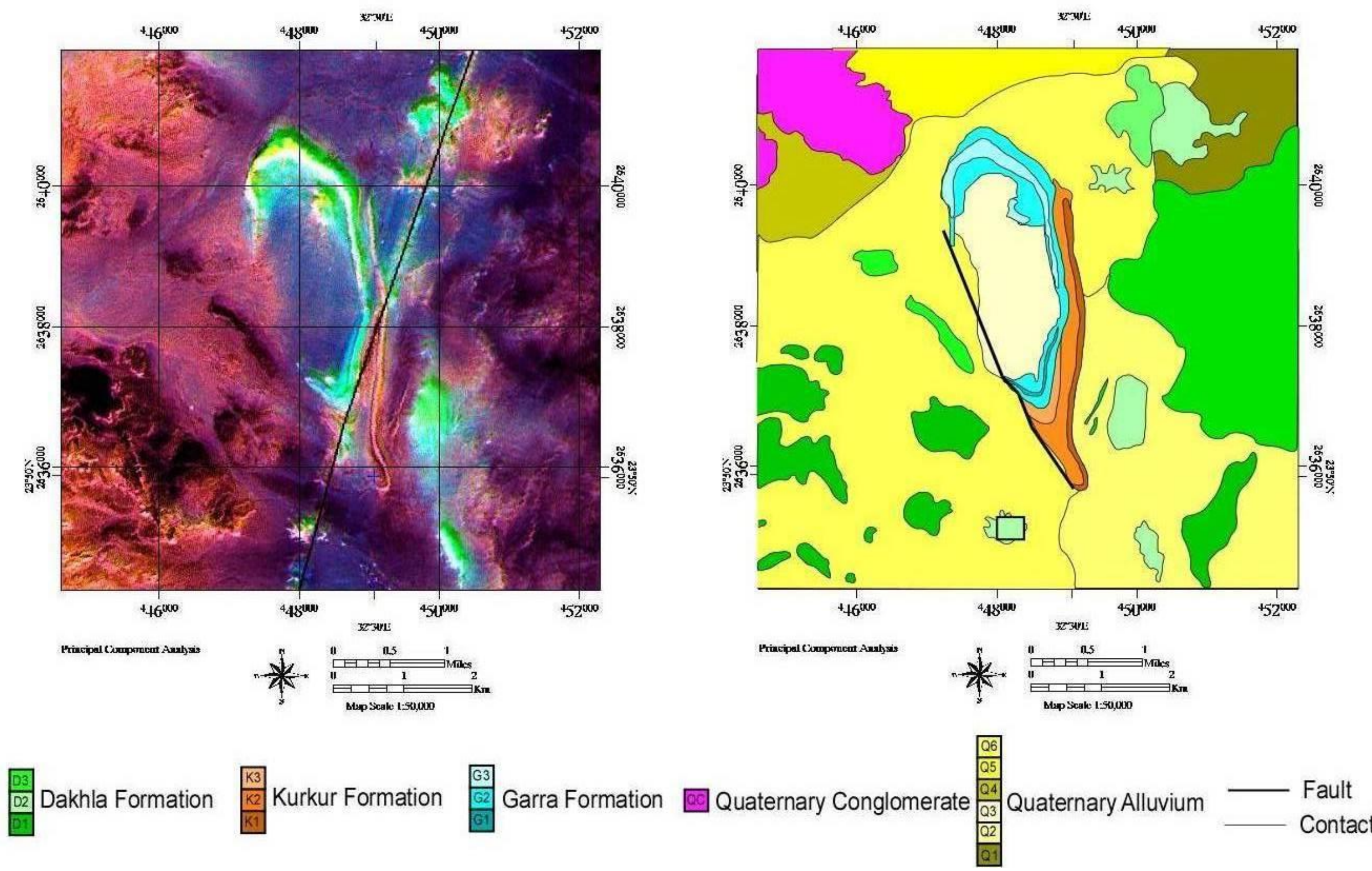

Figure 4.3 Principal Component Analysis image with geological interpretation.

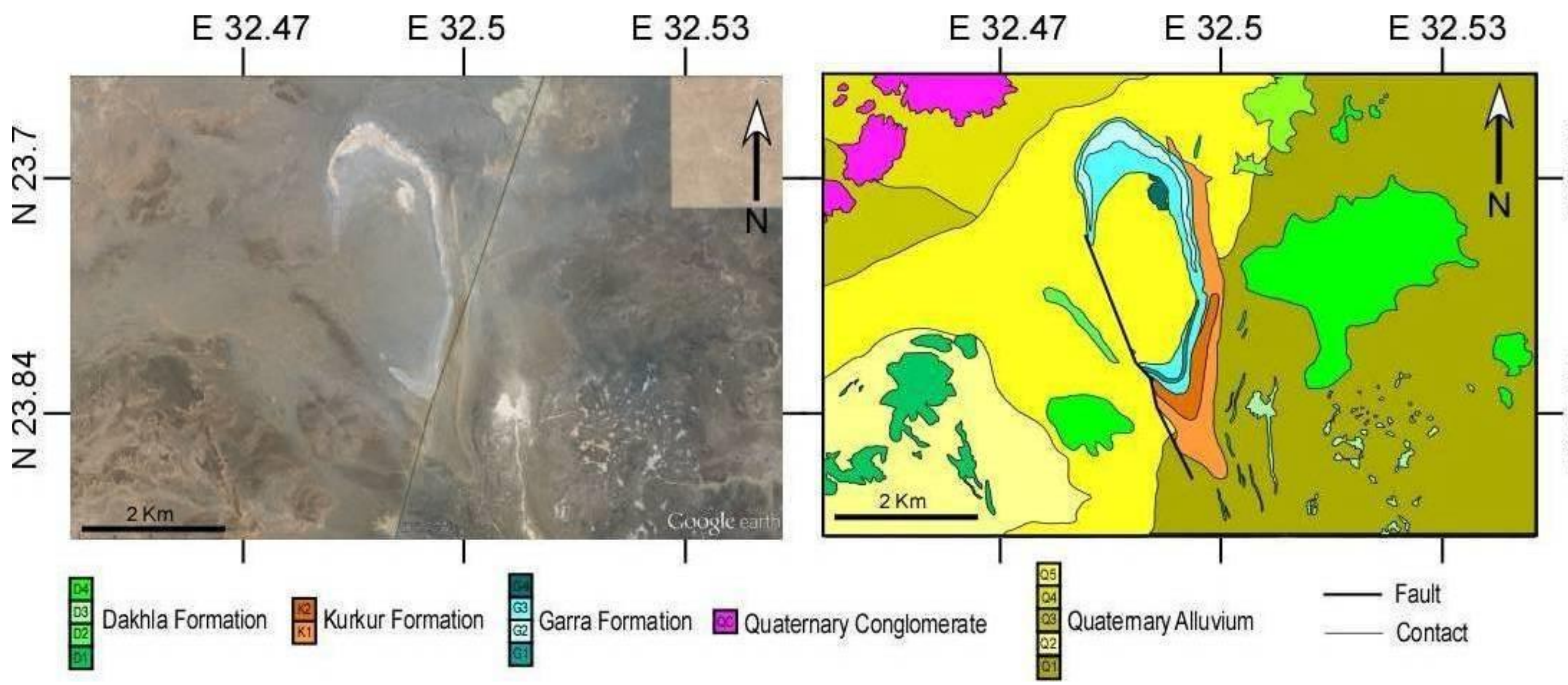

Figure 4.4 Google Earth image of the El Kasr structure with a geological interpretation.

To the south and east of the structures, the ridges seen in Google Earth imagery were identified as being the Dakhla Formation as well (Figure 4.4). These ridges are composed of the clean, well cemented sandstone members within the Dakhla and displayed moderate dips (~25°). It is possible the interbedded shale members of the Dakhla are present between the more resistant ridges. To the north and south of the structure, the Dakhla Formation cropped out as clean, well sorted, fine grained sand that was well cemented with calcite.

The Kurkur Formation is a massive fossiliferous limestone and prominent ridge forming unit (see Figure 4.6, UTM 36Q 449215.34 m E 2638503.93 m N). The unit appears as a dull gray and has a "spackle" appearance due to the severity of the erosion caused by wind. The unit also displays well developed spheroidal weathering, thereby making primary structures difficult to identify. In the north the Kurkur Formation dips toward the structure at a moderate angle (~25°) while in the south, in the smaller basin, it displays a range of dips (<10°-~25°).

Much of the northern basin is defined by the prominent ridge-forming Garra formation. The Garra formation is a gray to white, dominantly massive limestone interbedded with sparse, thinner and less resistant chalk, marl, and shale intercalations. In this region the Gara formation typically has dips of ~25°.

4.3 STRUCTURE

As seen in Figures 4.1-4.4, the El Kasr is a composite basin cut by a well constrained fault zone to the west. East of the structure the Dahkla Formation transitions from moderate dips (~32 to the west) to horizontal, from west to east. This constrains the folding in the eastern portion of the structure.

Figure 4.5 Field photo of the Dakhla Formation. The more massive sand rich unit is visible above the mud rich shale. To the left a hammer is seen for scale.

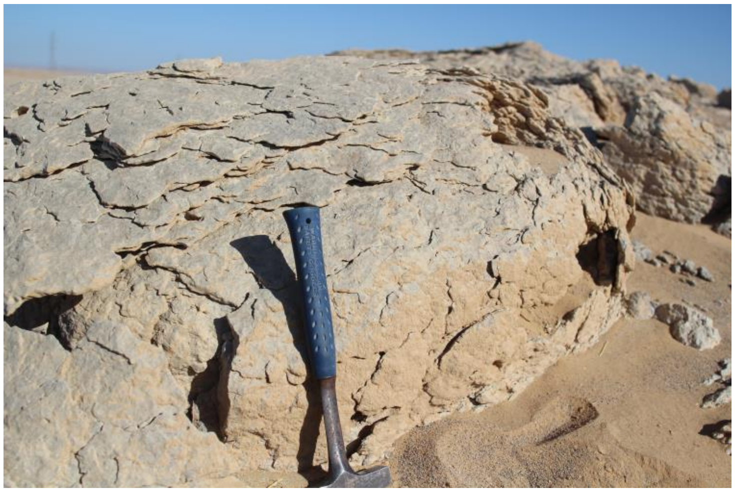

Figure 4.6 Field photo of Kurkur Formation. Evident is severe spheroidal weathering. Rock hammer is visible for scale

Similar relationships are seen to north and south, though alluvium is found in a strike valley between the ridges of the Kurkur Formation and the ridges of the Dakhla

Formation associated with the structure. To the west the orientation of the Dahkla Formation adjacent to the structure is unknown due to poor exposure. The Dakhla Formation seen on the scarp of the Sinn El-Kaddab Plateau reveals that the unit is flat-lying to the west (Figure 4.7).

4.3.1 Stereographic Analysis. Folding associated with the El Kasr structure was investigated by stereographic analysis. The geometric properties of each fold of the structure were determined through analysis of pairs of adjacent structural domains. Domains were defined by the attitudes of the rotated bedding and the location of structural elements (i.e. Fold axes) in such a way that the strike and dip data of each domain was consistent. Figure 4.8 displays the various domains into which the structure was divided for stereographic analysis (see Table 4.2). These divisions of the structure into structural domains allowed for stereographic analysis through the construction of Beta Diagrams.

These Beta Diagrams were constructed by plotting the poles to planes of adjacent domains using Stereonet 8 (Allmendinger et al., 2012). Best fits were then found to approximate each limb, allowing for the determination of the inter-limb angle as well as the strike and dip of the axial planes and trend and plunge of the hinge lines.

4.3.1.1 Major folds. The El Kasr structure is defined by a series of synclinal folds that share similar fold axial surfaces (345/89-158/89) and inter-limb angles (142-162). The northern basin is defined by two folds. The northern fold is defined by domains 1 and 8 while the southern fold is defined by domains 2 and 7. The southern basin is similarly defined by a pair of folds. The northern fold is defined by domains 3 and 6 while the southern. Each of these four folds defining the structure has a steeply dipping fold axial surface that varies in strike by 7° (Table 4.2). These major folds are classified as upright (due to steeply dipping fold axial surfaces) and subhorizontal (due to low plunge values) with the exception of the fold defined by the domains 2 and 7, which exhibits a slightly higher plunge value of 12 and is therefore gently dipping (Fleuty,1964; Figure 4.9).

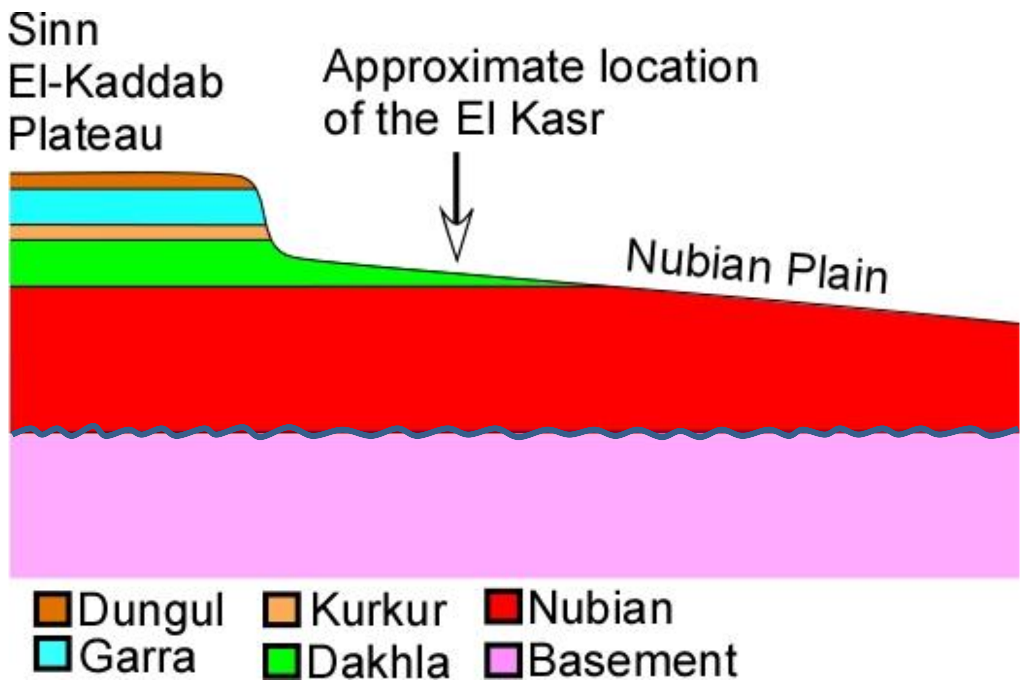

Figure 4.7 Schematic of relationship between stratigraphy and geomorphology. Slope of the Nubian Plain is exaggerated for purposes of visualization; The Dungul is seen capping the Sinn El-Kaddab, the horizontal nature of the stratigraphy is visible along the scarp of the plateau. The gentle dip of the Nubian plain exposes both the Dahkla and Nubian.

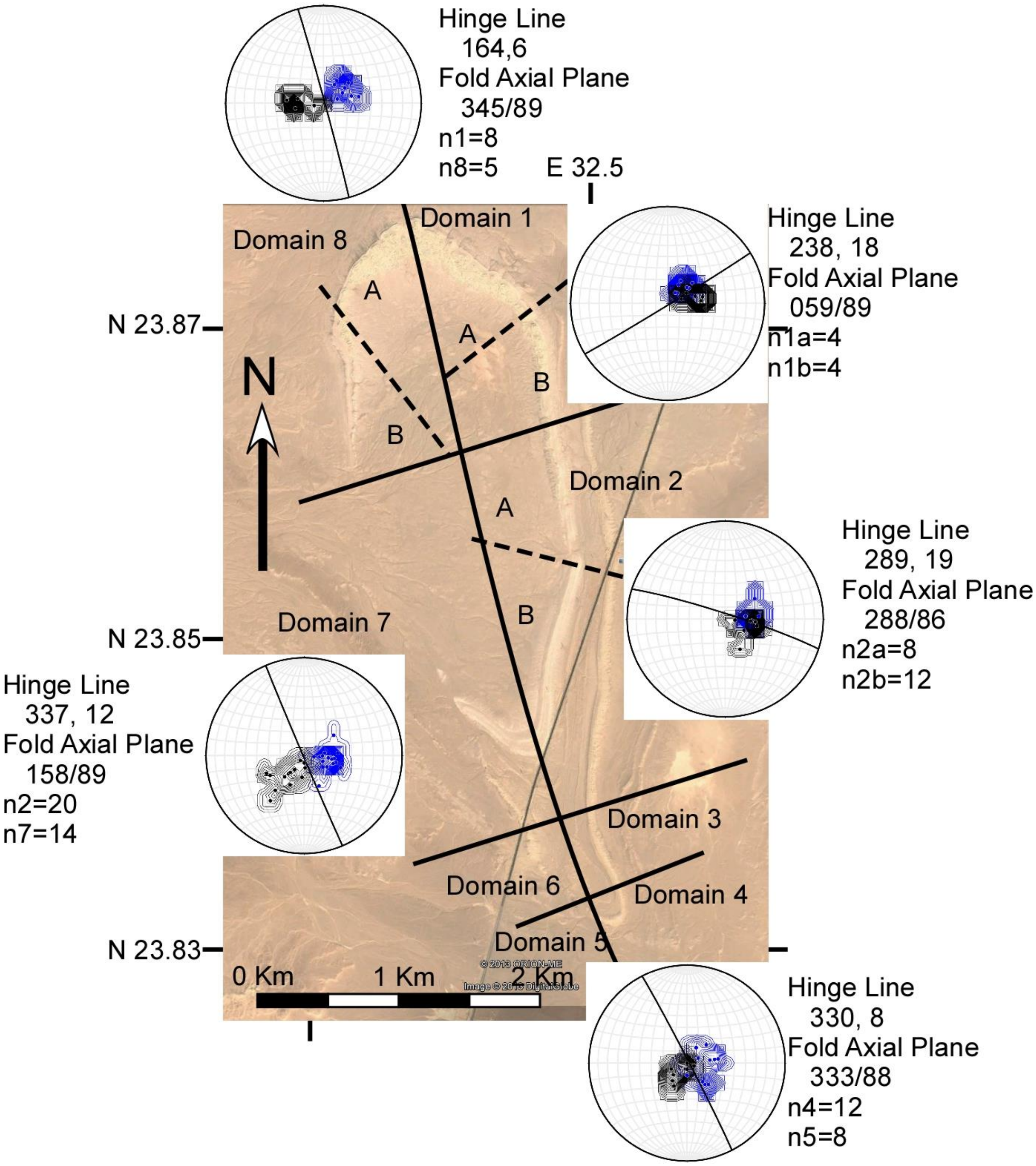

Figure 4.8 Structural Domains of the El Kasr. Select Beta Diagrams are displayed near the folds which they represent. In each diagram one domain is plotted in black and another in blue. The solid black line in each diagram represents the fold axial surface. The solid black lines on the map define the domain boundaries used for analyzing major folds.

Table 4.2 Stereographic analysis of the major and minor folds of the El Kasr structure

	Domains	Interlimb Angle	Fold Axial Plane	Hinge Line	Classification
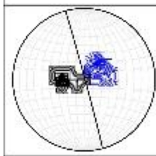	1 and 8 n_1=12 n_8= 5	142	345/89	164,6	Gentle, Upright, Sub-Horizontal
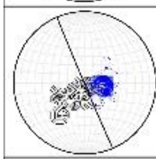	2 and 7 n_2=16 n_7= 13	144	158/89	337,12	Gentle, Upright, Gently Plunging
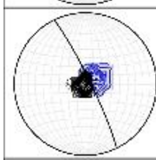	3 and 6 n_3=6 n_6= 12	156	334/84	153, 1	Gentle, Upright, Sub-Horizontal
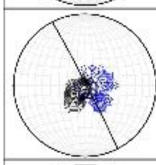	4 and 5 n_4=12 n_5= 8	162	333/88	330,8	Gentle, Upright, Sub-Horizontal
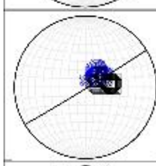	1a and 1b n_{1a}=7 n_{1b}=5	167	059/89	238, 18	Gentle, Upright, Gently Plunging
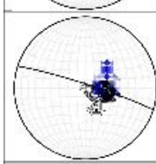	2a and 2b n_{2a}=8 n_{2b}= 8	160	288/86	289,19	Gentle, Upright, Gently Plunging
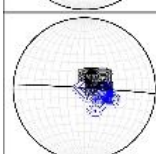	2b and 3 n_{2b}=8 n_3= 6	161	274/89	274, 14	Gentle, Upright, Gently Plunging
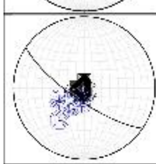	6 and 7 n_6=12 n_7= 13	161	122/76	123, 3	Gentle, Steeply Dipping, Subhorizontal

Folds defined by domain pairs 1/8, 2/7, 3/6, and 4/5 are referred to as “Major Folds”

Each of the major folds form dense and coherent populations within the constructed Beta Diagrams, the exception being the fold defined by domains 2 and 7. The cause of this lack of coherency in the data may be due to secondary deformation of the limb defined by domain 7 through folding and/or faulting. This limb is clearly truncated by the Western Fault Zone. Evidence gathered in the field suggested that fault-bound blocks within the fault zone have been rotated by motion along the fault segments.

Evident in the stereographic analysis is a distinct change in plunge of the hinge line of the folds defining the anticline between the basins. The syncline defined by domains 2 and 7 is categorized as gently plunging, reflecting the steeper plunge of the hinge line (12°) when compared to the other major folds. Conversely the syncline defined by domains 3 and 6 is categorized as subhorizontal, reflecting the gentle plunge (1°) of the hinge line.

4.3.1.2 Minor folds. Multiple minor folds deform the limbs of the El Kasr structure. These folds form complimentary pairs (e.g., domains 1a and 1b, 8a and 8b) on opposing limbs of the main basin defining synclines. The compliment to the syncline defined by domains 2a and 2b, however, has been obscured from view by a combination of faulting and burial by alluvium (Figures 4.8 and 4.9). A second pair of minor folds, defined by domains 2b and 3 and 6 and 7, are anticlines. This complimentary pair of anticlines crop out in the southern portion of the structure where the basin visibly necks down in width and serve to separate the larger northern basin from the smaller southern basin.

These minor folds are similar to the major folds in that they are upright (dips ~89°) with broad inter-limb angles (161°-167°) (Table 4.2). However, the plunge of these minor folds (18^o and 19^o) are steeper than those of the major northern and southern synclines (6^o and 8^o).

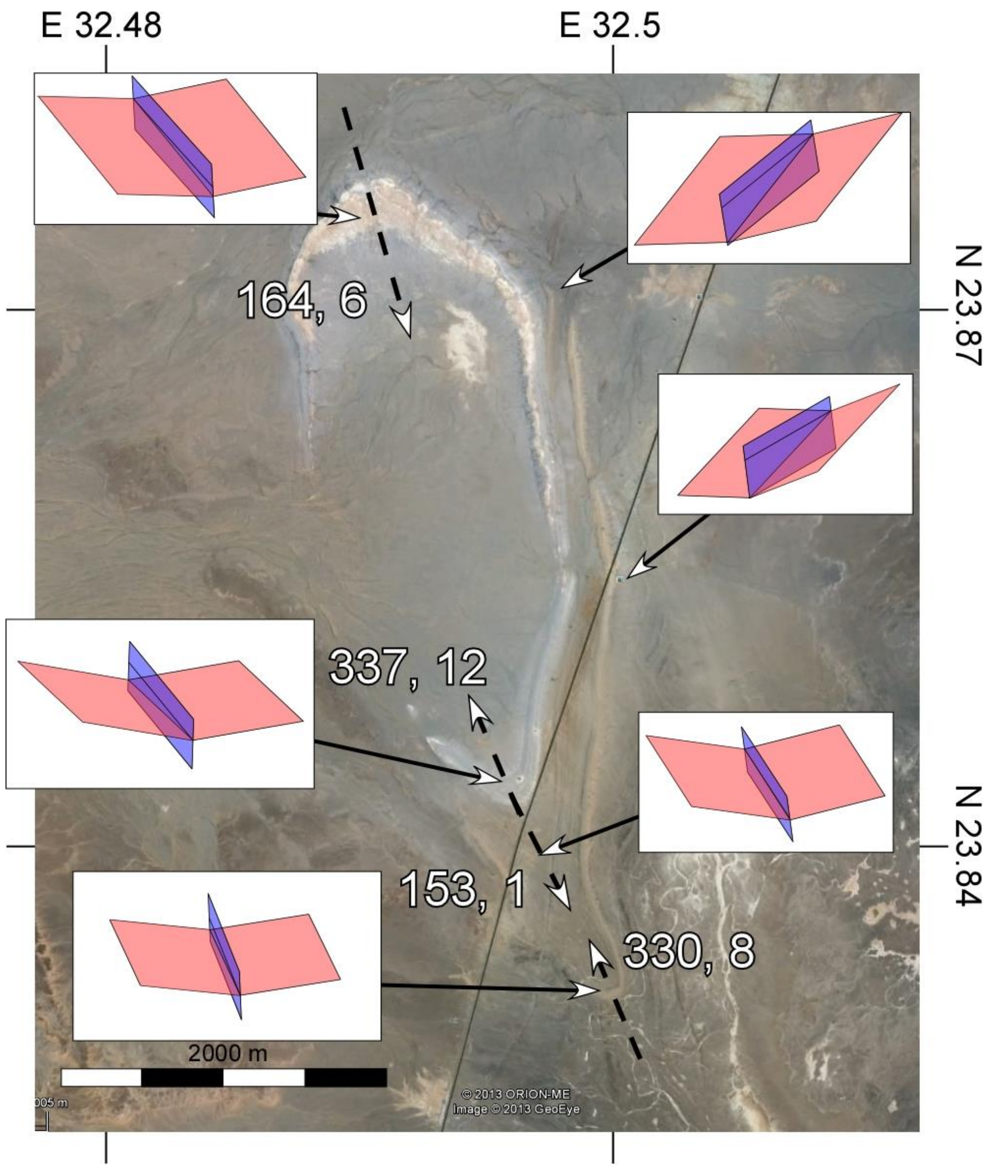

Figure 4.9 Google Earth image of the El Kasr with stereographically determined hinge lines of Major Folds as well as schematics of the folds.

The anticlinal minor folds differ in that the anticline to the west defined by domains 6 and 7 is steeply dipping (76°) and subhorizontal (3°). The fold defined by domains 2b and 3 is upright (89°) and gently plunging (14°). Both folds are gentle with identical interlimb angles of 161°. These anticlines potentially represent interference folds that develop during a subsequent deformation event that folded the original doubly plunging synclinal basin. This younger deformation event resulted in formation of a subtle dome that subdivides the El Kasr structure into a two structural basins. The doming steepens the plunge of one of the main basin forming synclines (defined by domains 2b and 7) in comparison with similar synclines defined by domains 1a and 8a and domains 4 and 5, is also rotates the plunge of the hinge line to the south for the portion of the fold defined by domains 3 and 6 (Table 4.2). The minor folds defined by the domains 2b and 3 and 6 and 7 are effected in a similar way. The plunge of the anticline defined by 6 and 7 is found to be much gentler (3°) than the minor folds in the northern basin (1a & 1b and 2a & 2b)

The field investigation of the El Kasr discovered the presence of a ridge of Dahkla Formation (seen in Figure 4.10) to the north of the structure with an associated fold. Data gathered on this fold reveals that its fold axial plane has an orientation of 076/80 and a hinge line with an orientation of 253, 15. These calculations were made on limited measurements (n=5). The discordant nature of the ridge relative to the structure as well as the presence of the drag fold indicates that a fault is present.

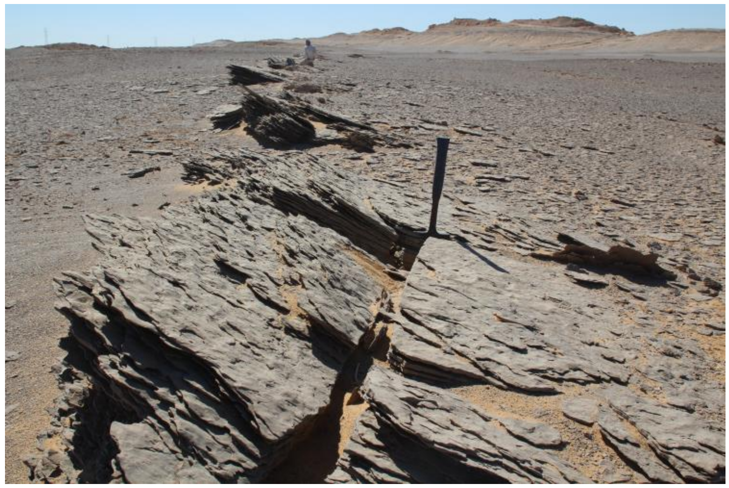

Figure 4.10 Field photo of Dahkla ridge. The El Kasr may be seen in the background. The presence of a drag fold at the southern end of the ridge indicates a left-lateral fault is present.

4.3.2 Faulting. Remote sensing and field observations demonstrate that the El Kasr structure is bounded on both sides by normal fault zones informally referred to here as the Western Fault zone (WFZ) and the Eastern Fault Zone (EFZ). Faults related to the WFZ, although not mapped as truncating the El Kasr structure, were previously mapped by Issawi (1968) and shown on the geologic map of Egypt (Conoco, 1981). Woodward-Clyde Consultants (1985) include the WFZ as part of a more laterally extensive north-south fault reffered to as the Gebel El-Barqa Fault and show it truncating a portion of the western limb of the El Kasr structure. The laterally extensive Gebel El-Barqa fault has previously been mapped as a continuous feature of approximately 110 Km.

Faulting associated with the EFZ was previously unrecognized. Evidence for the existence of the Eastern Fault Zone in the field included multiple offsets within Dahkla ridges to the south and east as well as the juxtaposition of a Dahkla ridge against a limb of the structure and an associated drag fold.

4.3.2.1Western fault zone. Along the southwestern limb of the structure the WFZ can be clearly seen in satellite imagery truncating resistant units of the Gara and Kurkur Formations near the nose of one of the synclines (Figure 4.11). In this location deformation related to fault slip is well defined by the presence of fault breccia (10's cm in thick), abundant veining filled with coarse crystalline calcite, and cataclasite along multiple fault planes. In addition, sand-filled ground fissures in pediment surfaces parallel the strike of the fault indicating a period of younger slip (Figure 4.12).

The fault plane(s) exhibit strikes of 295-310 and dip steeply to the east (73-87^{o}) or are vertical, suggesting that the fault zone is composed of subparallel fault segments. Fault ornamentation and the plunge and trend of slickenlines (57^{o}/335 and 65^{o}/300) indicate normal oblique-slip (sinistral) motion along the faults. Thin (~10cm) beds of resistant marl in shales of the Kurkur Formation are juxtaposed against massive limestone of the Garra Formation along the fault.

The strike and dip of the Kurkur Formation is variable within the fault zone but typically rotates towards the strike of the fault and steepens in dip (e.g., 307/48). A small triangular patch of Gara Formation, readily visible in satellite imagery (near 1 in Figure 4.9), has primary bedding that is highly discordant (025/14) to the structural trend of the WFZ or the western limb of the El Kasr structure and is likely a fault bounded block that was rotated within the WFZ.

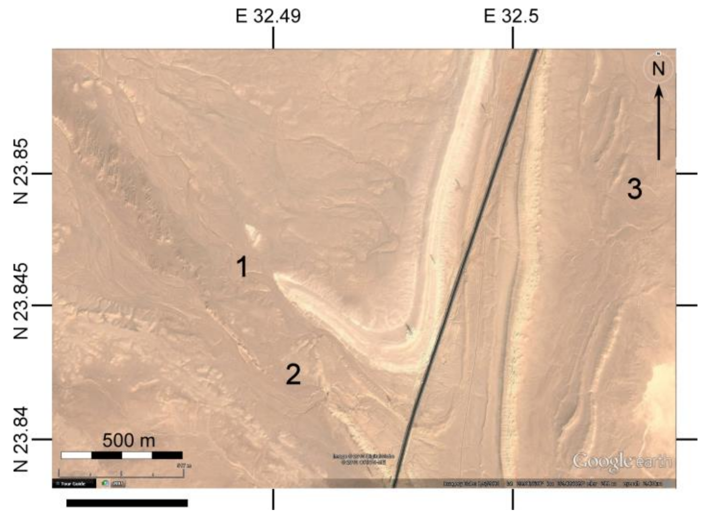

Figure 4.11 Google Earth image of a portion of the El Kasr structure. 1) Abrupt truncation of the Garra Formation; 2) Abrupt truncation of the Kurkur Formation; 3) Truncations of ridges of Dahkla.The solid black line that cuts across the structure in the image is a paved road.

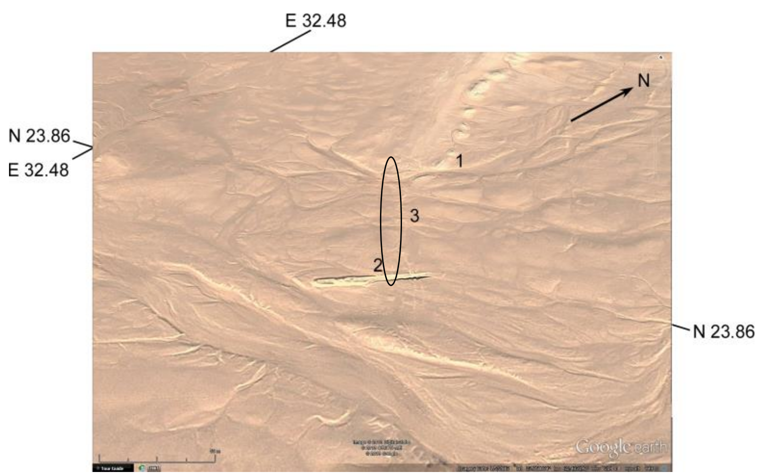

Figure 4.12 Google Earth image of the El Kasr. 1) Thinned and truncated Garra; 2) Woodward-Clyde Consultants trench; 3) Ground-cracks along the trace of the fault.

Along strike to the north, the western limb of the El Kasr structure also appears to have been thinned by faulting (Figure 4.11). In this region the trace of the fault zone has been obscured by deposition of younger alluvium that also fills in the center of the El Kasr structure. In this intervening area, the trace of the WFZ is locally marked by clusters of sand filled ground cracks and rare subdued fault scarps that develop in the quaternary alluvium pediments (see Figure 4.10 (circled) and 4.11). These features were not observed in the wadi channels that dissect these surfaces, suggesting the youngest displacement along the WFZ occurred in the Quaternary. However, in the face of the trench that exposes the WFZ surfaces defined by younger gravels appear to have been displaced (Figure 4.10) (see also Woodward Clyde Consultants, 1985).

4.3.2.2 Eastern fault zone Whereas the WFZ can be clearly seen, in both the field and in remote sensing imagery, truncating the Garra and Kurkur formations the EFZ is less well exposed in remote sensing imagery and in the field. The EFZ is inferred by the presence of numerous along strike structures. Multiple offsets within ridges of Dahkla Formation to the southeast of the structure define a splay of smaller faults originating from a larger master fault (Figures 4.13, 4.14, 4.15). The observed separation along these smaller faults can be as large as 2 meters. These faults displayed steep dips (near vertical) and dextral separation. It should be noted that separation is not the same as slip. Whereas slip is the true motion along a fault plane, separation is the apparent motion along a fault. While the offsets observed within the Dahkla appear to have been offset by dextral strike-slip faults, it is possible that these observations may have resulted from a combination of dip-slip motion and erosion. The truncation of larger ridges within the Dahkla also serves to constrain the location of the Eastern Fault Zone (Figure 4.15).

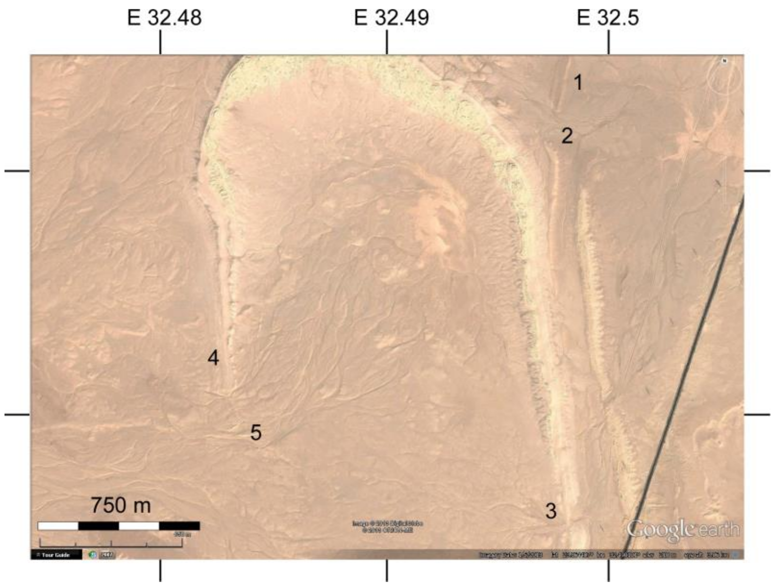

Figure 4.13 Google Earth image of a portion of the El Kasr. 1) Ridge of Dahkla; 2) Truncation of Kurkur; 3) Offset within Garra; 4) Truncation of Garra; 5.) Woodward-Clyde Consultants trench.

Figure 4.14 Field photo of dextral separation of Dahkla ridges

To the north a ridge of Dakhla Formation is discordant to the main synclinal structure oriented ~185/30. This ridge of Dahkla Formation displays moderate dips (18°-32°) and is cut by multiple joints forming approximate conjugate sets (Figure 4.8).

Figure 4.15 Google Earth image of a portion of the El Kasr. 1) Offset of Garra; 2) Truncated ridges of Dahkla; 3) Flat-lying and undeformed Dahkla.

4.4 INTEGRATED GEOLOGIC MAP

Field observations and the results of the remote sensing analysis were integrated with stereographic analysis to construct a geologic map of the El Kasr Desert Eye structure (Figure 4.16). The Dakhla Formation (in green) crops out to the east and west, forming an irregular shaped map pattern, reflecting its generally horizontal nature in this area. In contrast, it is exposed as linear ridges nearest to the El Kasr structure. The Dakhla ridges to the east were studied in detail by members of this team, but the ridges to the west have only been studied in remote sensing. These western ridges are located near the western-most fault (WFZ in Figures 4.1-4.4 and 4.9) and it is possible that these ridges also dip in toward the structure. If this is the case then these may represent possible drag folds along faults in the overlying Dakhla Formation. The Kurkur Formation (tan and orange) bound the Garra Formation in the north and form the ridges and smaller basin to the south (Figure 4.14). The Garra Formation (shades of blue) crops out in the center of the structure and contains multiple internal members (see Figure 4.14). Successive generations of alluvium, mapped in shades of yellow, cover much of the study area and may be seen filling the center of the basin. Consistent color changes visible in each ASTER image suggest that the alluvium filling the basin is different in some way from the alluvium immediately adjacent to it. Cross-cutting relationships indicate that the alluvium within the basin is older than that coming off of the plateau as is visible in Figure 4.14.While map patterns at first indicate that the QC units is younger than the surrounding Q3 and Q4 units, closer investigation in remote sensing images reveals that the QC is a consolidated unit whereas the Q3 and Q4 units appear to be unconsolidated alluvium filling channels cut into QC.

4.5 GEOLOGIC CROSS-SECTIONS

Geologic cross-sections of the El Kasr structure were constructed along section line A-A’ (Figure 4.14) through the center of the structure perpendicular to the strike of the main fold axis.

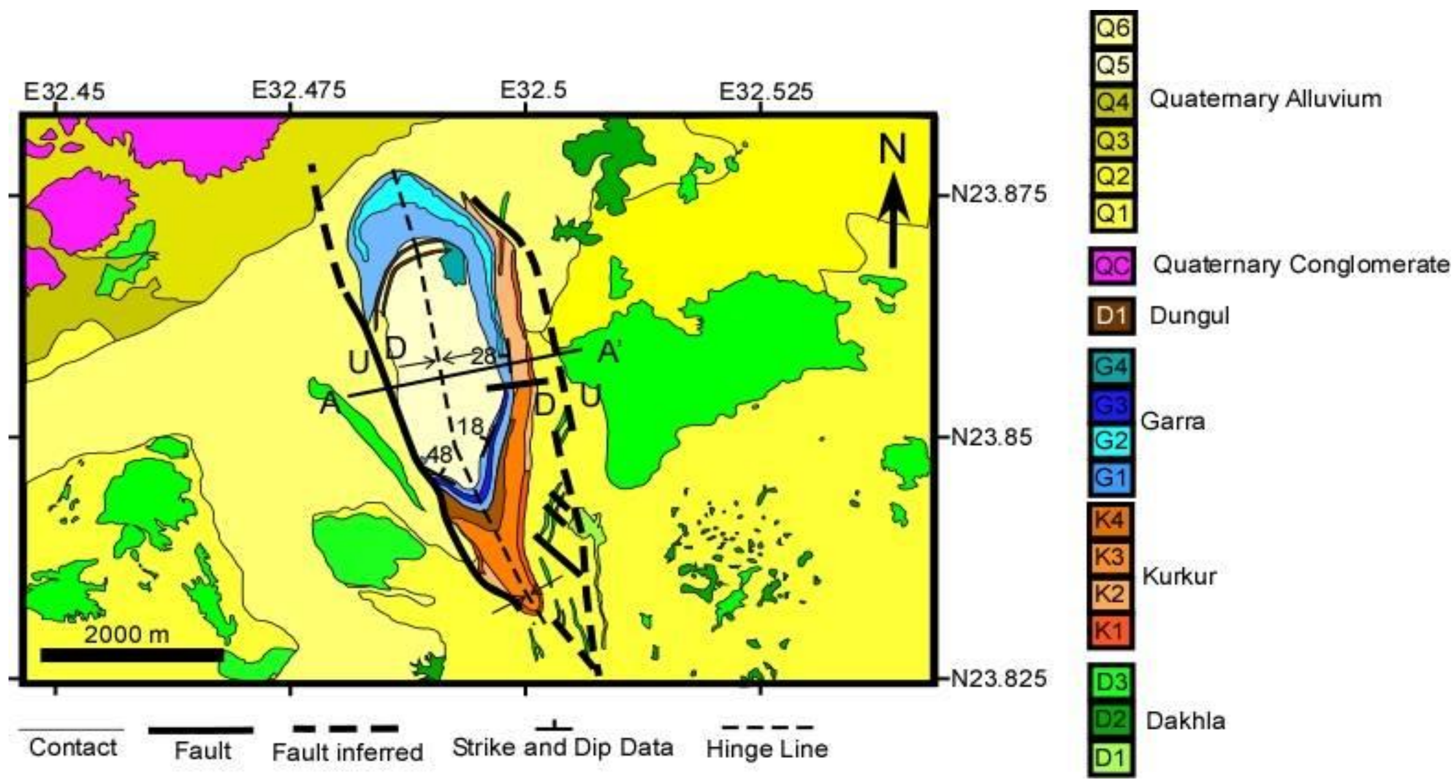

Figure 4.16 Integrated geological map of the El Kasr and surrounding area. Map incorporates field and remote sensing investigations.

These cross-sections were constrained by structural data including the orientation (strike and dip) of units, unit thicknesses, fault locations, dip of fault planes, and the location of unit contacts.

The EFZ was assumed to dip 75° into the structure, mirroring the dip measured for the WFZ. Remote sensing was used to supplement field data where necessary, particularly contact locations and orientations that were not collected in the field. All sedimentary units are *initially* assumed to maintain a constant thickness across the structure. Thicknesses of sedimentary units were calculated, where possible, using the location of contacts and the dip of the units as measured in the field (Appendices A, B, and C), otherwise measured thicknesses from well data were used (Table 4.1). Initially, constant slip along the fault is assumed where possible. Previous mapping in the region and formations seen on the scarp of the Sinn El Kaddab Plateau confirm that these units are in fact flat-lying to the west.

This study has constrained the vertical displacement along both the eastern and western bounding faults. This was done by employing the “three-point problem” procedure as described in Davis, et al., (2012). By mapping the Dahkla/Kurkur contact along the scarp of the Sinn El-Kaddab Plateau and projecting it over the El Kasr structure, it was found that approximately 200 meters of throw is necessary in order to account for the present location of the Kurkur - Daklha formation contact. It should be noted that this displacement may be accommodated by multiple subparallel faults between the Gebel El-Barqa Fault and the Sinn El-Kaddab Plateau.

4.5.1 Rollover Folding. Rollover was considered as a mechanism for the formation of the El Kasr structure and studied using balanced cross-sections. Xiao and

Suppe (1992) define rollover as the "folding of the hanging-wall fault blocks by bending or collapse in response to slip along nonplanar – commonly listric – normal faults". A structure similar to the El Kasr may reflect a change in dip of the Gebel El-Barqa fault at depth. A concave fault surface would result in a void space between the hanging wall and foot wall along the length of the steeper upper fault segment. The subsequent collapse/folding of the overlying rocks to fill the void would result in the formation of a structural basin. This mechanism could result in the prominent bounding fault and moderate dips that have been documented.

Xiao and Suppe (1992) quantitatively relate the shape of a fault and the shape of the fold forming above. The shape of the fault is defined by the change in dip of the fault (φ) and the cutoff angle of the bedding in the upper fault segment (θ). The fold above the fault is then defined by the collapse direction (ψ) and the dip of the bedding in the rollover measured relative to the undeformed bedding (δ). These variables are related by Equation 1.

$$\frac{Sin(\psi) * Sin(\psi - \delta)}{Sin(\Theta + \psi - \varphi) * Sin(theta + psi)} = \frac{Sin(\delta)}{Sin(\varphi)}$$

Equation 4.1. Relating fault shape (θ and φ) to fold shape (ψ and δ).

The collapse direction describes the relative particle motion in the deforming hanging wall. A pair of axial surfaces for the fold defines the transition from undeformed bedding to the thinned dipping limbs of the fold. These axial surfaces are parallel to the collapse direction of the hanging wall and are separated by a distance X, equal to the displacement along the lower fault segment. The orientation of the active axial surface is fixed to the bend in the fault (Xiao and Suppe, 1992).

Field investigations of the El Kasr structure by Dr. John Hogan, Dr. Barbara Tewksbury, and Trevor Ellis placed tight constraints on the dip of the upper segment of the fault, contacts between units, as well as the dip of the units to the east. This data collected in the field gives a value for the variables δ (25°) and θ (80°) and places constraints on the value of ψ (25°-90°). The range in values for ψ is derived from the orientation of the dipping beds to the east. Because the beds dip at 25° the collapse direction must be greater than 25° but less than 90° (vertical). The average of these values (57°) was used for ψ due to poor constraints. Solving for φ it was found that the change in dip of the fault was 25°, resulting in a dip of 50°. The change in dip of the fault plane was placed at the unconformity between the Nubian Formation and the Precambrian Basement, reflecting a change in mechanical strength properties of the materials.

Figure 4.17 displays the cross section created using a dip of 50° for the lower portion of the fault segment and a collapse direction of 57°. This cross section conforms to the constraints determined in the field and does result in a structural basin with a prominent bounding fault to the west.

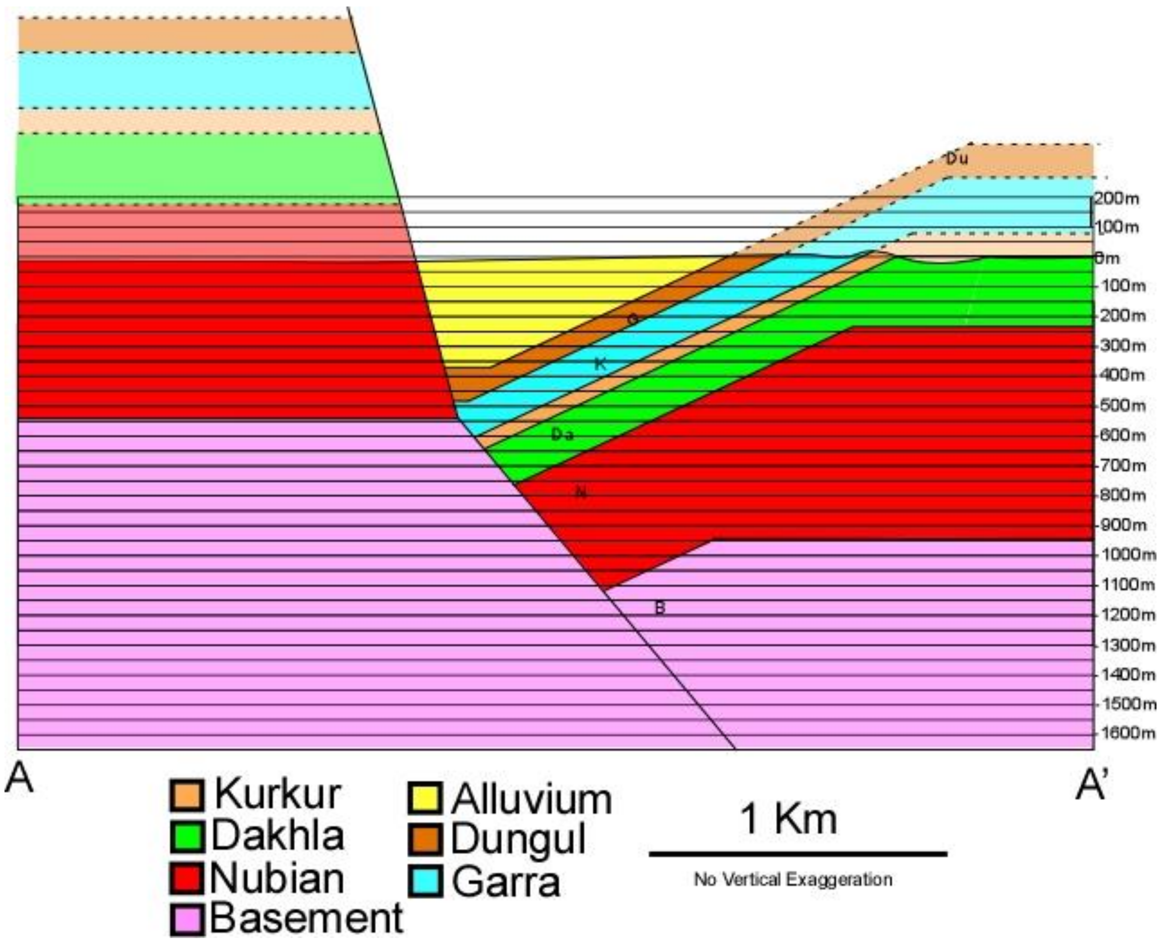

Figure 4.17 Rollover Cross-section of the El Kasr constraining the hanging wall**.** The model requires thinning of the deformed limb of the fold and exposure of the Nubian Formation at the surface of the footwall.

Evident in Figure 4.17 is the striking change in thickness of the units between the limb of the fold and the undeformed units to the east. In order to maintain equal area, rollover requires the thinning of the deformed limbs of the fold (Xiao and Suppe, 1992). As shown in Table 4.3, the model presented in Figure 4.17 is true to the unit contacts as mapped in the field and in remote sensing imagery and the unit thicknesses in this limb fall within the constraints given by previous studies (Issawi, 1968: Woodward-Clyde Consultants, 1985). Therefore the flat-lying units to the east as well as the flat-lying units within the structure must be thicker than the deformed limb. This new thickness was defined by the axial surfaces and it was found that the thickness of each unit increased by a factor of approximately 1.58. These results indicate that the undeformed Nubian would have a thickness of 710m while the undeformed Dahkla would have an undeformed thickness of 238m. Previous studies of the area have reported thicknesses of 39m-155m for the Dahkla and a maximum of 592m for the Nubian (Issawi, 1968). This drastic increase in unit thickness invalidates this construction of the rollover model for the formation of the El Kasr structure.

The cross-section in Figure 4.17 also requires folding of the rigid basement. In order to rectify this problem the axial surface may be moved west. This then requires that the angle of the collapse direction decrease in order to maintain the proper lithologic contacts as mapped in the field. This approach, however, results in further increase in thickness of the undeformed units resulting in thickness of approximately 2.5 times their measured thicknesses. The offset required along the fault in Figure 4.17 dictates that the orientation of the hanging wall would result in the exposure of the Nubian Formation to the west. While little data was gathered west of the fault by members of this team, previous authors have mapped Dahkla to the west (Conoco, 1981; Issawi, 1968; Woodward-Clyde, 1985).

Table 4.3 Comparison of models of formation of the El Kasr structure

Figure	Model	Constraints	Pros	Cons
4.15	Rollover (Constraining the Hanging Wall)	Unit thicknesses in limb of fold. Contacts on fold limb	Explains formation of structure with a single fault	Requires unrealistic thickening of units outside of the structure. Exposes Nubian to the west where Dahkla is mapped.
4.16	Rollover (Constraining the Foot Wall)	Dahkla Exposed to west. Unit thicknesses in limb of fold	Explains formation of structure with a single fault	Requires unrealistic thickening of units outside of the structure. Exposes Garra to the east where Dahkla is mapped.
4.18	Transtension/Drape Folding	Unit thicknesses, Maintain constant thickness, mapped contacts, mapped units exposed at surface	Incorporates both fault systems. Adheres to constraints mapped in the field	Maintaining constant thickness results in space problem between Nubian and Basement
4.19	Transtension/Drape Folding w/deformable Nubian	Unit thicknesses, Mapped contacts, Mapped units exposed at surface	Incorporates both fault systems. Adheres to constraints mapped in the field	Does not adhere to constant thickness constraint

The cross-section in Figure 4.17 investigates rollover as a mechanism of formation of the El Kasr by constraining the footwall of the Gebel El-Barqa, compared to the cross-section in Figure 4.18 in which the hanging wall is constrained. In Figure 4.17 the footwall is fixed, exposing Dahkla Formation at the surface as previously mapped. This position of the footwall in turn dictates the position of the hanging wall, resulting in the exposure of the Garra Formation to the east, as well as obscuring most of the contacts mapped in the field and in remote sensing imagery. This model also suggests the presence of approximately 450m of alluvium within the structure. Similar to Figure 4.17, Figure 4.18 suggests that the rigid basement is behaving ductily. Attempts to correct this error result in similar thicknesses as those previously discussed related to Figure 4.17.

4.5.2 Transtensional/Drape Folding Model. Transtension was investigated as a model of formation of the El Kasr in which overlapping fault zones would result in a local region of extension. This extension would be accommodated by the formation of normal faults within the zone as well as normal motion along the east and west bounding faults. Initially the units were projected into the subsurface from both east and west with a constant dip until they merged beneath the structure. This result predicted approximately 250 m of alluvium to be present in the basin. It was determined that this

thickness of alluvium allowed for the presence of the Dungul Formation within the center of the structure. The addition of the Dungul Formation still allowed for over 100 m of alluvium within the structure, suggesting that the units are flat-lying in the center of the structure, a style of folding more consistent with folds associated with extensional faulting (Sylvester, 1988). This approach reduced the alluvium in the center of the basin to 10-20 m while still allowing for the presence of the unmapped Dungul Formation (see Figure 4.19).

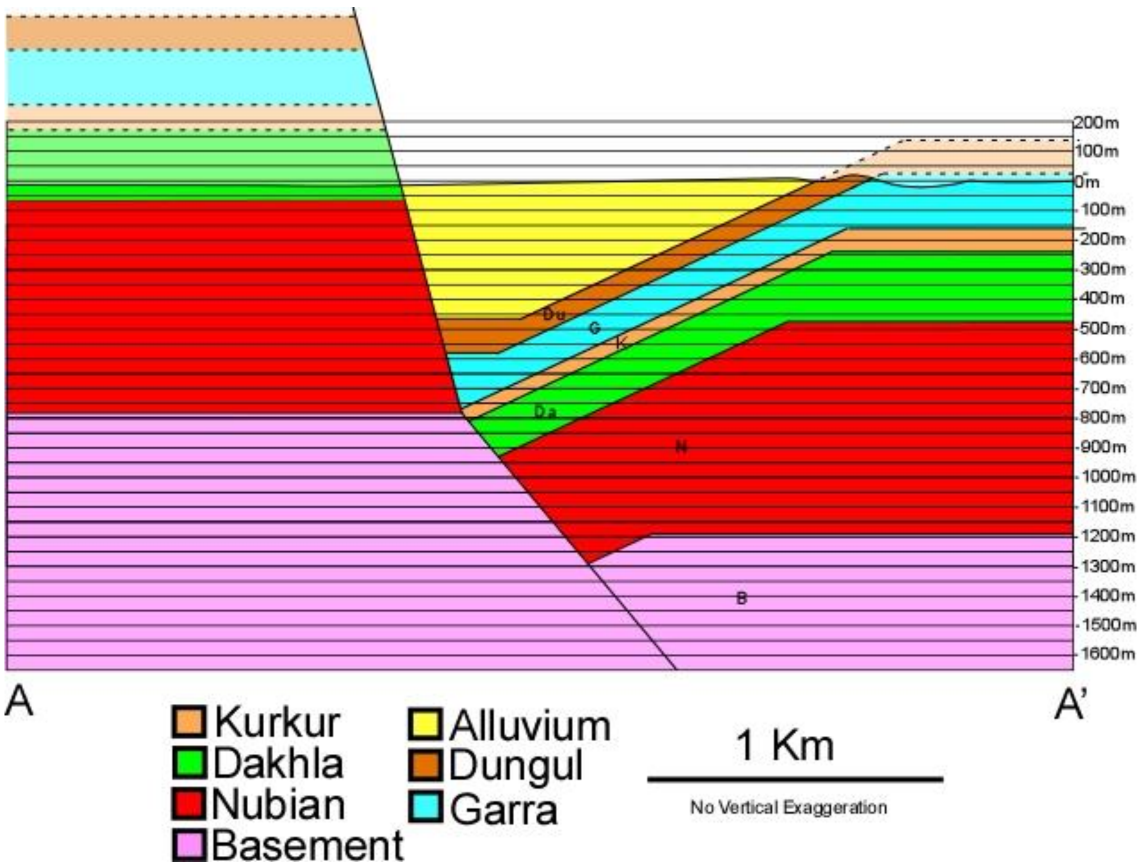

Figure 4.18 Rollover Cross-section of the El Kasr constraining the foot wall. The footwall is fixed adhering to the constraints from the field investigation, forcing the hanging wall into the location shown, exposing flat-lying Garra at the surface.

The cross-section in Figure 4.19 predicts that the basement is divided into fault bound blocks with the outermost blocks rotated and dipping into the structure. These faults are not visible at the surface and are inferred to be blind, propagating an unknown distance into the cover. These faults are inferred by the dipping limbs of the structure, allowing the limbs to dip into the structure without overlapping the basement. These inferred faults therefore allow for grabens to develop below the limbs of the structure. The constraints within the structure dictated that one of these faults would be located west of the previously mapped Gebel El-Barqa fault trace. The geometry of the structure to the east suggests that the eastern fault zone dies out near the surface within the Dahkla.

Not visible in Figure 4.19 are the complexities of each fault zone manifested as offsets and multiple fault traces. Field and remote sensing investigations of both fault systems revealed that both zones are composed of these complexities. These secondary structures may be explained using the drape fold model as discussed by Withjack et al. (1990) and Sharp et al., (2000) in which secondary faults propagate up through the cover in order to accommodate folding.

Draped folding involves the propagation of normal and reverse faults from the basement into the ductile cover. This results in the thinning and flexing of the limb of the folded sedimentary cover over the down-thrown basement. Sharp et al. (2000) outlines the growth and propagation of normal faults and associated normal and reverse faults as well as the folding of the cover. As normal faulting progresses, the basement behaves as a rigid “forcing member” while the sedimentary cover folds ductily. As the normal fault continues to propagate into the cover the monocline steepens and a series of upward-steepening normal and reverse faults form subparallel to the normal fault in the immediate hanging wall in order to accommodate deformation (Sharp et al., 2000).

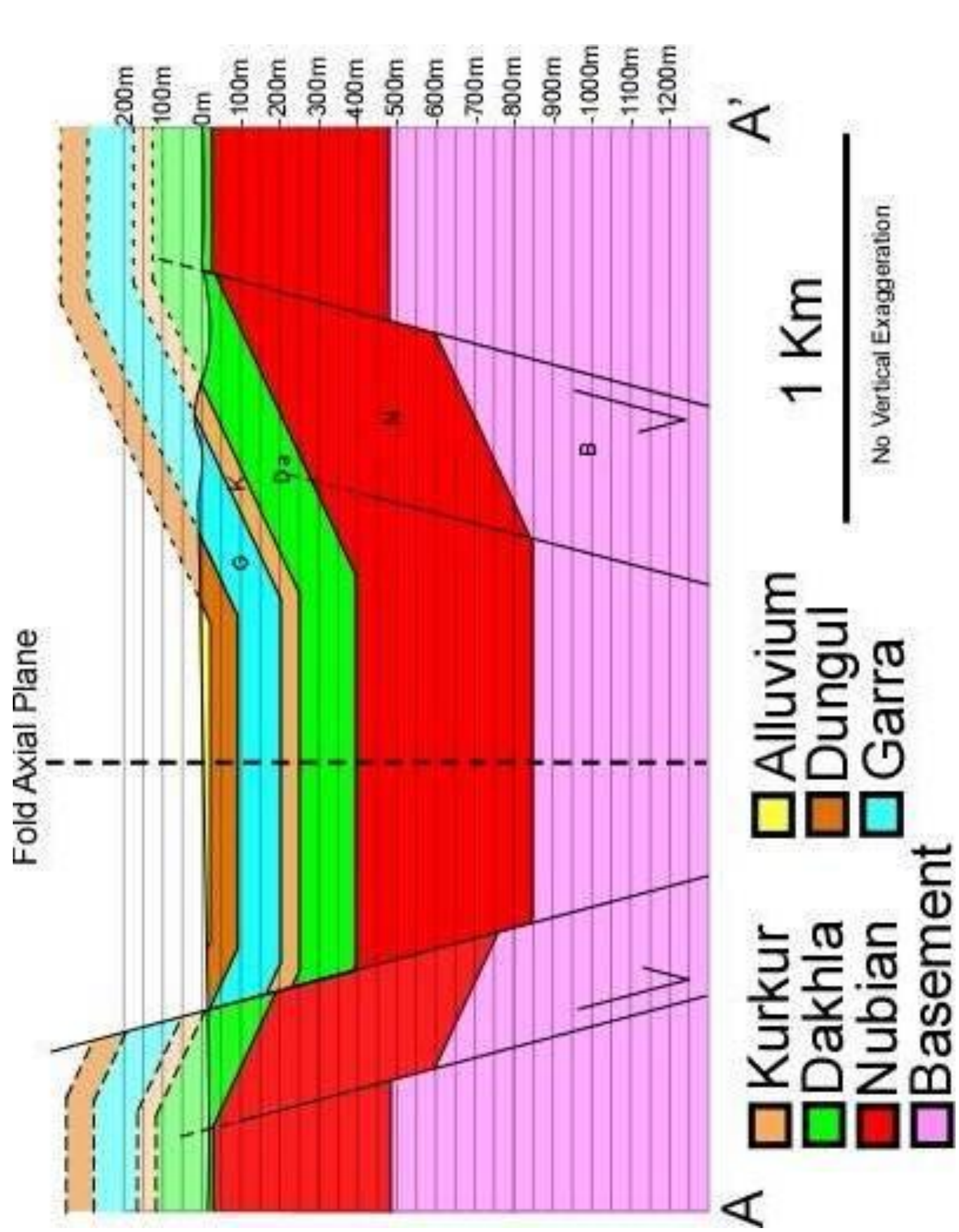

Figure 4.19. Transtensional Cross-section of the El Kasr with basement rotation. Surface contacts and unit thicknesses fall within constraints. Basement rotation and fault displacement remain unresolved.

The observed offsets within the Dahkla Formation suggest that in the case of the El Kasr structure these normal and reverse faults may allow for the thinning and folding of the Nubian and Dahkla formations over the displaced basement below to the east. These secondary faults may not propagate into the Kurkur and Garra formations, which may simply fold over the Dahkla and Nubian below in response to the displacement. Within the WFZ these secondary faults may cut up through the entire sedimentary section. This difference may be attributed to the maturity of each fault zone, where the WFZ is more mature than that to the EFZ and therefore contains both a greater number of faults as well as more extensive faults.

While the cross-section in Figure 4.19 conforms to the constraints dictated by field and remote sensing investigations several unresolved questions remain. The cross-section in Figure 4.19 predicts that fault-bound blocks within the basement have rotated in response to extension. Without this rotation the cross-section predicts a void space along the Nubian-Basement contact as seen in Figure 4.20. This rotation is poorly explained and appears to suggest that the brittle basement behaves in a ductile manner. However, Moretti et al. (1988) discusses rotation of rigid blocks in which the void spaces resulting from the rotation were filled with a softer material, such as catalysis.It is possible that the strain is taken up by motion along secondary structures (faults/joints). It is also possible that the basement within the structure is composed of grabens above which the sedimentary cover is deformed at the tips of the propagating normal faults according to the principles of trishear (Erslev, 1991).

The void spaces visible in Figure 4.20 indicate that the El Kasr structure cannot be modeled by a balanced, restorable cross-section. This then indicates that the sedimentary cover is accommodating the strain in a manner shown in Figure 4.19 in which the Nubian Formation deforms to fill the potential void space. The Nubian is reported to be a poorly cemented sandstone (Issawi, 1968) and could therefore potentially deform in such a way as to address the potential space problem.

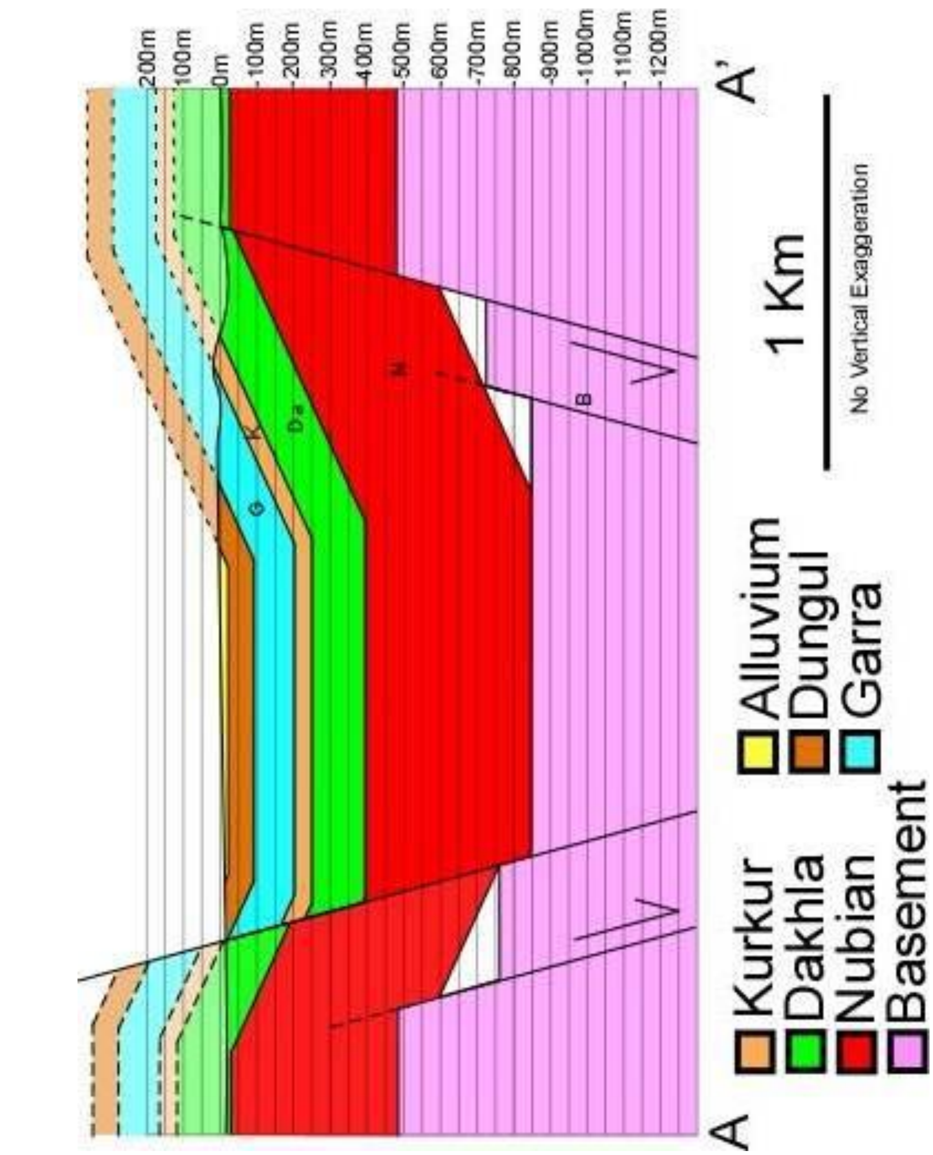

Figure 4.20. Transtensional Cross-section of the El Kasr with void spaces. Void spaces may be seen along the Basement/Nubian contact due to the brittle behavior of the basement and the ductile behavior of the sedimentary cover.

The Navajo sandstone of the southwestern Unites States is of a similar well sorted, poorly cemented lithology. Studies on the Navajo indicate that this lithology is readily deformable through such mechanisms as deformation bands and "short unconnected slip surfaces" (Shipton and Cowie, 2001). It is possible that the Nubian Formation accommodates the strain in a similar way. It is also predicted that this accommodation of stress decreases up section, exploiting the poorly cemented Nubian Formation and shale layers within the Dahkla Formation.

While the Nubian and Dahkla formations may accommodate the strain above the normal faults within the basement, the conservation of matter dictates that the units must thin at some point in order to account for the extra material required for the model as seen in Figure 4. 21. Moretti and Callot (2012) discuss the validity of the assumptions that bed thickness and bed length remain constant in the kink-band approach to geologic cross-sections. They found that the thickness, and therefore the length, of soft layers did not remain constant throughout deformation.

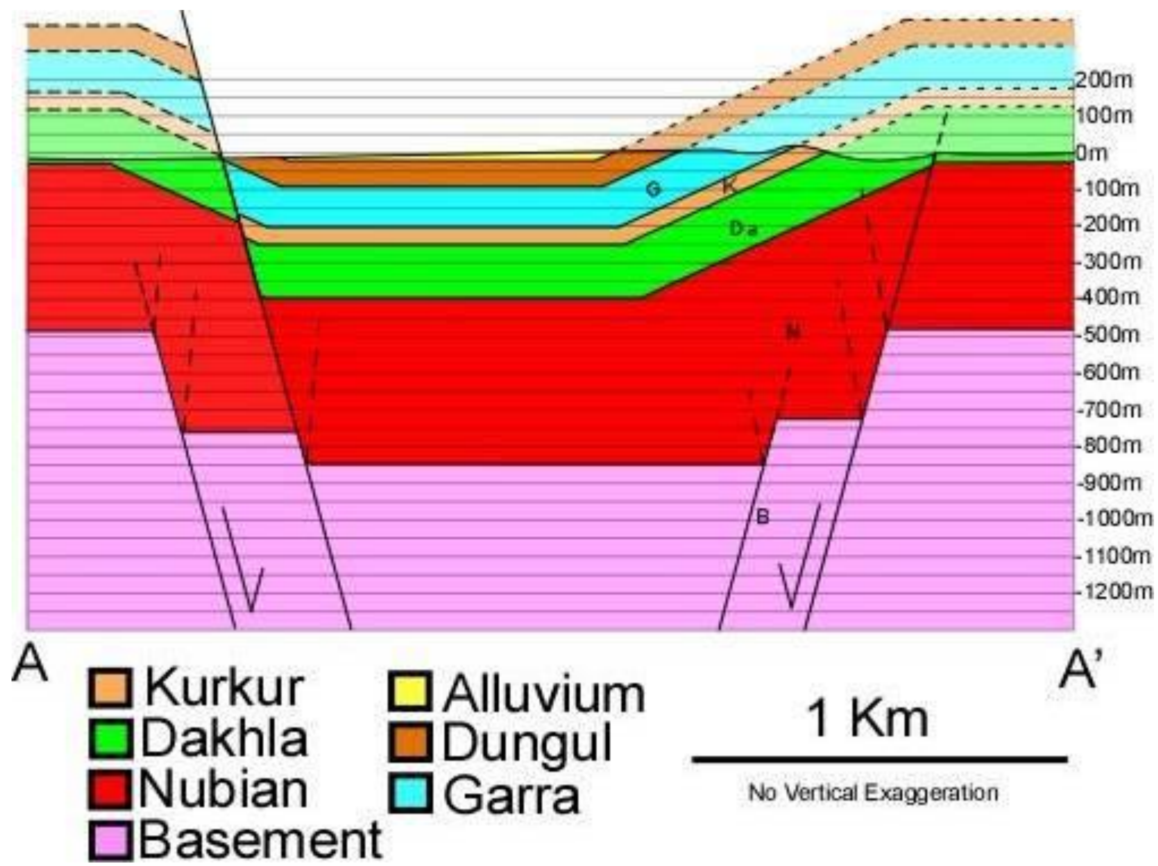

Figure 4.21 Transtensional Cross-Section of the El Kasr structure in which the Nubian Formation has accommodated the strain. Possible secondary faults are shown propagating into the cover in dashed lines.

5. DISCUSSION

Previous work in the study area has mapped the Gebel El-Barqa as a continuous single fault trace. However, this study has found that it is much more likely that the fault associated with the El Kasr structure are zones comprised of multiple fault segments as opposed to continuous faults. These findings are consistent with those concerning the east-west faults in the region including the Seiyal and Kalabsha faults (El Etr et al., 1982). These previously unreported fault segments likely influenced the formation and evolution of the El Kasr structure.

The El Kasr synclinal basin may be the result of deformation within a local region of extension related to strike-slip faulting. Transtension would require the presence of a second fault or fault segment bounding the structure to the east in conjunction with the well studied fault to the west. This study has mapped a previously unrecognized fault zone to the east of the structure. The presence of multiple offsets within the Dahkla Formation, truncations of Dahkla ridges as well as a fold and ridge within the Dakhla Formation to the northeast of the structure serve to constrain its location. Mapping of these fault systems suggests that they may merge to both the north and south of the structure, though this is as of yet unconfirmed. As seen in Figure 5.1 a left-handed step-over of left-lateral faults would result in the predicted zone of extension.

Woodward-Clyde Consultants (1985) reported that sinistral motion has occurred along the Gebel El-Barqa fault. Similar motion occurred along the north-south trending faults of northeast Africa during the Late Eocene as Africa and Eurasia began to collide (Guiraud et al., 2001). This left-lateral motion along with the observed relationship between the El Kasr and the fault zones would result in the predicted region of transtension (Figure 5.1).

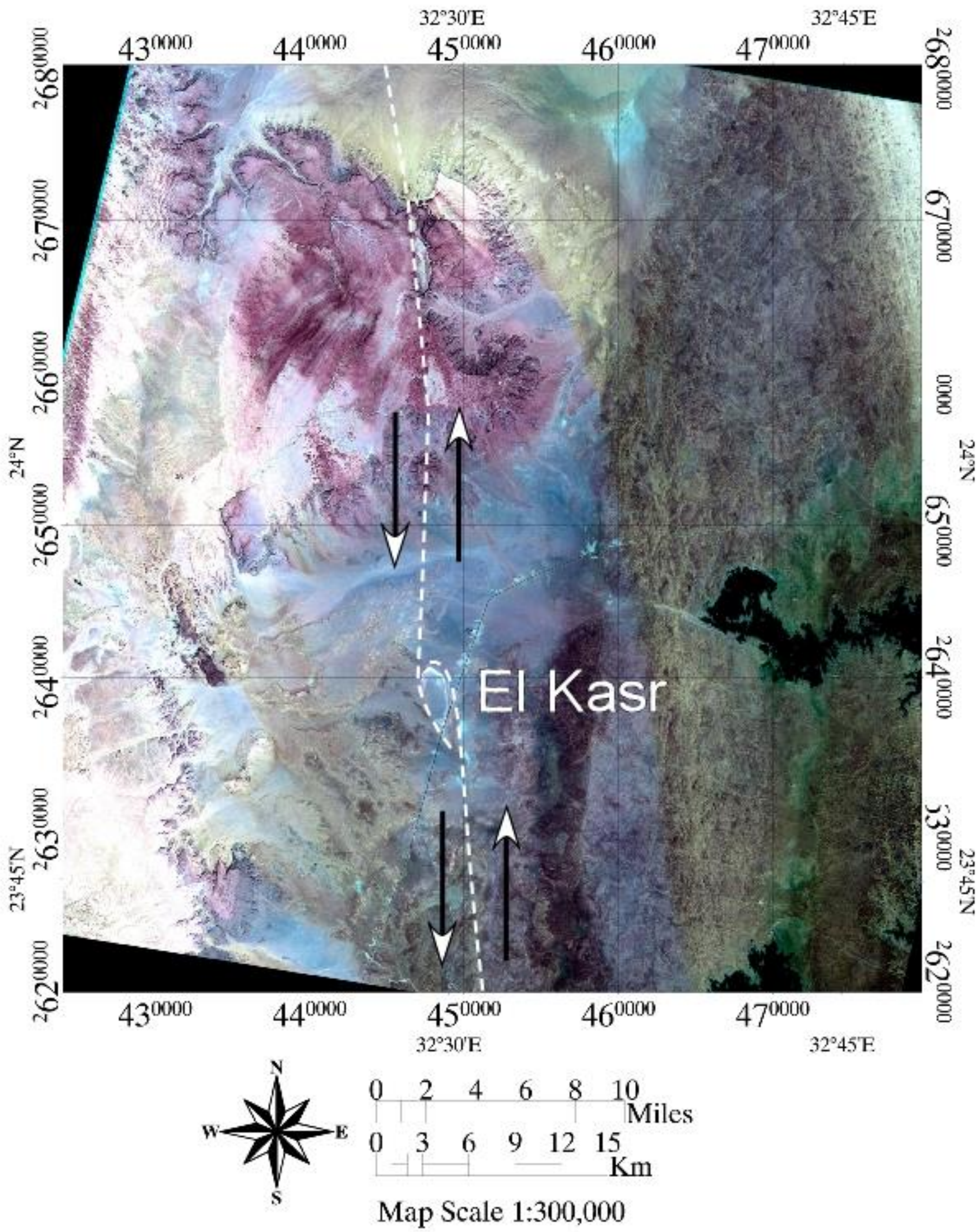

Figure 5.1 ASTER of the El Kasr structure and Gebel El-Barqa Fault. Relative motion of the faults is shown by the arrows. This geometry would result in the predicted region of extension

Folding of the Garra and Kurkur formations within the structure may be explained through folding of the sedimentary cover over the displaced basement blocks below. To the east, offsets were observed within the Dakhla Formation. Because the younger units have been eroded way, it is not possible to determine if these offsets had yet propagated up section. These offsets may represent the normal and reverse faults that accompany propagating normal faults into the sedimentary cover and the subsequent drape folding, as predicted by the models of Withjack et al., (1990) and Sharp et al., (2000). If this is the case, then it is likely that the Garra and Kurkur are folding in response to the down-thrown basement blocks.

The inability of balanced cross-sections to completely analyze the structure suggests that some mechanism is operating in order to resolve the space problem along the unconformity. It appears that the poorly cemented Nubian and possible the incompetent shales within the Dahkla have deformed in such a way as to thicken and accommodate the strain. This thickening of these formations near the uncomformity must in turn require that the units be thinned elsewhere in order to maintain equal volume within the structure.

Wu et al. (2009) investigated the effect of transtension on pull-apart basins opposed to simple strike-slip using analogue models. Many of the characteristics of the El Kasr structure appear to match the characteristics of transtensional analogue models that have undergone moderate displacement. The transtensional model that underwent moderate displacement displayed two distinct depocenters, one larger than the other, bounding normal fault along the larger depocenter, and a through-going dextral fault found between the depocenters. These characteristics are all found in the El Kasr structure which has a composite nature and a prominent western bounding-fault. A dextral offset trending 060 (36 Q 448860.69 m E, 2636985.05 m N) was reported from the field near the interbasin high. This offset is not readily apparent in remote sensing imagery but is consistent with predictions made with analogue models (Wu et al., 2009).

Competing models for the composite nature of the El Kasr structure include initial formation of adjacent structures, refolding of the original basin, and differential displacement along normal fault planes. The analogue models performed by Wu et al., (2009) resulted in the formation of adjacent depocenters similar to the El Kasr structure. Stereographic analysis demonstrates the presence of anticlines that define an anticlinal dome which separates the northern and southern basins. This anticlinal dome within the El Kasr structure may be an interference fold pattern indicating that the structure was subsequently deformed, possibly by brief reactivation of the Gebel El-Barqa fault system as right-lateral, resulting in transpression. If the northern portion of the structure subsided as the southern portion remained fixed, an anticline with the observed features as well as expose the Garra in the north as seen.

This thinning may also serve to explain the formation of the fold above the extensional zone. Folds often occur in compressional regimes, though many are found in extension, in which horizontal shortening is accommodated by folding of the units. The El Kasr occurs within an extensional zone and therefore the folding must

The Western Desert of Egypt represents a unique setting that may promote the formation of the Desert Eye structures. El Etr et al. (1982) reported that the major E-W faults in the region are not continuous features but are instead discontinuous segments. Similarly, El-Khashab et al. (1991) note that many of the faults in the region branch, forming smaller faults. These complexities within the fault systems of the region may indicate that many of the Desert Eyes form through processes similar to that of the El Kasr structure in which the interactions of fault segments results in local stresses that result in the formation of the observed structures. Tewksbury et al. (2009) discuss the possibility that shale mobilization within various units of the stratigraphy may be related to the formation of these structures and identify mass movement features visible in Google Earth imagery. It is possible that locally rheology plays a significant role in the formation of these structures, particularly ductile shales and weakly cemented sandstones, both of which are prominent in the stratigraphy of the Western Desert .

6. CONCLUSIONS

Detailed field and remote sensing investigation of the El Kasr structure has revealed that the structure is closely associated with a pair of bounding fault zones. Previous authors have mapped the western-most fault as a portion of the more laterally extensive Gebel El-Barqa Fault (Woodward-Clyde Consultants, 1985) which has been shown to have accommodated dip-slip (Issawi, 1978) motion as well as strike-slip (Guiraud et al., 2001; Abdeen et al., 2000) motion throughout its history.

Based on detailed field study the Western Fault Zone is composed of steeply dipping (73°-87°) subparallel fault segments striking 295-310. Truncated units within the fault zone were found to be rotated towards the strike of the fault. The Eastern Fault Zone is inferred from the presence of a variety of associated structures. The presence of a Dahkla ridge that is discordant with the structure, as well as an associated drag fold constrain the location of a fault. To the east of the structure the truncation of multiple ridges of the Dahkla Formation as well as multiple offsets within the Dakhla Formation suggest the presence of a fault zone.

Stereographic analysis of the folds defining the El Kasr structure demonstrates that both the major and minor folds of the structure have broad inter-limb angles. The northern and southern major folds of the structure display similar plunge values of 6 and 8 respectively. Stereographic analysis suggests that the central folds of the structure appear to have been rotated, steepening the hinge line of one fold while an adjacent fold became subhorizontal. A similar pattern is visible in the adjacent minor folds of the structure where the hinge line of the minor folds adjoining the larger and smaller basins display strikingly different plunge values of 14° and 3°.

Cross-sections constructed of the structure predict that the El Kasr structure has formed in a zone of transtension as the sedimentary cover folds over fault-bound blocks within the basement, employing drape folding near the margins to thin and deform the cover. These cross-sections do not properly address the motion along the westernmost fault or the rotation of fault-bound blocks within the basement.

Detailed field and remote sensing study of the El Kasr structure as well as stereographic analysis and the construction of balanced cross-sections indicate that the El Kasr structure has formed over an extensional zone along the trace of a strike-slip fault. The left-handed step-over of the left-lateral fault traces would result in the predicted zone of transtension (Figure 5.1). Drape folding as discussed by Withjack and Peterson (1990) and Sharp et al. (2000) induces the propagation of normal and reverse faults into the deformable sedimentary cover. The space problem presented by Figure 4.18 is still unresolved, but it is believed that the majority of the strain is accommodated by the Nubian Formation and decreases up section (Figure 4.19). This is supported by the multiple off-sets and truncations found within the Dahkla Formation and the relatively undeformed Kurkur and Garra formations.

As reported in Guiraud et al. (2001), North Africa was subjected to a brief yet strong compressional event with the main shortening in the NW-SE direction in the Late Eocene. The stress Late Pleistocene stress field as described by Bosworth and Strecker (1997) may have induced sinistral motion along N-S trending faults in the region. This motion along the fault would have resulted in the predicted transtensional motion and potential formation of the El Kasr structure.

The counterclockwise rotation of the stress field in eastern Africa places constraints on the formation of the El Kasr structure (Bosworth and Strecker, 1997). This rotation is suspected to be a plate-wide event and occurred prior to 125,000 years ago.

This study has found that the El Kasr structure has likely developed due to transtension and it is possible that similar mechanisms are responsible for the formation of other Desert Eye structures. El Etr et al. (1982) stated that the east-west oriented faults are discontinuous and El-Khashab et al. (1991) describe the branching of faults as “a normal feature in the area”. These discontinuous and branching faults may allow for regions of transtension, resulting in basins, and regions of transpression, resulting in domes. The inability to construct a balanced cross-section of the El Kasr structure indicates that deformation within the sedimentary cover played a significant role in the formation of the structure.

APPENDIX A

"REMOTE MAPPING" INDICATORS

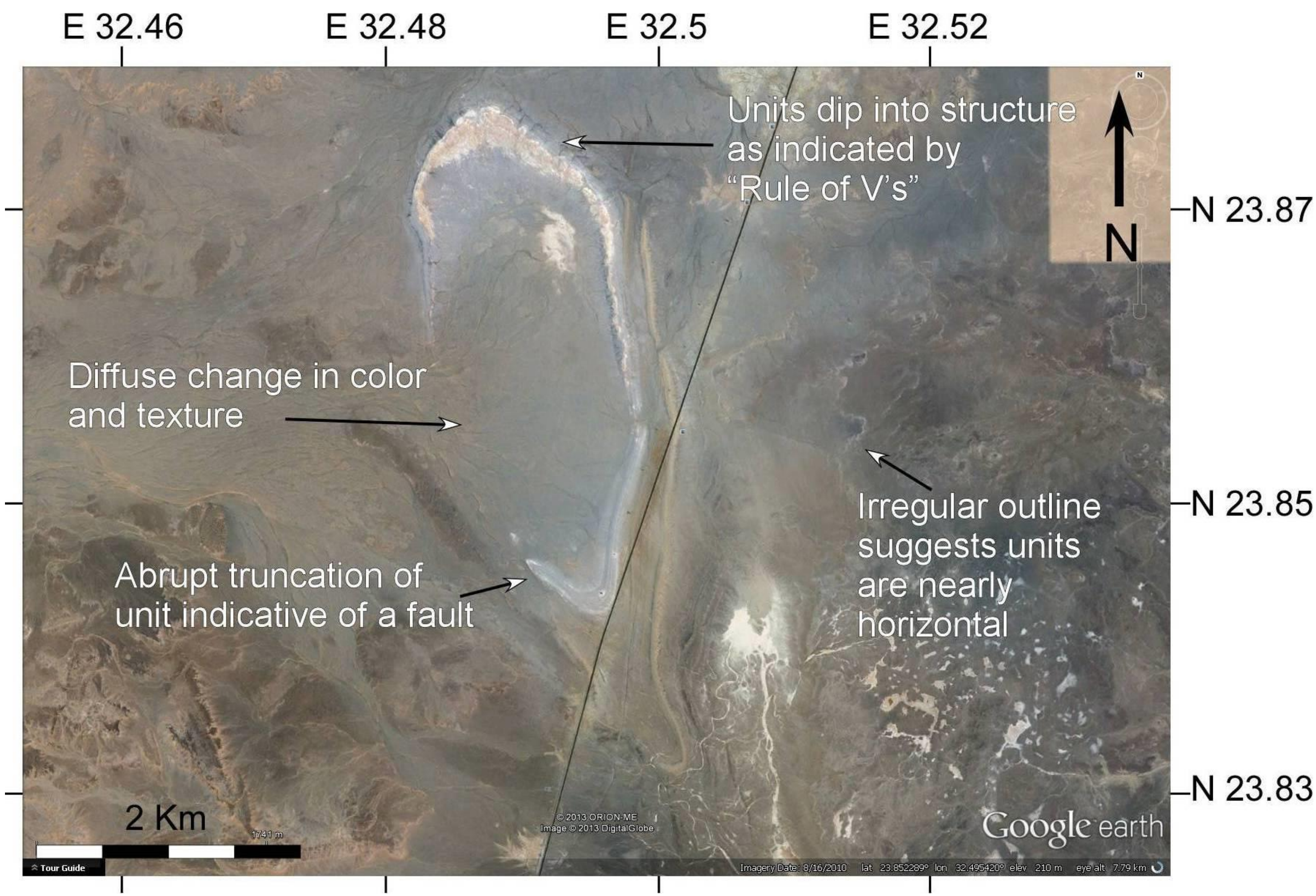
E 32.46
E 32.48
E 32.5
E 32.52
N 23.87
N 23.85
N 23.83
N
Units dip into structure as indicated by "Rule of V's"
Diffuse change in color and texture
Irregular outline suggests units are nearly horizontal
Abrupt truncation of unit indicative of a fault
2 Km
© 2013 ORION-ME
Image © 2013 DigitalGlobe
Google earth
Tour Guide
Imagery Date: 8/16/2010 lat 23.852289° lon 32.495420° elev 210 m eye alt 7.79 km

APPENDIX B.

DR. JOHN HOGAN FIELD NOTES,
2010

	Dr. Hogan Data, 2010					
	Stop	Lat/Northing	Lon/Easting	Strike	Dip	Notes
1	1.2	2633251	44886	244	28	Low whitish grey mound of very fine grained massive limestone, rises ~2m above basin floor. Rock breaks into thin "flag stones" @ surface- along bedding (?) below surface more massive blocks (so could be exfoliation feature) defined by joints. Rock has a very peculiar texture on bedding planes accentuated by wind abrasion (micro ripples) or some dessication feature. Dips may reflect exfoliation rather than primary bedding.
				192	27	
				54	57	Joint
				67	70	Joint
				149	85	Joint
2	1.3	2638329	448914	172	17	Possible fault, located in drainage cross cutting structure, beds truncated and offset. Strike and Dip taken on N-side of drainage. Resistant unit truncated. Possible drag.
3	1.4	2638648	448873	175	28	Distance determination of strike and dip by settign a point in distance @ same elevation (strike line). "grey unit" below white with several alternating resistant units location is on the S edge of a V notch in structure. White unit has been disrupted by bulldozing, it contains good stromatolite mound almost a meter in size.
4	1.5	2638188	449240			otc of "Limestone Spatter" lifht tan-buff limestone, not bedding visible, crops out in irregular blocks on slopes seperated by sand and as a irregular loose material on flats, ridge former. Blocks are several meters on sides, and are composed of very irregular shaped pieces of limestone stuck together, edges of pieces defined by irregular cracks. "Appearance of spatter stuck together" high surface roughness (show up on radar) cantact to the east is sharp but boulders end and sandy gravel begins.

5	1.6	2636219	448659	357	12	Dip slope of massive light grey limestone surface polished by wind abrasion, scalloped, holes cross-cut by multiple joints very common. Strike and dip best estimate based on dip slope. Contact with "spatter limestone" (older) along ridge crest light grey limestone (younger)
6	2.1	23.84134	32.4925	330	33	Following ridge of "spatter limstone", bedding difficult to observe, here best chance @ strike and dip. (330 33 "average") Here is where the ridge dramatically thins to the south is a good size wadi (beds have slumped into the wadi) N-side als a wadi-could less resistant unit have been buried after being eroded down? (alternative to faulting)
				310	38	
				335	35	
7	2.2	23.84472	32.49159	307	48	along the edge of the wadi, adjacent to the white-grey massive limestone area dramatically changes in dip, breccia, and calcite filling fractures, and slickenlines indicate fault (dip slip) Fault has more than one trace.
				310	75	Of Fault
				296	73	measurements taken drirectly on fault plane
				310	18	
				296	87	
8	2.3	23.84546	32.49073			Ground cracks within a raised surface comprised of abundant angular fragments of the whote/grey limestone. Trend 320-325 recent? Of slumping reactivated?
9	2.4	23.84596	32.49021	270	6	excellent example of a cataclastic fault rock! Thinly bedded marl juxtaposed against white-grey massive limestone, along edge of the wadi to this tip where we are now-massive gray/white limestone brecciated the entire way, wadi probably exploited the main fault (? notes unclear) and we are on the edge. Cataclastis dominated by vertical fractures parallel to trce of fault ~325+/-5 (strike and dip taken on marl, but variable "flat-lying") marl cataclasite-not well cememnted or indurated, in contrast the white-grey limestone is...age of fault...older

10	2.6	23.84755	32.4893	25	14	isolated block of rock in wadi, visible on Google image, beds are "rotated" relative to the trend of our basin, the color banding on Googl matches this change. -This is the unit with the alternating thin tarnish resistant beds seperated by less resistant unit (several meter spacing) capped by the white/grey massive limestone (strike and dip variable)
11	2.7	23.84802	32.48967	300	5-14	Low otc in a thin band silty-very fine grained sandstone. Grityy; massive, no obvious bedding, orange brown-orange buff color. Otc x-cut by abundant joints, at leat 3 prominent sets (160, 82; 090, 80; 180, 90) not a "fault rock" but showing lots of brittle strain
				285	20	
12	2.8	23.84698	32.4931			Several scattered otc of the very fine grained red-brown sandstone- form a strike line ~060 but dip not possible- spheroidal weathering along fractures is excellent
13	2.9	23.34795	32.49654	185	23	Low ridge west of poer lines, grey/white massive limestone, ridge is all loose broken rock, with several ridges that are slightly more resistant (ridge is ~3m high)
14	2.10	23.84595	32.49614	185	25	Scruffy layer on side of ridge using for strike and dip
				184	21	
15	2.11	23.84421	32.49615	187	23	following ridge, collecting strike and dip to characterize fold
				197	16	
16	2.12	23.84343	32.49521	276	18	around the nose of the fold following the limestone ridge (dip may be high, looked shallower, hard to get) thin scruffy layer was measured
17	2.14	23.84437	32.49342	313	24	taken in the unit just above the grey/white ridge, 10m to the north
				296	27	
				309	5	
				305	14	
				311	20	
18	2.15	23.8426	32.49486	266	10	light tan to buff thinly bedded limestone, looks flat (nose of fold)

19	3.1	23.83542	32.49598			Otc between "spatter" limstone same as knobbly limestone of barb and red flaggy limestone +Fe concretions. This otc is first appearnce of otc this side of road. Red sandstone fine-medium grained well sorted, very well indurated with silica and Fe cement broken surfaces have a quartzite appearance contains good current ripples, interbedded with light brown-tan sandstone below "Dakhla Formation"
20	3.2	23.83455	32.49641	225	5	"Flat-lying" subtle dip on the light tan, soft, thinly bedded sandstone, not indurate, friable. Bedding is highly disrupted as the unit breaks into various size flag stones and rotates from collapse so south side up based on stratigraphy
21	3.3	23.83389	32.49801	300	22	On contact between Fe rich red brown flaggy sandstone (Dakhla) and spatter knobby limestone (kurkur). Dakhla is "disrupted" by mass wasting movement, probaly cloe to horizontal. Strike and dip are of "bedding in Kurkur
				310	19	
22	3.4	23.83322	32.49845	340	14	In this location on google map it has a sense of a small syncline on s side of fault in Dakhla. Here Dakhla is dipping consistently over a 10's of meter range but on other hill dips are variable
				320	15	
23	3.5	23.83188	32.5005	287	5	Fault contact between red brown Fe rich sandstone(Dakhla) and whitish spatter limestone(Kurkur) contact not exposed but can be "straddled". Contact trend 126
				200	6	
				297	6	
				270	5	on limestone
24	3.6					Barb collected data on Dakhla near nose of fold, strike and dips were @ high angle to structure
25	3.7	23.83214	32.50155	225	24	collecting strike and dip near nose of fold in kurkur limestone; primary bedding is impossible to see, so best guess
				230	23	
				230	20	
				225	25	
26	3.8	23.83314	32.50089	270	10	unit with very thin flaggy resistant layers seperated by several meters of

						shale?
27	3.9	23.83338	32.50178	172	26	strike and dip in kurkur-better chance of bedding
				172	23	
				172	19	might be better indicator of bedding
28	3.10a	23.83313	32.50361	169	42	Dakhla, surprising steep dips
				170	50	
				169	48	
29	3.10b	23.83306	32.50345	160	43	
				164	43	
				155	51	
				159	32	
30	3.10c	23.83309	32.50338	158	68	
				157	70	
				160	76	
				160	62	
31	3.10d	23.83331	32.50304	164	35	series of linear steeply dipping ridges of resistant red brown sandstone with friable tan sandstone in between. Ridges are 10's of meters long and offset-probably by splays of faults coming off of the fault between these ridges and the kurkur, this fault probably merges with the other fault
				170	42	
32	3.11	23.83071	32.50364	185	82	ridges of Dakhla sandstone, part of this fault system
33	3.13	23.83531	32.50418	155	18	bedding on chalky white friable surface. Dakhla tan-buff friable, red cometatn and tan competant sandstone layers in a small wadi buried beneath pediment surface highly weatherd beneath last outcrop for km's east
34	3.14	23.83993	32.50313	192	21	High long ridge of Dakhla. Last ridge east, steep slope on east side cut by a wide wadi. Sand sheets and small dunes to NE. Height of ridge ~similar to other ridges in syncline, surface seems to be an old pediment
				172	17	
				183	25	
35	3.12	23.84035	32.50201	184	37	another ridge of Dakhla. Fairly linear and sinuous.
36	3.15	23.84044	32.50147	165	67	Dips are variable-rotated beds(locally) how? Kinks? Drag fold? (Dakhla)
				168	38	
				175	53	

37	3.16	23.84035	32.49973	184	13	Bedding as best we can tell. Kurkur limestone defining the ridge on east side of syncline. Dakhla obvious thinned stratigraphically on the se side of the basin-reverse fault?
				180	15	
38	3.17	23.83904	32.49855	203	17	in desperation a strike and dip was taken on a thin tan-buff shell hash limestone, not sure if this is real bedding, very thin scruffy low ridge cropping up in gravelly wadi within basin.
39	3.18	23.8375	32.49653	027	3	other side of fold, same as tan-buff limestone as in 17. Shell hash, again a desperate attempt at strike and dip as bedding is hard to see
				345	3-5	

APPENDIX C.

DR. JOHN HOGAN FIELD NOTES, 2011-2012

	Dr. Hogan Data				
Stop	Lat/Northing	Lon/Easting	Strike	Dip	Notes
1/1/2012	23.85718	32.50125	183	22	Kurkur Limestone (?), weathers buff, light gray with a vuggy appearance and "spatter"-which may be an erosional feature mssu with poorly develpoed bedding
1/1/2012			145	30	
1/1/2012			40	45	(?)
1/2/2012	23.85705	32.50333	196	20	Low SW dipping continuous ridge of fossiliferous light gray weathering Limestone (fizzes vigourously) broken surface is a mottled white, orange-red, and fine black lines, possibly outlines of shells.-Lots of broken shel fragments (nearshore?) Kurkur Limestone
1/2/2012			192	23	(shooting across outcrop)
1/3/2013	23.85692	32.50361			Irregularly bedded calcareous sandstone with smooth round-angular grains-pebbles of quarts, chert, and ? Poorly sorted. Flaggy weathering - Could be a much younger unit? -Could be an angular unconformity and a younger fault (less likely) sample taken
1/4/2012	23.85602	32.50509	142	4	Outcrop defining the "horizontal" irregular ridge on google earth. Outcrop capped by a "mssu" indurated .5m thick that is actually very finely bedded with local mounds- when broken open coarse cc can be seen in places but its fine sandstone below this unit is a more "shaly" in appearance unit that is argillaceous fine grained sandstone (pebbles absent) weathered surface light gray, fresh orange brown, Can have vuggy horizons. Photos show outcrop and rip up clasts. shallow shelf?
1/5/2012	23.85617	32.50308	186	32	Back of dipping ridge, gray-buff weathering, orange rusty fresh, shell fragments common also pebbles, near shore? Oyster shell fragments large 5-6 cm

1/6/2012	23.85543	32.50324	142	45	Change in unit, change in strike and dip. Well sorted very fine grained sandstone, slight fizz, iron stain, ripples give a chippy appearance to the outcrop. Fault splays? Pebble sand, oyster bed, fine grained sandstone, and pebble sand all same unit, near shore, interbedded
1/6/2012			155	39	Trevor
1/6/2012			130	44	Eman
1/7/2012	23.8552	32.50332	155	30	"same unit" pebble sand above oyster lag, near shore
1/8/2012	449548	2638021	174	58	Ridge of coarse grained pebbly sanstone with round and angular fragments, poorly sorted. Weathers buff gray, dark brow-orange on fresh surface
1/8/2012			180	29	
1/8/2012			186	34	
1/8/2012			174	43	
1/9/2012	23.8528	32.50409	187	30	cross-strike taverse towards road, thin ridges cropping out of pediment deflation surface. Bedding very fine grained well indurted well sorted sandstone. Gray weathering, dark blackish gray fresh, wavy chippy bedding.
1/10/2012	449392	2638019	198	24	Rusty shell fragment limestone
2/1/2012	449427	2638098	174	24	Ridge of Dakla-must be careful as spherodial weathering creates a secondary fabric that can appear as a psuedo bedding and when buried is confusing. "fibrous" cc occurs with this feature
2/2/2012	23.85245	32.50452	178	27	Dakla ridge interbedded fine grained sand pebbly sandstone, several cm thick. Pebbly sandstone misture of shell fragments and rock fragments , dark blackish color on fresh surface gray on weathered. Matrix supported? Sample taken.
2/2/2012			182	17	
2/3/2012	23.85153	32.5029	184	21	Low ridge at edge of valley before kurkur limestone ridge, light gray orange pebbles , shell fragments, fizz. Based on

					dip slope on weathered rock
2/4/2012	23.85032	32.50278	180	32	fine grained, well sorted sandstone. Buff wethering, maroon on fresh surface, well indurated, hummocky appearance, good bedding.
2/5/2012	23.8489	32.50306	155	38	small group of outcrops in middle of waddi low ridges, very thin wavy bedding light gray weathering, dark blackish brown on fresh surface. Looks like a fine grained sandstone with a lot of cc cement. 328 43 cc filled fracture fairly common but hard to see blend in coarse dark red brown cc. ? change in strike, cc-fractures...fault? close by?
2/6/2012	23.84805	32.50324	154	34	Continuing along ridge-low fins of scattered outcrop all along this trend. Fine grained well indurated sandstone gray weathering, orange brown when fresh, lacks the dark cc of last stop
2/7/2012	23.84755	32.50345	157	46	Continuation of same ridge of low outcrop, strike seems to be slowly rotating, same gray buff fine grained sandstone, orange brown fresh
2/8/2012	23.84731	32.50362	130	51	Last bit of outcrop on this ridge, flat pavement, thinly bedded small wavelength cross-bedded sandstone. -Mapping consistent ridges as we are on the edge of a hummocky topography where mound are "rock" and depressions may have held water-in this area the strike from mound to mound is inconsistent so disrupted by weathering and fault, or what?
2/8/2012			123	45	
2/8/2012			134	42	looks to be best
2/9/2012	23.8476	32.5041	153	74	fine grained well sorted buff inside and out sandstone, thin beds and small ripples. Small ridge in wadi.
2/9/2012			160	76	

2/10/2012	23.84655	32.50388	183	30	Low ridge of fine grained gray sandstone that is rusty red brown on broken surface. Well sorted, we indurated, thinly bedded on a wavy surface
2/10/2012			180	32	
2/11/2012	23.84585	32.50461	70	76	Dramatic change in strike suggests possible drag fold related to displacement along a fault which may go through the "disrupted" outcrop/mound area. Fine grained buff sandstone
2-11a-12	23.84582	32.50447	245	63	fine grained buff sandstone
2-11b-12	23.84571	32.50434	215	64	fine grained sandstone, dark gray inside
2-11c-12	23.84553	32.50425	190	36	fine grain sandstone, gray inside and out
2/12/2012	449595	2637249			photos of deformation bands. Rubly outcrop, flat pavement float with deformation bands abundant. Fine grained well sorted light gray sandstone deformation bands have cement halos not enough outcrop to get a sense of shear, sandstone weathers to a bumpy surface-cement spheroids? -Ridge where we had lunch lots of float with deformtion bands, however finding stuff in place is impossible.
2/13/2012	23.84427	32.5035	176	48	Low ridge of fine grained well sorted sandstone with iron oxide specs scattered throughout, buff weathering light orange buff inside
2/14/2012	23.84467	32.502753	204	33	very low fins of the same fine grained sandstone as last stop-in middle of wadi all cover until kurkur ridge very thin bedding planes forms a chippy outcrop
2/15/2012	23.84369	32.50222	198	46	same fine grained sandstone, very small exposure
2/15/2012			205	44	Better
2/16/2012	23.84344	32.50299	188	63	Med ridge "bumps" of aligned outcrop of the fine grained sandstone, light gray weathering but blackish mottled gray fresh surface flaggy bedding.
2/16/2012			195	48	
2/16/2012			190	50	

2/18/2012	23.84287	32.5035			Finally outcrop with deformation bands in place, deformation bands seem to be confined to this ridge of fine grained well sorted sandstone. Deformation bands have cement halos. Ladders suggest sinistral. 295 68 for main set, 078 85 for ladder
2/19/2012	23.84082	32.50362	167	50	Low low ridge of clean sandstone. Barely crops out. Very fine grained well sorted, tan buff inside and out.
2/19/2012			166	53	
2/20/2012	23.84123	32.50264	196	20	Outcrop along mod size ridge mottled black gray sandstone
2/21/2012	23.84171	32.50124	195	35	Low pavement in wadi fine grained well sorted sandstone buff to rusty orange
2/21/2012			183	42	
2/22/2012	23.84031	32.50197	206	16	fine grained well sorted sandstone with abundant cc cement flaggy wavy bedding forms low ridge
2/22/2012			203	17	
2/23/2012	23.83538	32.50423	143	24	Near seismic line outcrop in wadi tough shape fine grained sandstone well sorted rusty and Mn oxide
3-1-12	23.83753	32.49654	280	6	Low outcrop of fossiliferous limestone is in syncline 9280 6 is best estimate as clear bedding surfaces are in?)
3/1/2012			330	10	another estimate, sample collected
3/2/2012	23.83723	32.49847	153	14	Outcrop of buff weathering fossiliferous limestone (same as 3-1) sub-horizontal dips but sag on outcrop. 153 14 taken from dip surface
3/3/2012	23.83924	32.49862	207	25	same limestone measing a pavement surface that may or may not reflect bedding
3/3/2012			188	15	
3/3/2012			179	5	
3/3/2012			180	16	
3/4/2012	23.83957	32.49941	171	20	light gray-dirty white weathered light brown tan fresh fossiliferous limestone, 171 20 taken from dip slope
3/5/2012	23.842	32.49894	195	25	low ridge of fossiliferous limestone, buff light gray weathering light brown inside
3/5/2012			198	32	

3/6/2012	23.84203	32.49955	185	20	long ridge of fossiliferous limestone (kurkur) 185 20 taken from well developed flat flaggy surface
3/7/2012	23.83545	32.50012	136	22	(?) best chance for being "in place" among rubble (kurkur limestone)
3/7/2012			120	15	
3/8/2012	23.8347	32.50077	155	10	another scruffy kurkur limestone outcrop amongst rubble, could be weathering surface
3/9/2012	23.83625	32.50034	155	25	kurkur limestone base of ridge "shooting" the dip slope in an area that may reflect bedding
3/10/2012	23.83665	32.50184	155	76	thin shark fins in the desert, several along strike steeply dipping thin wavy bedding well indurated, fine grained well sorted brown weathering smooth surface orange tan brown on fresh surface. Sample taken. Second normal fault down to the west, steep dips from drag on fault, younger against older instead of out of the syncline thrust
3/11/2012	23.83581	32.50223	141	60	shark fin red-brown thinly bedded fine grained sandstone same as 3-10 cross-cut by cc viens (275 43)
3/12/2012	23.8354	32.50239	138	83	outcrop of "clean" buff sandstone cross-bedded, good bedding, right side up, sample taken
3/12/2012			140	88	
3/13/2012	23.83468	32.5027	153	69	shark fin same sandstone layer wavy bedding just past old seismic survey -Found a good fault, looks like bedding plane faults with ramps, Trevor and Eman working on it
3/14/2012	23.83219	32.50413	174	22	red-brown flaggy fine grained sandstone well indurated brown on fresh surface
3/14/2012			158	36	good bedding, clean sandstone, sample taken
3/15/2012	23.83094	32.50434	172	32	low fins of red brown sandstone from last stop
3/16/2012	23.82884	32.50455	165	6	Low pavement shallow dips - variable strike, clean light tan fine grained sandstone with desert varnish
3/17/2012	23.82838	32.50428	118	18	several thin ridges parallel to strike spaced 10's of meters

					apart, big change in strike (cross fault line?)
3/18/2012	23.82941	32.50363	170	67	low fins of the red brown well indurated fine grained sandstone looks "cleaved", 170 67 bedding or cleavage? ?the fault splay heading up the valley, sample takend
3/19/2012	23.83241	32.50375	165	36	fine, dark gray (fresh) light gray weathered sandstone. Thick 3cm and thin flaggy bedding. Good bedding
4/1/2012	23.8761	32.49913	197	27	NE corner of structure, edge of large gravel fan in wadi. Low ridges of the fine grained well sorted well indurated thinly bedded sandstone. Weathers light gray-gray fresh surface, over all orange sandstone
4/1/2012			198	26	
4/2/2012	23.87702	32.49907	177	22	Contact, angular unconformity between a well indurated conglomerate of sand grains and rounded sub rounded clasts supported on top of dakla (?) Sandstone (same as last stop), conglomerate looks horizontal. Small outcrops of conglomerate scattered on edge of stream cut as well as dakla with shallow dips
4/3/2012	23.84734	32.49638	211	18	low pavement ridges of the light tan sandstone fine grained well sorted but with something weathering out, 2nd porostiy thinly bedded
4/3/2012			185	8	
4/4/2012	23.87502	32.4981	185	20	N end of prominent low ridge thinly bedded "slaby" wavy fine grained sandstone red brown weathering charcoal gray inside fine grained well sorted well indurated -ridge cut by small faults -look to be offsets across strike on conjugate sets, which in places may connect to bedding plane parallel faults
4/5/2012	23.87476	32.49807	186	18	Same unit, good main bedding trend
4/6/2012	23.84345	32.49782	206	21	along dextral offset, trend approx 060, good regional bedding
4/7/2012	23.87458	32.49806	199	33	same ridge, locally dips will steepen, good bedding -drag

					on hanging wall of a normal fault?
4/8/2012	23.87385	32.49797	196	37	same ridge, here steppening of dips and break drag fold on hanging wall normal fault
4/8/2012			174	18	
4/9/2012	23.87267	32.49757	230	34	good pavement of the clean thinly bedded sandstone light tan weathered, light brown fresh, very fine grained, well sorted.collecting data on a drag fold (?) units strike at high angle to syncline, possible fault?
4/9/2012	23.87272	32.4976	205	20	same outcrop, bedding changing
4/10/2012	23.87375	32.49644	205	30	clean fine grained well sorted sandstone, light brown inside and out. Good bedding, low pavementscruffy outcrop, high angle to el kasr
4/11/2012	23.87401	32.4963	210	34	same stuff as 4-10 last ridge to west scruffy outcrop, then buried by gravel
4/12/2012	23.87304	32.49517	120	18	low ridge of kurkur limestone has that appearance…on west end (shooting the outcrop)
4/13/2012	23.87262	32.49575	120	22	bumps of kurkur
4/14/2012	23.87213	32.49565	140	27	low scruffy ridge of kurkur limestone, light gray with fresh pinkish gray, very fine grained, could be bedding
4/15/2012	23.87144	32.49568	144	22	at slope break thinly bedded limestone, chippy weathering, light gray light pink gray fresh, very fine grained
4/15/2012			140	21	
4/17/2012	23.86515	32.49775	165	24	low linear ridge of kurkur limestone in valley fine grained and full of pellets
4/18/2012	23.8584	32.5041	168	10	flat gravel pavement eroded edge light tan and black pebbles with red orange brown fresh matrix supported matrix very fine grained, looks more horizontal overall
4/19/2012	23.83755	32.50187			gigapan
4/20/2012	23.83362	32.50179			gigapan
4/21/2012	23.834856	32.5014			gigapan
4/22/2012	448523	2636096	298	4	"flat" thinly bedded friable clean sandston weathers tan same inside

APPENDIX D.

TREVOR ELLIS FIELD NOTES,
2011-2012

		Trevor Data				
	Stop	Northing	Easting	Strike	Dip	Notes
1	1-1	2638521	449210	183	22	Massive gray limestone. Vuggy, some rust stains. Primary structures difficult to find
1	1-1			145	30	
1	1-1			40	45	
2	1-2	2638489	449426	190	23	Massive, gray, vuggy limestone, fossiliferous. Effervesces with HC. Ridge east of road, dips toward El Kasr
3	1-3	2638477	449453	350	18	Small outcropjeast of ridge. Rust colored marl. Smooth pebbles abundant, reacts with HCL, no fossils. Dips east away from El Kasr. Flaggy weathering
4	1-4	2638377	449603	142	4	Rust colored fine grained sand with calcareous cement, laminated, few pebbles, no fossils. Apparently continuous with 1-2. Interbedded massive layers. Some pebbly pieces found with shell fragments
5	1-5	2638343	449419	166	38	Massive Gray unit. Ridge east of El Kasr. Large shel fragments, 7cm
6	1-6	2638311	449423	155	39	Small ridge. Well sorted, very fine grained, sligh fizz with HCL, flaggy. Some Fe rich clasts. Sandstone thinly bedded, some ripple marks or cross bedding
7	1-7	2638285	449427	155	30	Ridge east of El Kasr dipping toward El Kasr, pebbly marl
8	1-8	2638021	449548	180	29	Ridge East of El Kasr, flaggy marl
9	1-9	2637999	449490	188	34	Flaggy ridge marl
10	1-10	2638019	449392	186	22	rusty marl, pebbles, shell fragments
11	2-1	2638098	449427	174	24	pebbly marl ridgesare dakla formation. Formation exhibits spheroidal weathering that may be taken as bedding if not careful
12	2-2	2637976	449545	182	17	dakla ridge, just above compositional change. Dips towards El Kasr dark gray, pebbles, some Fe
13	2-3	2637906	449513	189	49	dakla ridge, south of change in strike
14	2-4	2637812	449474	214	32	dakla ridge, south of change in strike
15	2-5	2637741	449368	171	32	Dakla ridge west of ridge at 2-4, East of Road
16	2-6	2637688	449522	219	13	Ridge East of road. Fine to Very Fine grained, well sorted, well cemented, Fe stained. Nearly horizontal, may be weathering. Layers seem too consistent to be weathering. No pebbles or shells
17	2-7	2637614	449486	205	34	Dakla ridge cut by wadi
18	2-8	2637575	449479	217	11	low ridge of very fine grained, well sorted, Fe stained unit. East of road

19	2-9	2637411	449452	130	62	fine grained to very fine grained sandstone unit flush with ground surface, does not form ridge. Strike and dip difficult to get due to poor exposure. Strike of beds appears to change from N-S to E-W
20	2-10	2637430	449518	123	55	Very fine grained, well sorted, well cemented sandstone with some Fe stains. Low lying, does not form ridges. Some Fe found along strike. Strike curves south.
21	2-11	2637414	449541	148	58	Low lying well sorted very fine grained tan sand interbedded with more resistent gray fins
22	2-12	2637411	449538	140	40	Resistant gray fin within tan sand
23	2-13	2637363	449605			Hummocky topography outcrops at tops of hills show huge variation in strike. Very difficult to tell what is in place, hills form small rises aprox 1m high. Few larger depressions aprox 10 m across
24	2-14	2637353	449583			Last exposure of tan sand before hummocky topography approx 7m from hummocks
25	2-15	2637248	449590			deformation bands present in fine grained gray unit. Some in place, some not. Appears to trend 175 chalk found a few cm below surface
26	2-16	2637060	449502			top of ridge. Gray sand. Some dark coarser grains present.
27	2-17	2637070	449520	176	6	East side of ridge from 2-16. Clean tan sand, interbedded with Fe. Nearly horizontal
28	2-18	2637058	449499	181	50	Fins of gray sand at top of ridge. Deformation bands abundant, but nothing in place
29	2-19	2636999	449492			Clean tan sand on side of ridge, nearly horizontal
30	2-20	2636983	449467			deformation bands present on top of ridge. None in place though follows general trend of 152. Bands so far only observed in gray unit.
31	2-21	2636942	449448	311	86	Deformation bands on top of ridge in gray unit
32	2-22	2636851	449442	330	82	In place deformation bands in gray unit on top of ridge
33	2-23	2636853	449434	1	39	Clean tan sand on side of ridge. Some Fe
34	2-24	2636824	449426	151	27	clean tan sandat base of ridge. Strike and Dip of layers change
35	2-25	2636818	449423	190	22	clean tan sand at base of ridge
36	2-26	2636722	449416	230	43	Clean tan sand. Fresh surface is rusty color. Edge of ridge
37	2-27	2636530	449370	202	16	Gray unit on top of ridge
38	2-28	2636306	449309	127	21	dark gray unit, very fine grained, Fe inclusions
39	3-1	2636329	448731	280	6	Small outcrop in drainage, strike and dip approx., bedding difficult to find. Fine grained shell fragments, Fe

40	3-2	2636358	448957	181	17	Small outcrop, appears to be same unit as 3-1. fine grained, shell fragments, bedding difficult to see. Strike and dip approx.
41	3-3	2636518	448938	174	15	dip of surface, same limestone as 3-1 and 3-2
42	3-4	2636551	449041			Prominent ridge of highly weathered fossiliferous limestone. Bedding impossible to find.
43	3-5	2636465	449218	215	24	small dipping fins of dakla. 3-1 through 3-4 kurkur formation. Small dakla fins closest to kurkur formation
44	3-6	2636432	449256			offset en-echelon pattern of dakla ridges, offset approx 2m
45	3-7	2636396	449271			apparent right-lateral offset of gray unit within dakla. Dark gray fins stand up out of low lying clean tan sand. Dark gray unit continuous, showing drag of fault. Total offset approx 3m 152 54, 145 45, 145 49
46	3-8	2636403	449269	141	65	deformation bands present in dark gray layer and clean tan sand. Bands appear to be on strike but have different dip than beds
47	3-9	2636408	449272			distinct right lateral offset of dark gray layer within clean tan sand dark gray layer cleanly broken and translated 15-75 cm. Faults seem to have slightly different orientations.strike and dip measurements on offset layer 150 60, 149 60. trends of "faults" 214, 227
48	3-10	2636421	449273			right lateral offset of dark gray layer. Layer not continuous. Offset approx 2m, trend of fault 205
49	3-11	2636421	449273			Offset dark gray, right lateral. Offset approx 3.5m. Gray layer not continuous. Fault trends 210
50	3-12	2636347	449272			Deformation bands present near right lateral offset. Deformation bands run along strike of displaced gray layer. Deformation bands trend 151, fault trends 206
51	3-13	2635838	449426	161	52	Possible normal fault motion along bedding. Strike of bedding changes where fault transfers to new planes.
	3-13			179	19	
52	3-14	263589	449422	159	80	Clean tan sand
53	3-15	2635855	449395	161	52	Clean tan sand
54	4-1	2640605	449006	162	24	Northeast corner of structure. Small outcrop of gently dipping beds. Weathered dark gray, fresh surface very fine grained, orange, speckled with dark brown. Dakla

55	4-2	2640625	449049	171	48	Northeast corner of structure. Steeply dipping dakla. Dipping toward structure. Possibly drag fold
56	4-3	2640701	449002			unconformity between very fine grained dakla and gravel conglomerate. Dakla dips gently west toward structure, conglomerate appears to be horizontal. Conglomerate consists of pebbles a mm to 10 cm. Grain supported
57	4-4	2640476	449771			dahkla and conglomerate side by side, though nonein place. Ptotentially faulted. Conglomerate displays some fabric, possiblye bedding.
58	4-5	2640476	448740			small conglomerate outcrop. Conglomerate exhibits fabric resembling bedding. Fabric appears to be nearly horizontal.
59	4-6	2640413	448888	186	29	Northeast corner. Dahkla ridge. Ridge dips toward El Kasr, though dips vary. Dips steepen suddenly up dip, folds seen down dip, forming horse-shoe like structures. Some features may be visisble in high-res imagery. Structures may form conjugate sets, limbs cure toward one another.
60	4-7	2640380	448888	175	32	Dahkla ridge, down strike of 4-6. Pictures show offset of ridge down strike. Pictures show fins cutting across bedding and changing strike.
61	4-8	2640387	448889	199	16	Down strike on dahkla ridge. Ridge cut by joints, beds steepen across joint. Pictures display joints and steepening beds.
62	4-9	2640277	448856	197	11	Down strike of ridge. Strike of ridge changes, wraps around, coming in line with syncline.
63	4-10	2640272	448852	202	13	Down strike of 4-9
64	4-11	2640255	448845	186	12	Down strike of 4-10
65	4-12	2640250	448848	172	19	Down strike of 4-11. Dark gray resistant layers interbedded with low lying clean tan sand.
66	4-13	2640241	448847	175	17	Down strike of 4-12. Farther down strike beds curve again to a high angle with syncline. Pictures show changes in strike, conjugate sets, joints and bedding, beds approaching syncline at high angle.
67	4-14	2640041	448847	12	20	Kurkur highly weathered gray limestone. No visible bedding, but unit appears to be nearly horizontal.
68	4-15	2640037	448845			Near base of ridge, slightly higher topographically from 4-14. Fins that appear to be Dahkla. Possible contact between Dahkla nad Kurkur. In place kurkur present above, but no dahkla

69	4-16	2639948	448758	162	12	Small kurkur outcrop at base of outcrop at base of ridge some layering perhaps bedding or weathering.
70	4-17	2639936	448721	151	18	Side of ridge, thinly bedded limestone
71	4-18	2639736	448431			Sample taken from within structure
72	4-19	2639421	448915	169	30	Small low lying ridge east of structure. Bedding difficult to find. Surface may be weathering
73	4-20	2638695	449426	125	10	East of structure. Gently dipping rust colored limestone.

APPENDIX E.

CHARACTERISITICS OF STRUCTURES ALONG THE GEBEL EL-BARQA FAULT

Table 3. Characteristics of Structures found along the Gebel El-Baqa Fault

	36 R 446657 E 2669952 N	Elongate structural basin, fold nose easily identifiable, narrow (~1 Km), filled with sediment, 8 Km long	Possibly Garra
	36 R 446657 E 2669952 N	Elongated, basin, filled with sediment, smaller than other observed folds along Gebel El-Barqa, dip of bed difficult to determine, possible bounding fault to the west, 1 Km long	Possibly Dungul
	36 R 447168 E 2667360 N	Elongated, narrow (~1 Km), structural basin, filled with sediment, few observable dipping beds, no obvious faults or offsets. 3.5 Km long	Possibly Dungul
	36 R 448002 E 2659026 N	Asymmetric, elongated, beds appear to dip in toward a single bounding fault, approx 3 Km long	Possibly Dungul
	36 Q 448205 E 2638640 N	Elongated composite basin. Oriented N-S, Multiple offsets, multiple faults, Approx 5 Km long	Garra, Kurukur, Dakhla

APPENDIX F.

CALCULATION OF DISPLACEMENT ACROSS THE GEBEL EL-BARQA FAULT

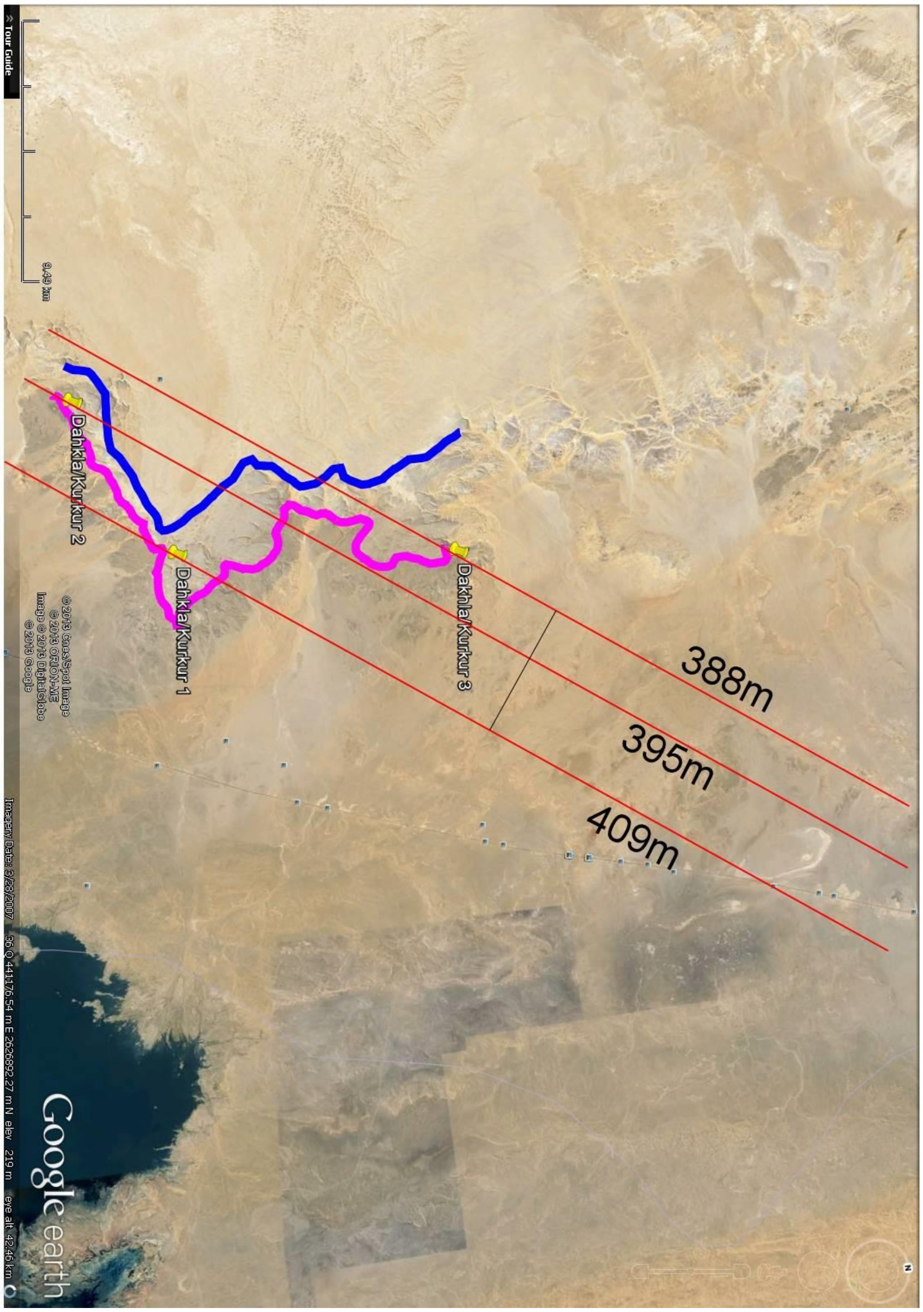

The Dahkla/Kurkur contact was mapped along scarp of the Sinn El-Kaddab Plateau on Google Earth using maps as a reference (Conoco, 1981). Control points were then used to collect elevation data and calculate the orientation of the contact. The strike and dip of the contact was found to be 209/<1. Structural contours were then projected over the El Kasr and the elevation difference was calculated.

BIBLIOGRAPHY

Abdeen, M.M., Abdelsalam, M.G., Nielsen, K.C., Yehia, M.A., Cherif, O.H., 2000. Active dextral wrenching in southern Egypt. In: 38th Annunal Meeting of the Geological Society of Egypt, Cairo, November

Abdel-Monem, M.S., Haggag, H.M., Saleh, M., Abou-Aly, N., 2012. Seismicity and 10-years recent crustal deformation studies at Aswan region, Egypt. Acta Geodyn. Geomater. 9, 221-236.

Allmendinger, R.W., Cordozo, N., and Fisher, D., 2012. Structural geology algorithms: Vectors and tensors in structural geology. Cambridge University Press, New York, 6-8.

Badawy, A., 2001. The present-day stress field in Egypt. Annals of Geophysics 44, 557-570.

Bosworth, W., Guiraud, R., Kessler, L.G. 1999. Late Cretaceous (ca. 84 Ma) Compressive Deformation of the Stable Platform of Northeast Africa(Egypt): Far-Field Stress Effects of the “Santonian Event” and origin of the Syrian Arc Deformation Belt. Geology 27. 633-636.

Bosworth, W. and Strecker, M.R., 1997. Stress field changes in the Afro-Arabian rift system during the Miocene to Recent period. Tectonophysics 278, 47-62.

Bosworth, W., El-Hawat, A.S., Helgeson, D.E., Burke, K., 2008. Cyrenaican “shock absorber” and associated inversion strain shadow in the collision zone of northeast Africa. Geology 36, 695-698.

Bucher, S., Schmid, S.M., Bousquet, R., Fugenschu, B., 2003. Late-stage deformation in a collisional orogen (Western Alps): nappe refolding, back-thrusting or normal faulting? Terra Nova 14, 109-117.

Conoco, 1981, "Geologic Map of Egypt" Map. Ministry of Industry and Mineral Resources. The Egyptian Geological Survey and Mining Authority.

Davis, G.H. Reynolds, S.J. and Kluth, C.F., 2012. Structural Geology of Rocks and Regions. 3th ed. John Wiley and Sons, New York, p 718-726.

Dibblee, T.W.Jr.,1977. Relations of hydrocarbon accumulations to strike-slip tectonics of the San Andreas fault system, in Nielsen, T.H., ed., Late Mesozoic and Cenozoic sedimentation and tectonics in California: Bakersfield, California. San Joaquin Geological Society, p. 135-143.

El-Araby, H., and Sultain, M., 2000. Integrated seismic risk map of Egypt. Seismological Research Letters 71, 53-66

El Etr, H.A., Yehia, M.A., and Dowidar, H., 1982. Fault pattern in the southwestern desert of Egypt. Ain Shams University, Science Research Series 2. 123-152.

Erickson, S.G., 1995. Influence of mechanical stratigraphy on folding vs faulting. Journal of Structural Geology 18, 443-450.

Erslev, E.A., 1991. Trishear Fault-Propagation Folding. Geology 19, 617-620.

Fleuty, M.J., 1964. The description of folds. Proceeding of the Geologists' Association 75, 461-492.

Gomez, C., Delacourt, C., Allemand, P., Ledru, P., Wackerle, R., 2004. Using ASTER remote sensing data for geological mapping in Namibia. Physics and Chemistry of the Earth 30, 97-108.

Guiraud, R. and Bosworth, W., 1999. Phanerozoice geodynamic evolution of northeastern Africa and northwestern Arabian platform. Tectonophysics 315, 73-108.

Guiraud, R., Issawi, B., and Bosworth, W., 2001. Phanerozoic History of Egypt and surrounding areas. Peri-Tethyan rift/wrench basins and passive margins 186, 469-509.

Guiraud, R., Bosworth, W., Thierry, J., Delplanque, A., 2005. Phanerozoic geological evolution of Northern and Central Africa: an overview. Journal of African Earth Sciences 43, 83-143.

Harding, T., 1974. Petroleum Traps Associated with Wrench Faults. AAPG Bulletin 7, 1290-1304.

Henson, F., 1951. Observations on the geology and petroleum occurrences in the Middle East. Proceedings of the Third World Petroleum Congress. Sect. I. Leiden 118-140.

Hosny, A., Ali, S. M., Abed, A., 2013. Study of the 26 December 2011 Aswan earthquake, Aswan area, south of Egypt. Arabian Journal of Geosciences, (Online First Article) not in an issue

Issawi, B., 1968. The Geology of the Kurkur Dungul Area. General Egyptian Organization for Geological Research and Mining, Geological Survey 46.

Issawi, B., Anonymous 1978. Geology of Nubia West area, Western Desert, Egypt. Annals of the Geological Survey of Egypt 8, 237-253.

Janecke, S., 1998. Geometry, mechanisms, and significance of extensional folds from examples in the Rocky Mountain Basin and Range province, USA. Journal of Structural Geology 20, 841-856.

Khalil, S.M. and McClay, K.R., 2002. Extensional fault-related folding, northwestern Red Sea, Egypt. Journal of Structural Geology 24, 743-762.

Mekkawi, M., Schnegg, P.A., Arafa-Hamed, T., Elathy, E., 2005. Electrical structure of the tectonically active Kalabsha Fault, Aswan, Egypt. Earth and Planetary Science Letters 240, 764-773.

Mohamed, H.H., Kang, T.S., and Baag, C.E., 2001. Focal mechanism determination based on the polarity and SV-P amplitude ratio in the Kalabsha area, Aswan, Egypt. Geosciences Journal 5, 165-171.

Rich, J., 1934. Mechanics of Low-angle overthrust faulting as illustrated by Cumberland thrust block Va., Ky., and Tenn.. American Association of Petroleum Geologists Bulletin 18, 1584-1596.

Robert-Charrue, C. and Burkhard, M., 2008. Inversion tectonics, interference pattern and extensional fault-related folding in the Eastern Anti-Atlas, Morocco. Swiss Journal of Geosciences 101, 397-408.

Roden, J., Abdelsalam, M.G., Atekwana, E., El-Qady, G., Tarabees, E.A., 2011. Structural influence of the evolution of the pre-Eonile drainage system of southern Egypt: Insights from magnetotelluric and gravity data. Journal of African Earth Sciences 61, 358-368.

Rowan, L.C., and Mars, J.C., 2002. Lithologic Mapping in the Mountain Pass, California area using Advanced Spaceborne Thermal Emission and Relfection Radiometer (ASTER) data. Remote Sensing of the Environment 84, 350-366 .

Schlische, R.W., 1995. Folds in Extensional Settings. AAPG Bulletin 79, 1661-1678.

Sharp, I.R, Gawthorpe, R.L., Underhill, J.R., Gupta, S., 2000. Fault-Propagation folding in extensional settings: Examples of structural style and synrift sedimentary response from the Suez rift, Sinai, Egypt. Geological Society of America Bulletin, 112, 1877-1899.

Shipton, Z.K. and Cowie, P.A., 2001. Damage zone and slip-surface evolution of um to km scales in high-porosity Navajo sandstone, Utah. Journal of Structural Geology 23, 1825-1844.

Simpson, D., Kebeasy, R., Maamoun, M.M., Ibrahim, E., Megahed, A., 1986. Induced seismicity around Aswan lake. Tectonophysics 118, 281.

Storti, F., Salvini, F., and McClay, K., 1997. Fault Related folding in Sandbox Analogue Models of Thrust Wedges. Journal of Structural Geology 19, 583-602.

Suppe, J., 1983. Geometry and Kinematics of Fault-Bend Folding. American Journal of Science 283, 684-721.

Sylvester, A.G., and Smith, R.R., 1976. Tectonic Transpression and Basement-Controlled Deformation in San Andreas Fault Zone, Salton Trough, California. The American Association of Petroleum Geologists Bulletin 60, 225-299.

Sylvester, A.G.,1988. Strike-Slip Faults. Geological Society of America Bulletin 100, 1666-1703.

Tewksbury,B., Abdelsalam, M.G., Tewksbury-Christle, C., Hogan, J.P., Pandey, A., and Jerris, T., 2009. Reconnaissance study of domes and basins in Tertiary sedimentary rocks in the Western Desert of Egypt using high resolution satellite imagery. Geological Society of America annual meeting, Portland Oregon, Oct 19-21, 2009.

Tewksbury,B., Dokmak, A.A., Tarabees, E.A., Mansour, A.S., Fattah, T.A., and Rashad, M.A., 2010. A Previously Unrecognized System of Folds and Related Faults in the Stable Platform Limestones of the El Rufuf and Drunka Formations, Western Desert, Egypt. Geological Society of America annual meeting, Minneapolis Minnesota, October 9-12, 2011.

Tewksbury, B.J., Dokmak, A.A.K., Tarabees, E.A., Mansour, A.S., 2012. Google Earth and Geologic Research in Remote Regions of the Developing World: An Example from the Western Desert of Egypt. In Whitmeyer, S.J., Bailey, J.E., De Paor, D.G., and Ornduff, T., eds., Google Earth and Virtual Visualizations in Geoscience Education and Research: Geological Society of America Special Paper 492, 23-36.

Thurmond, A.K., Stern, R.J., Abdelesalam, M.G., Nielsen, K.C., Abdeen, M.M., and Hinz, E., 2004. The Nubian Swell. Journal of African Earth Sciences 39, 401-407.

Withjack, M.O., Olson, J., and Peterson, E., 1990. Experimental models of Extensional Forced Folds. AAPG Bulletin 74, 1038-1054.

Woodward-Clyde Consultants, 1985. Seismic hazards in the vicinity of the Aswan Dam and Lake Nasser. Internal Report, Geological Survey of Egypt, 2, 16-27.

Wu, J., McClay, K., Whitehouse, P., and Dooley, T., 2009. 4D analogue modelling of transtensional pull-apart basins. Marine and Petroleum Geology 26, 1608-1623.

Youssef, M.M., 2003. Structural Setting of Central and South Egypt: An Overview. Micropaleontology 49, 1-13.

Xiao, H. and Suppe, J., 1992. Origin of Rollover. AAPG Bulletin 76, 509-529.

VITA

Trevor Charles Ellis was born on in Troy, Missouri to Charles and Carmen Ellis. He attended Silex High School and graduated in 2006 as Salutatorian. He continued his education and enrolled in Missouri University of Science and Technology in 2006, graduating with a BS in Geology and Geophysics in 2010. He then enrolled as a Master's student in Geology and Geophysics at Missouri University of Science and Technology, studying under Dr. John Hogan. He married Sara Elizabeth Cook on June 15, 2013 and received his MS in Geology and Geophysics in 2013. He and his wife currently live in Independence, Missouri.